SONIC HEDGEHOG SIGNALING IN INNER EAR ORGANOID DEVELOPMENT

Emma Longworth-Mills

Submitted to the faculty of the University Graduate School
in partial fulfillment of the requirements
for the degree
Doctor of Philosophy
in the Department of Anatomy and Cell Biology,
Indiana University

August 2019

Accepted by the Graduate Faculty of Indiana University, in partial fulfillment of the requirements for the degree of Doctor of Philosophy.

Doctoral Committee

_____
Eri Hashino, Ph.D., Chair

_____
Kathryn Jones, Ph.D.

June 21, 2019

_____
Alexander Robling, Ph.D.

_____
Teresa Zimmers, Ph.D.

_____
Jinhui Chen, Ph.D.

DEDICATION

I would like to dedicate this work to my parents, to my sister and brother-in-law, and to my friends, all of whom have been the absolute guiding force in getting me here—to this moment wherein there is work to dedicate to anyone in the first place.

ACKNOWLEDGEMENTS

This work would not have been possible without the leadership of my mentor, Dr. Eri Hashino. I would like to acknowledge and thank Dr. Hashino for the tremendous support she has provided throughout my graduate experience. I would additionally like to thank the members of my graduate committee, Dr. Kathryn Jones, Dr. Teresa Zimmers, Dr. Alexander Robling, and Dr. Jinhui Chen, for further guiding my research career at the IU School of Medicine—your input has been valuable throughout my time here.

The members of the Hashino lab, past and present, have additionally been an amazing source of guidance throughout my time as a student, and are every bit responsible for having made the lab an enjoyable place to spend my days. I sincerely thank them, along with the members of the Nelson and Koehler labs, for all of their valuable input over the years. Among my co-workers, I would especially like to thank Jing Nie, whose patience, meticulousness, and unshakeable work ethic has served as a model for me of what it means to be a scientist. Thank you as well to Jade Harkin, who has provided crucial assistance during this last portion of my dissertation research. A profound thank you is owed to Karl Koehler, who has played an intrinsic role in my success as a graduate student, and served as a source of guidance and experimental know-how that has been absolutely indispensable. Finally, both inside and outside the lab, I have learned so much and found incredible joy throughout my time spent with Jiyoon Lee and Pei-Ciao Tang. To you both: thank you for everything you have taught me, in science and in life; thank you for being my dear friends.

I would like to acknowledge my fellow graduate students in the IBMG program; among them, I would especially like to thank Lakshmi Prabhu, Rochelle Frankson, Danting Cao, Xiaoting Wang, Yu-Hsiang Chen, and Eshaani Mitra. Sincere thanks as well to Rachel and Shawn Moore, for being excellent neighbors and friends.

At IUSM, I would additionally like to thank the Department of Otolaryngology-Head & Neck Surgery, in particular Linette Staley, who has been incredibly helpful in managing my F31 award and has been an absolute pleasure to communicate with over the years. In the Department of Anatomy & Cell Biology, I would like to thank Dr. Joseph Bidwell for the guidance and encouragement he has given me throughout my graduate experience, and Kate McMillan for top-notch administrative support. The IUSM graduate division has been amazing as well, in particular Tara Hobson, who has gone above and beyond to help me during my time as a student, as well as Brandy Woods and Lauren Easterling for all of their expertise.

Finally, I would like to thank my family for their love and support over the course of this experience—it would not have happened without you!

Emma Longworth-Mills

SONIC HEDGEHOG SIGNALING IN INNER EAR ORGANOID DEVELOPMENT

Loss of the finite cochlear hair cells of the inner ear results in sensorineural deafness. Human cochlear hair cells do not regenerate, and there is no cure for deafness. Our laboratory has established a three-dimensional culture system for deriving functional sensory hair cells from human pluripotent stem cells. A major limitation of this approach is that derived hair cells exhibit a morphological and gene expression phenotype reflective of native vestibular hair cells. Previous studies have shown that establishment of localized domains of gene expression along the dorso-ventral axis of the developing otic vesicle is necessary for proper morphogenesis of both auditory and vestibular inner ear structures. Sonic hedgehog (SHH) signaling has been shown to play a key role in specification of the ventral otic vesicle and subsequent cochlear development. Here, SHH treatment was pursued as a potential strategy for inducing a patterning phenotype permissive to cochlear induction *in vitro*. Single-cell RNA-sequencing analysis revealed that while treatment with the SHH pathway agonist Purmorphamine reduced expression of markers for the vestibular-yielding dorsal otic vesicle, upregulation of ventral otic marker genes was modest. More strikingly, the number of otic progenitors exhibiting a neuroprogenitor phenotype increased in response to Purmorphamine treatment. These results suggest that SHH pathway modulation in early-stage inner ear organoids may bias their differentiation toward a neural lineage at the expense of an epithelial lineage. The present study is the first to evaluate the patterning phenotype of human stem

cell derived otic progenitors, and sheds light on the transcriptomic profile at this critical point of inner ear development. This study may also cultivate future efforts to derive cochlear cell types as well as inner ear neural cell types from human pluripotent stem cells, and contribute to the establishment of a more complete *in vitro* model of inner ear development.

Eri Hashino, Ph.D., Chair

TABLE OF CONTENTS

LIST OF TABLES xii

LIST OF FIGURES xiii

LIST OF ABBREVIATIONS xvi

CHAPTER ONE: INTRODUCTION 1

The mammalian ear 3

Anatomy and physiology of the human ear 3

Inner ear development 8

Modeling inner ear development *in vitro* 11

Pluripotent stem cells 13

Differentiation of human 3D inner ear organoids 14

Previous in vitro studies for the differentiation of inner ear cell types 17

Single-cell RNA-sequencing analysis of the inner ear 24

The role of Sonic hedgehog signaling in inner ear development 28

Sonic hedgehog signaling pathway 28

Dorso-ventral patterning of the otic vesicle 31

Research aims 35

CHAPTER TWO: MATERIALS AND METHODS 38

Embryonic stem cell culture 38

Signaling molecules and recombinant proteins 39

Inner ear organoid differentiation 40

Quantitative PCR 42

Immunohistochemistry 43

Fluorescence activated cell sorting 45
Single-cell RNA-sequencing 48
Statistical analysis 51
CHAPTER THREE: RESULTS 52
Validation of inner ear organoid differentiation 52
PAX2-2A-nGFP reporter line allows for monitoring the development of derived otic progenitors 55
SHH pathway modulation in early stage inner ear organoids 60
Isolation and FACS analysis of *PAX2*-2A-nGFP+ derived cell populations 66
Evaluation of control and treated cell populations via single-cell RNA-sequencing 70
Evaluation of dorso-ventral patterning markers 75
Otic marker expression observed in *PAX2*-2A-nGFP+ populations 76
Expression of SHH pathway components 79
Ventral patterning marker analysis 82
Dorsal patterning marker analysis 85
Increased neural population observed in SHH pathway modulated cell population 88
Temporal gene expression changes in Purmorphamine treated cultures 99
Late stage evaluation of Purmorphamine treatment 99
CHAPTER FOUR: DISCUSSION 105
What underlies the apparent commitment to vestibular fate within the inner ear organoid model? 106

What factors may be applied in order to guide differentiation of otic progenitors toward a cochlear fate? 110

CHAPTER FIVE: FUTURE DIRECTIONS 118

Improving efficiency of otic induction 118

Toward cochlear differentiation 120

Fine-tuning SHH pathway modulation 120

Additional pathway modulation 121

The potential impact of the in vivo microenvironment 122

Assessing late stage neural identity 123

REFERENCES 125

CURRICULUM VITAE

LIST OF TABLES

Table 1: Organoid maturation medium (OMM) components 41

Table 2: Chemically defined medium (CDM) components 41

Table 3: qRT-PCR primers 44

Table 4: Primary antibodies 46

LIST OF FIGURES

Figure 1: Anatomy of the human ear 4

Figure 2: Vestibular and cochlear sensory hair cells and synaptic innervation 7

Figure 3: Auditory neural pathway from the inner ear 9

Figure 4: Timeline and key markers of otic cell type induction 12

Figure 5: Droplet-based single-cell RNA-sequencing 27

Figure 6: Hedgehog signaling pathway 30

Figure 7: SHH signaling in inner ear development 32

Figure 8: Hypothesis 37

Figure 9: Morphological progression observed in inner ear organoid culture 53

Figure 10: Immunohistochemistry of early and late stage inner ear organoids confirms expression of markers of otic development 54

Figure 11: Live imaging of *PAX2*-2A-nGFP aggregates 57

Figure 12: PAX2 and GFP expression overlaps completely in *PAX2*-2A-nGFP aggregates 58

Figure 13: Expression of otic markers supports otic identity of *PAX2*-2A-nGFP+ cell population 59

Figure 14: Purmorphamine treatment alone fails to induce presumptive otic vesicles 62

Figure 15: Size phenotype observed in CH+PUR treated aggregates 63

Figure 16: Purmorphamine dose response 65

Figure 17: Fluorescence activated cell sorting of *PAX2*-2A-nGFP aggregates allows for isolation of GFP+ cell population 67

Figure 18: Fluorescence activated cell sorting of CH and CH+PUR treated aggregates 69
Figure 19: Quality control analysis of CH and CH+PUR treated *PAX2*-2A-nGFP+ cell populations for comparative analysis..... 72
Figure 20: Clustering of CH treated single-cell population 73
Figure 21: Clustering of CH+PUR treated single-cell population..... 74
Figure 22: Integrated analysis of CH and CH+PUR datasets..... 77
Figure 23: Otic marker expression in single-cell datasets 78
Figure 24: SHH pathway component expression 81
Figure 25: Ventral patterning marker analysis..... 83
Figure 26: Immunohistochemical analysis of ventral marker OTX2 in CH and CH+PUR treated aggregates..... 84
Figure 27: Expression of dorsal markers DLX3, DLX5 and DLX6 in CH and CH+PUR treated populations 86
Figure 28: Immunohistochemical analysis of dorsal marker DLX3 in CH and CH+PUR treated aggregates..... 87
Figure 29: Evaluation of additional dorsal markers within the CH and CH+PUR sorted populations 89
Figure 30: CH+PUR treated cultures exhibit an increased neural population 90
Figure 31: Immunohistochemical analysis of inner ear neuroprogenitor marker NEUROD1 in CH and CH+PUR treated aggregates..... 92
Figure 32: Additional neural marker expression in CH and CH+PUR treated

populations 93

Figure 33: Markers of vestibular ganglion neuron development 96

Figure 34: Markers of spiral ganglion neuron development 97

Figure 35: Temporal analysis of CH+PUR treatment 98

Figure 36: *ATOH1*-2A-GFP+ population appears reduced in late stage CH+PUR treated aggregates 102

Figure 37: Late stage inner ear organoids do not express cochlear hair cell marker LMOD3 103

Figure 38: Late stage inner ear organoids express neural marker TUJ1 104

Figure 39: Summary of findings 107

LIST OF ABBREVIATIONS

BMP	Bone morphogenic protein
CDM	Chemically defined medium
CHIR	CHIR99021; small molecule inhibitor of GSK3β and GSK3α, functioning in WNT pathway activation
DHH	Desert hedgehog
DIC	Differential interference contrast
ESC	Embryonic stem cell
EGF	Epidermal growth factor
E8f	Essential 8 flex; embryonic stem cell medium
FACS	Fluorescent activated cell sorting
FGF	Fibroblast growth factor
GFP	Green fluorescent protein
HH	Hedgehog
IGF	Insulin-like growth factor
IHH	Indian hedgehog
iPSC	Induced pluripotent stem cell
KSR	Knockout serum replacement
LDN	LDN-193189 dihydrochloride; small molecule inhibitor of BMP receptors ALK2 and ALK3
nGFP	Nuclear green fluorescent protein
OMM	Organoid maturation medium
PSC	Pluripotent stem cell
PUR	Purmorphamine; small molecule agonist for SHH pathway effector Smoothened

RNA-seq	RNA sequencing
ROCK	Rho-associated, coiled-coil containing protein kinase
SB	SB-431542; small molecule inhibitor of TGF-β type I receptor activin receptor-like kinases ALK4, ALK5, ALK7
scRNA-seq	Single-cell RNA sequencing
SFEB	Serum-free culture of embryoid-like bodies
SGN	Spiral ganglion neuron
SHH	Sonic hedgehog
SNHL	Sensorineural hearing loss
TGF-β	Transforming growth factor beta
UMI	Unique molecular identifier
VGN	Vestibular ganglion neuron
WG	Weeks gestation

CHAPTER ONE: INTRODUCTION

Sensorineural hearing loss (SNHL) is caused by the incomplete formation or degeneration of mechanosensitive hair cells within the spiral-shaped inner ear structure known as the cochlea. This sensory cell population is found in the Organ of Corti, a specialized epithelium running through the cochlea, and is responsible for converting sound vibrations into electrical signals, a process termed mechanotransduction. Loss of the neural population innervating the inner ear hair cells, termed spiral ganglion neurons (SGNs), may additionally contribute to SNHL. According to a report from the National Institute on Deafness and Other Communication Disorders, approximately 15 percent of Americans experience noise-induced hearing loss [1], while 2-3 out of every 1,000 children are born with profound hearing loss [2]. The current treatment strategies for SNHL focus on the amplification of acoustic or electric signals, and do not address the underlying pathology, which includes loss of sensory hair cells and SGNs. An *in vitro* system for the derivation of cochlear hair cells from pluripotent stem cells (PSCs) represents a potential means to augment or replace this finite cell population. Furthermore, such a platform would offer a valuable model for recapitulating the pathophysiology of certain types of inner ear disorders.

PSCs are capable of self-renewing indefinitely and generating all cell types from the three germ layers of the body. Three-dimensional (3D) culture systems offer a useful tool for the guided differentiation of PSCs into specific cell populations. Culture in a 3D format permits stem cells to interact in a manner that more closely mimics *in vivo* cell-cell and cell-extracellular matrix interactions,

allowing for self-organized differentiation, and often facilitating more faithful recapitulation of organ development [3-5]. 3D organoid systems have previously been employed in the generation of retinal [6, 7], cerebral [8, 9], lung [10], intestinal [10, 11], and kidney organoids [12-14], among others, representing a platform for disease modeling and drug screening [5, 15-18]. Potential application in the development of cell-based therapies is another appealing aspect of these systems.

Our laboratory has developed a novel 3D *in vitro* system for generating, from mouse and human PSCs, inner ear sensory epithelia, including sensory hair cells, supporting cells, and concurrently arising neuronal populations [19, 20]. This system employs 3D floating cell culture techniques (described [21]) and precisely timed manipulation of several key signaling pathways in order to recapitulate inner ear development. However, it is important to note that the derived sensory hair cells resulting from this model bear morphological and functional properties of the gravity-sensing hair cells of the vestibular end organ [19, 20, 22]. Cochlear cell types have not been observed within the system.

This lack of cochlear induction has spurred the study described here, which set out to investigate the cause of the apparent vestibular bias within this model, and to evaluate what factors may lead to the induction of cochlear cell types *in vitro*. The subsequent work focuses primarily on defining the gene expression patterns of the early-stage PSC-derived otic progenitors. *In vivo,* the otic vesicle serves as the anlage of the inner ear sensory structures and contains multipotent otic progenitors competent to give rise to cochlear or vestibular cell

types. Rigorous analysis of the “default state” derived otic vesicle may shed light on how to increase efficiency of inner ear sensory cell differentiation, and furthermore develop strategies to induce differentiation of cochlear cell types. Additionally, one such strategy is investigated here: the introduction of Sonic hedgehog (SHH) pathway modulation in the 3D inner ear culture model. SHH pathway modulation is evaluated as a potential means to alter the early stage gene expression phenotype of the derived otic vesicles and subsequently bias differentiation toward a cochlear fate.

In order to understand the experimental processes and rationale carried out in the subsequent work, I will begin with an overview of several primary areas of significance, including inner ear anatomy and development, SHH pathway signaling, and a review of previous efforts to model inner ear development *in vitro*. Furthermore, I will discuss single-cell RNA-sequencing, a major component of the approaches used in this investigation.

The mammalian ear

Anatomy and physiology of the human ear

The human ear consists of three main areas—the outer, middle, and inner ear—each of which contributes to the overall function of the ear in hearing and balance (Figure 1). The outer ear consists the pinna and the earlobe, which comprise the external portion of the ear, and the external auditory meatus, which is responsible for conducting sound toward the tympanic membrane, or eardrum.

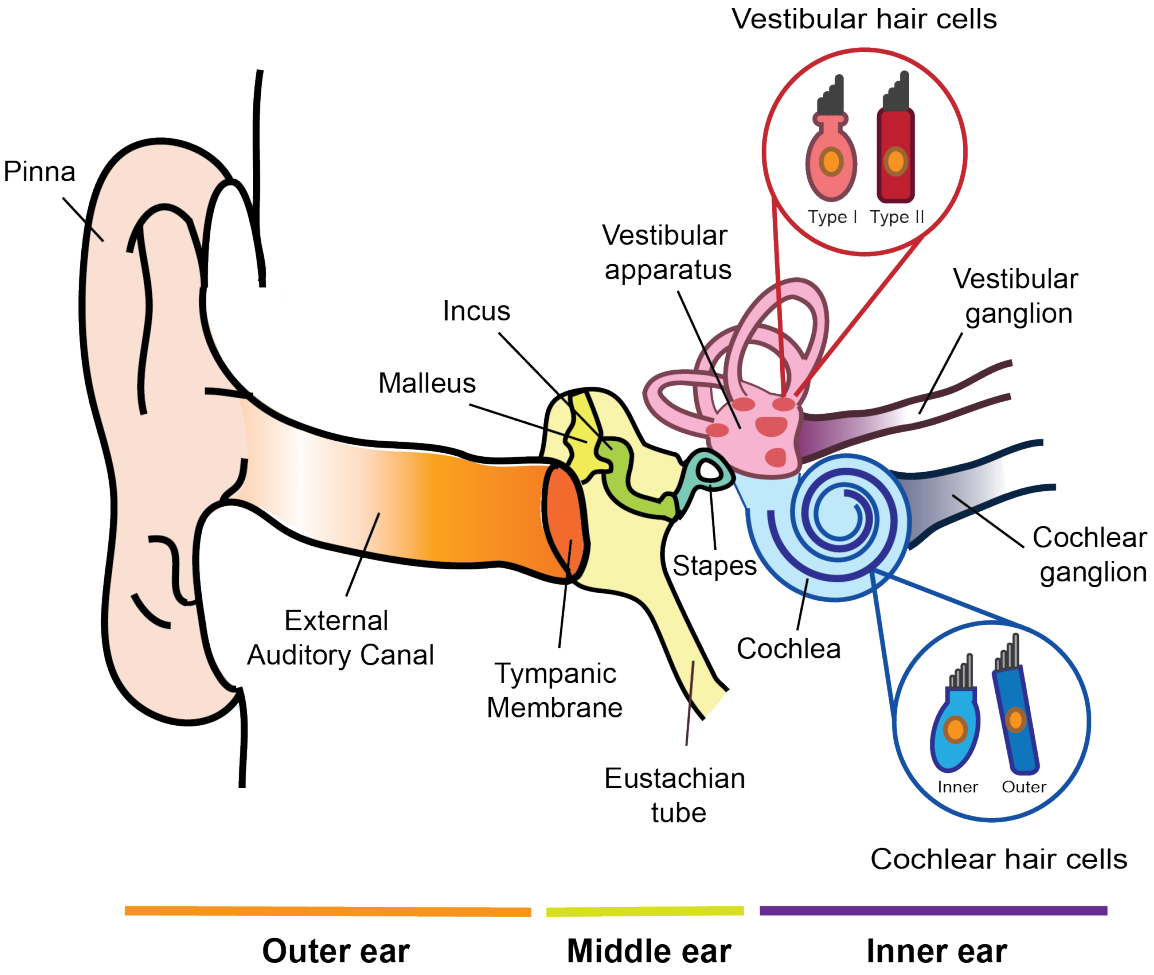

Figure 1: Anatomy of the human ear.

The human ear comprises the outer ear, middle ear, and inner ear. The outer ear and middle ear function primarily in receiving and transmitting vibrations in the air to the inner ear, where mechanical signals are transduced into sensory signals that are relayed to the brain.

The tympanic membrane divides the outer ear and middle ear, and is responsible for conveying sound vibrations to the auditory ossicles of the air-filled middle ear. The middle ear, or tympanic cavity, contains these three auditory ossicles, known as the malleus, incus, and stapes, which serve to convert the mechanical energy of sound vibrations in the air to fluid motion within the inner ear.

The inner ear contains the auditory-sensing cochlea and the gravity-sensing vestibular apparatus, the latter of which comprises the semicircular canals, saccule, and utricle. Both the cochlea and the vestibular organs house sensory epithelia containing mechanosensitive hair cells and non-sensory supporting cell types (for review, see [23]) (Figure 2).

Within the vestibular organs, sensory hair cells are found in patches referred to as maculae in the saccule and utricle, and cristae in the semicircular canals. These sensory hair cells serve as the receptors for balance, detecting angular acceleration (semicircular canals), linear acceleration (saccule), and gravity (utricle). Two types of vestibular hair cells, type I and type II, are found randomly dispersed throughout the maculae and cristae. Type I and type II vestibular hair cells differ with respect to morphology, wherein type I hair cells exhibit an amphora or “vase”-shaped tapered morphology, and type II hair cells exhibit a cylindrical shape [24]. Additionally, type I and type II hair cells also differ with respect to the nature of their synaptic connections; neurons innervating type I hair cells exhibit a cup-like or calyx nerve terminal, while type II hair cells are contacted with a bouton nerve terminal [24, 25] (Figure 2).

The cochlea is a spiral-shaped structure that houses the hair cell-containing Organ of Corti (Figure 2). The Organ of Corti contains two types of hair cells that function in sound transduction and are designated with respect to their relative positions: inner hair cells (IHCs) are found in one continuous row lining the spiral of the Organ of Corti, and outer hair cells (OHCs) are organized in three rows adjacent to the inner hair cells. Morphologically, IHCs exhibit a pear-like shape, whereas OHCs exhibit a longer, “cigar”- like shape [26].

All hair cell types, both vestibular and cochlear, possess epithelial protrusions termed hair bundles that are required for their function. Hair bundles consist of groups of highly organized structures called stereocilia that are found grouped together on the apical surface of the hair cell. The organization of these hair bundles may additionally be used to distinguish between cochlear and vestibular hair cells. Both type I and type II vestibular hair cells contain hair bundles with stereocilia organized from shortest to tallest, with a single motile kinocilium at the highest length of the bundle. Cochlear hair cells lack a kinocilium, and display stereocilia organized in several rows of ascending height.

These hair bundles play an essential role in mechanosensory transduction. In the cochlea, hair cells are affixed to the basilar membrane, with their stereocilia contacting a structure termed the tectorial membrane. Sound waves are transmitted from the auditory ossicles through the round window, and translated into fluid waves within the cochlea. These waves cause flexion of the basilar membrane, which in turn causes the stereocilia attached to the tectorial

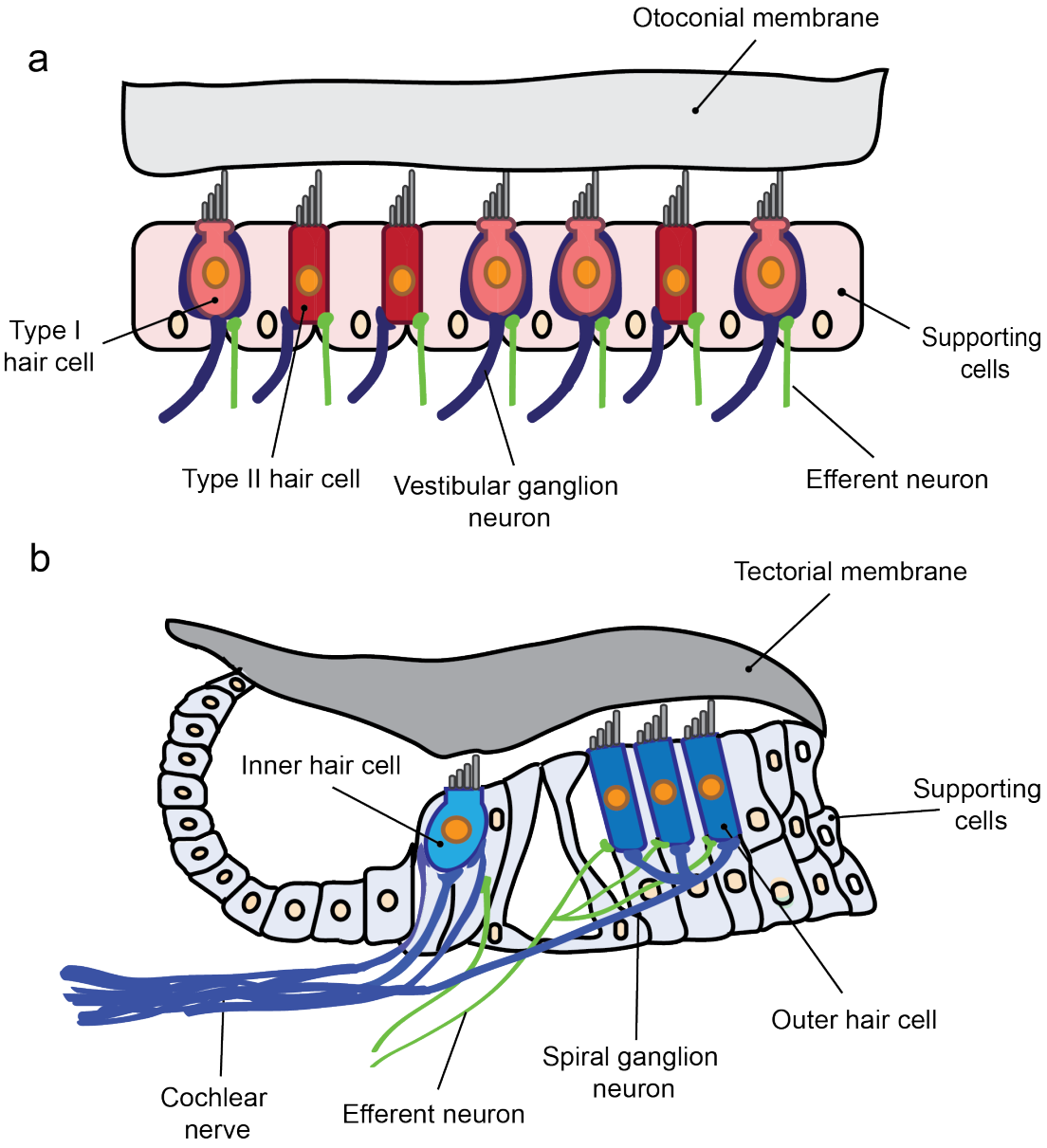

Figure 2: Vestibular and cochlear sensory hair cells and synaptic innervation.

(**a**) Type I and type II hair cells exhibit random organization in the sensory patches of the vestibular organs. Within the saccule and utricle, hair bundles contact an otoconial membrane, which functions in hair cell mechanotransduction. Synaptic innervation to efferent vestibular ganglion neurons may resemble calyx or bouton morphology. (**b**) Within the cochlea, hair cells are organized into one row of inner hair cells flanked by three rows of outer hair cells. Each inner hair cell is contacted by multiple spiral ganglion neurons, whereas one spiral ganglion neuron may synapse on multiple outer hair cells. For (**a**) and (**b**), efferent connections are illustrated in green.

membrane to bend. This movement results in the opening of a gated ion channel within the hair cell, which triggers depolarization and subsequent signal transmission to the cochlear nerve. Within the vestibular organs synaptic transmission occurs in a similar manner, with mechanical movement, i.e. head rotation, leading to deflection of the stereociliary bundles of hair cells. This deflection results in depolarization, and subsequent synaptic transmission to neurons of the vestibular ganglion.

The neural population associated with the sensory hair cells of the cochlea and the vestibular organs differs, with vestibular ganglion neurons (VGNs) synapsing on hair cells in the vestibular apparatus, and spiral ganglion neurons (SGNs) contacting hair cells in the cochlea. Both VGNs and SGNs are bipolar primary afferent neurons, the axons of which make up the VIIIth cranial nerve, also known as the cochleo-vestibular nerve. This nerve is responsible for relaying auditory and balance information to higher centers of the brain. For the process of afferent cochlear transmission, signals are initially relayed from SGNs to secondary sensory neurons in the cochlear nuclei in the brainstem (Figure 3). From the cochlear nuclei, sound information is transmitted through a series of relay centers including the superior olive, the inferior colliculus, and the medial geniculate body, before reaching the auditory cortex.

Inner ear development

The inner ear is an ectodermally-derived structure. During embryonic development, the definitive ectoderm specifies into neural and non-neural

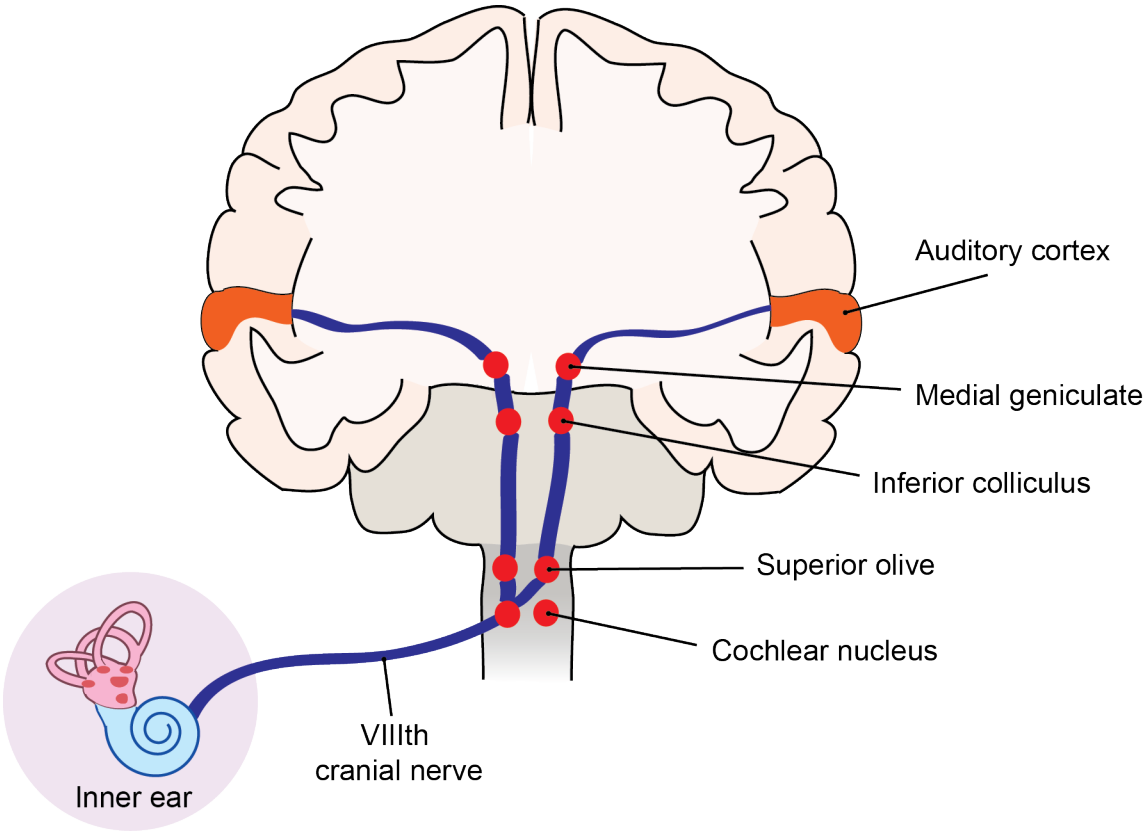

Figure 3: Auditory neural pathway from the inner ear.

Spiral ganglion neurons innervate sensory cells of the cochlea and contribute to the VIIIth cranial nerve, which synapses in the cochlear nucleus. The ascending pathway includes relays in the superior olive, inferior colliculus, and medial geniculate body before reaching the auditory cortex.

ectoderm, the latter of which gives rise to the sensory placodes that serve as the anlage for structures of the cranial sensory ganglia, including the otic, lens, and olfactory placodes (for review, [27]). In humans, the otic placode is characterized as a thickened region of surface ectoderm adjacent to the hindbrain. The otic placode invaginates to form the otic pit, which pinches off to form a structure referred to as the otocyst or otic vesicle. Otic vesicle formation occurs during week 4 of pregnancy in humans [28].

Precise patterning of the otic vesicle is responsible for establishing sensory and non-sensory domains and morphogenesis of the inner ear structures [29-31]. Several key signaling pathways are involved in specification of the dorsal and ventral regions of the otic vesicle, and will be discussed at length further in this introduction. The vestibular apparatus arises from a more dorsal aspect of the otic vesicle, whereas the cochlea first appears as an outgrowth from the ventral aspect of the otic vesicle. Vestibular development precedes cochlear development, with semicircular canal formation and enlargement of the vestibule, which gives rise to the saccule and utricle, beginning at embryonic week 5 [32]. By week 7, formation of the sensory cristae associated with each semicircular canal is evident, coinciding with partitioning of the saccular macula and the utricular macula [32]. Vestibular hair cell development occurs between weeks 8-9, with nascent stereocilia bundles evident at week 8.

Cochlear outgrowth from the ventral otic vesicle is evident at week 5, and continues over the next several weeks, with rotation to form the characteristic 2.5 turns of the cochlea occurring between weeks 8-9. Growth continues until

approximately weeks 18-19, when cochlear size reaches that of the adult form. Cochlear hair cell development occurs two weeks later than vestibular hair cell development, with nascent hair cells first observed during weeks 11-12. IHC development occurs first at week 12, with OHC development following. All three rows of OHCs are evident by week 14.

The cochleovestibular ganglion arises as a population of neural progenitors termed neuroblasts that delaminate from the antero-ventral portion of the otic vesicle. VGNs are first observed in humans at embryonic week 4. Nerve fibers from VGNs begin to extend toward the brain stem at week 5, and enter the putative vestibulum at week 6, with afferent nerve fibers observed contacting vestibular hair cells during weeks 8-9. SGN development succeeds that of VGN development, with the first observations of SGNs during week 8 of embryonic development [33].

Figure 4 illustrates a timeline for key hallmarks of inner ear sensory development, and additionally features specific markers indicative of each of these developmental timepoints (Figure 4).

Modeling inner ear development *in vitro*

Efforts toward modeling inner ear cell types *in* vitro have taken many approaches, among them guided differentiation strategies to induce sensory cell types by recapitulating the hallmarks of inner ear development. PSCs serve as the foundation for these efforts, due to their capacity to differentiate into specialized cell types. Our established inner ear differentiation protocol

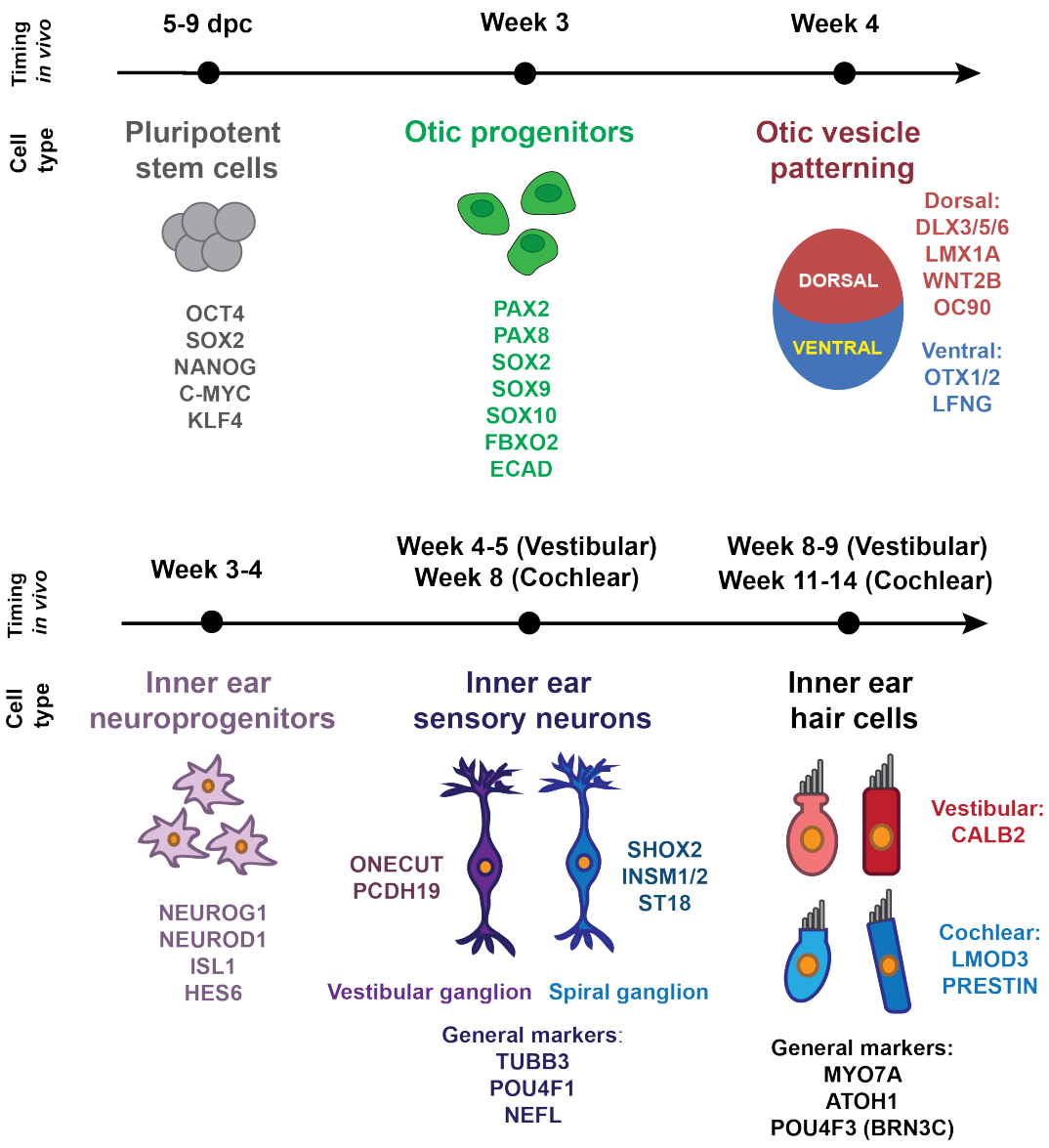

Figure 4: Timeline and key markers of otic cell type induction.

Developmental timeline for inner ear development, including specific markers expressed for each timepoint/cell type. dpc = days post conception.

recapitulates inner ear development through the aggregation of PSCs and introduction of signaling cues necessary to induce an inner ear hair cell-specific developmental program. Prior to a review of the previous efforts to generate inner ear cell types *in vitro*, I will detail the protocol our lab has employed toward this effort, beginning with an exploration of stem cells as a model system.

Pluripotent stem cells

Stem cells are defined by the properties of 1) infinite self-renewal, meaning the ability to divide and proliferate long-term, and 2) pluripotency, meaning the capacity to differentiate into specialized cell types from all three germ layers of the body (mesoderm, endoderm, and ectoderm). There are two types of PSCs: embryonic stem cells (ESCs) and induced pluripotent stem cells (iPSCs).

ESCs are derived from the inner cell mass of the blastocyst of the pre-implantation embryo. A battery of transcription factors, including OCT4, SOX2, and NANOG, function in maintaining pluripotency of these cells [34, 35]. iPSCs are terminally differentiated somatic cells that have been re-programmed to a pluripotent state through the introduction of specific transcription factors. In a landmark series of papers by Takahashi and Yamanaka, mouse and human adult fibroblasts were re-programmed to a pluripotent state by the introduction of OCT4 and SOX2, along with pluripotency markers C-MYC and KLF4, via retroviral vectors [36, 37]. The resulting iPSCs resembled ESCs with respect to

morphology, proliferative capacity, and transcriptional profile, and furthermore were capable of differentiating into cell types of the three germ layers [36].

Pluripotency may be characterized by either a naive or primed state. Naive state stem cells are equivalent to cells of the inner cell mass that exhibit stable pluripotency and express so-called pluripotency markers. Primed state stem cells are equivalent to cells of the epiblast that are capable of self-renewal and differentiation, but are considered to be more readily “primed” to differentiate than naïve state stem cells. Human ESCs are considered to exhibit a primed state, akin to mouse epiblast stem cells, rather than a naïve state [38, 39]. Accordingly, culture of inner ear organoids from human ESCs requires modification from our laboratory’s original published mouse inner ear organoid protocol [20], potentially due to these differences in initial “ground state” of the stem cells.

Differentiation of human 3D inner ear organoids

The generation of human 3D inner ear organoids begins with the aggregation of human PSCs. For the purposes of this study, the term “aggregate” will be used to describe a single 3D mass of aggregated cells, whereas the term inner ear “organoid” will refer to the vesicle-like structures within the aggregates in which otic tissue arises. One aggregate may give rise to multiple inner ear organoids.

Floating stem cell culture techniques were pioneered by Sasai and colleagues in a series of landmark papers published in the mid-to-late 2000s [21,

40, 41]. Watanabe et al first demonstrated the aggregation of mouse ESCs for the differentiation of telencephalic progenitors in a process termed serum-free culture of embryoid-like bodies (SFEB) [40]. Under the original SFEB protocol, spontaneous aggregation of mouse ESCs into embryoid bodies occurred following 1-2 days in suspension or “floating” culture. After eight days in floating culture, embryoid bodies were then plated in Petri dishes for two days of adherent culture, and induction of telencephalic progenitor cell types was observed. This process was later adapted for use with human PSCs, where the noted addition of Rho-associated kinase (ROCK) inhibitor Y-27632 promoted survival and aggregation of human PSCs [41].

Eiraku et al optimized the SFEB protocol by introducing the concept of aggregating mouse ESCs in low-adhesion U-bottom 96-well plates [21]. The low-adhesion properties combined with the U-shaped format of the wells prevented cells from adhering to the culture dish, thereby encouraging aggregation. This modification to the SFEB format allowed for the formation of embryoid bodies in a matter of hours, as compared to days in the Watanabe et al protocols [21]. The modified protocol also served to increase the efficiency of differentiation, as evidence by an increased number of cells expressing telencephalic progenitor markers as compared to the previous SFEB study [40]; furthermore, self-organization and a more complex degree of differentiation were observed. The optimized method, termed SFEBq for the “quick” aggregation step, would serve as the foundation for many organoid studies in years to come, including the inner ear organoid protocol pioneered by our laboratory [20].

For the generation of inner ear organoids from human PSCs, cells are initially aggregated in V-bottom plates, a modification to the SFEBq method [21] that was found to promote aggregate formation using human WA25 ESCs [19]. Following two days of culture in the V-bottom format, aggregates are transferred to U-bottom plates in chemically defined medium (CDM) containing extracellular matrix compound Matrigel to promote epithelialization and TGF-β inhibitor in order to induce formation of non-neural ectoderm. Subsequent treatments with small molecules for activation of Fibroblast Growth Factor (FGF) signaling and inhibition of Bone Morphogenic Protein (BMP) signaling are applied on culture day 4 in order to specify pre-placodal ectoderm, and WNT pathway agonist is applied on culture day 8 to help promote induction of the otic placode. Additional treatment with WNT agonist at culture day 11 promotes otic vesicle induction [19]. Following transfer to a long-term culture format on day 18, no additional treatments are applied, and induction of sensory and supporting cell populations occurs in a self-directed manner. Hair cells are typically observed between day 40 to day 60 of culture, typified by expression of hair cell markers MYO7A, ATOH1, and POU4F3 [19].

It is important to note that characterization of the derived hair cells arising in this system has corresponded with properties of vestibular type I and type II hair cells [19]. Hair cells arising in mouse inner ear organoids exhibit expression of vestibular marker Calbindin-2 (Calb2), and extensive electrophysiological analysis has revealed derived mouse hair cells appear to be comparable to hair cells of the post-natal mouse utricle [22]. Additionally, derived stereocilia bundles

exhibit a vestibular morphology, and observed synaptic connections appear to mirror the calyx or bouton-like synapse observed at nerve terminals of vestibular type I and type II hair cells. In the derived hair cells of human inner ear organoids, expression of CALB2 has also been observed, along with hair bundle morphology similar to that of vestibular hair bundles, with a single acetylated-alpha-Tubulin (TUBA4A) positive kinocilium observed with among apical protrusions co-expressing stereocilia markers F-ACTIN and ESPIN. Clusters of hair cells are observed in human inner ear organoids, reminiscent of the randomized organization of hair cells observed in the maculae and cristae of vestibular organs. Functional analysis has additionally indicated that derived hair cells exhibited a similar electrophysiological profile to mouse and human vestibular organs [19].

Previous in vitro studies for the differentiation of inner ear cell types

Previous otic differentiation studies have investigated both direct conversion and guided differentiation approaches to inducing inner ear sensory hair cells from PSCs. Direct conversion involves the overexpression of cell type-specific transcription factors that target cell identity toward a particular lineage [42]. A study by Costa and colleagues explored the combined expression of hair cell transcription factors Gfi1, Pou4f3, and Atoh1 to induce hair cell differentiation in mouse ESCs [43]. Induced hair cells expressed hair cell-specific markers and morphology, including the development of hair bundle-like protrusions. However, the protrusions displayed heterogeneous morphology and

poor organization, indicating incomplete maturation. Notably, the converted cell population lacked corresponding induction of a supporting cell population, which may be necessary for establishing an environment for proper hair cell induction. One advantage to our guided differentiation approach is that a progenitor population is not bypassed as in direct conversion, meaning multipotent progenitor cells capable of giving rise to both supporting cells and sensory cell types are achieved in culture. Accordingly, we have confirmed the appearance of a supporting cell population arising in our inner ear organoid model [19, 20].

An early guided differentiation study by Li and colleagues demonstrated induction of an otic progenitor-like cell population from mouse ESCs using an embryoid body culture technique and timed treatment with epidermal growth factor (EGF), insulin-like growth factor 1 (IGF-1), and FGF to induce a cell population expressing early otic progenitor markers [44]. Further culture induced expression of hair cell markers Myo7a, Atoh1 and Brn3c in a small percentage of the derived cell population. Oshima et al employed this stepwise guidance protocol using mouse ESCs and iPSCs to induce an otic progenitor population, and found that co-culture of these cells on mitotically inactivated chicken utricle stromal cells was necessary to promote hair cell marker expression and acquisition of hair bundle-like protrusions expressing bundle-specific marker Espin [45]. As co-culture with stromal cells was shown to be necessary for hair cell-like induction in this culture model, this further indicates the potential role of a supporting cell population in contributing to hair cell identity.

Ouji et al employed a method for the generation of otic-like cells wherein mouse PSCs were first aggregated into embryoid bodies using a hanging drop method [46] and then cultured in conditioned medium from bone marrow-derived ST2 stromal cells for a subsequent 14 days [47]. The embryoid bodies produced cells expressing hair cell markers Atoh1, Myo7a, and Brn3c. A hair cell-like morphology was not observed, although this culture method did produce rudimentary hair bundle-like protrusions from the surface of hair cell marker-expressing cells.

It is important to note that all of the previously mentioned studies employed mouse PSCs. There are fundamental differences between mouse and human development [48, 49], and this is apparent in the inner ear. The mouse cochlea is not yet mature at birth, whereas the human cochlea is functional by embryonic week 20 [50]. These differences may need to be taken into account in establishing methods for the generation of inner ear sensory cells. While mouse stem cells may be easier to acquire, the generation of inner ear cell types from human tissue presents a clearer avenue toward clinical translation, and more potent relevance toward human health.

Chen et al first developed a guided differentiation model for otic differentiation using human ESCs [51]. This protocol employed timed treatments of FGF-3 and FGF-10 in early stage culture to produce an otic progenitor population capable of giving rise to sensory hair cell-like cells and neurons. The derived sensory cells were found to express hair cell markers MYO7A and ATOH1, and additionally bore morphological protrusions reminiscent of hair

bundles. However, similar to the Costa et al direct conversion study, the protrusions did not display morphology consistent with native hair cells [43, 51].

Ding and colleagues also developed a protocol for the differentiation of otic progenitors from human ESCs employing FGF-3 and FGF-10 pathway activation [52]. This study made use of co-culture with mitotically inactivated chicken utricle stromal cells to further promote otic induction. The resulting otic epithelial progenitors gave rise to hair cell-like cells bearing stereocilia-like bundles that exhibited functional capability. However, this group found that co-culture was indispensable for induction of hair cell-like cells; cells cultured on laminin alone and subjected to the same protocol did not yield derived hair cells with proper hair cell morphology. Furthermore, derived cells exhibited short apical protrusions lacking bundle morphology and organization, and experienced a loss of functional capability as well. Chicken utricle stromal cell conditioned media supplemented with EGF and retinoic acid was able to rescue some of the effects observed in the laminin-cultured cells; however, efficiency of the generation of ESPIN-positive cells was low.

Unlike these studies, our laboratory's model represents a "developmentally faithful approach" [19], meaning the progression through the hallmarks involved in inner ear development occurs, as opposed to forced otic progenitor induction occurring without first "passing through" the necessary developmental steps. Ohnishi and colleagues employed a stepwise method for the induction of inner hair cell-like cells from human iPSCs that similarly emphasized induction of non-neural ectoderm, the preplacodal region, and otic

placode prior to otic progenitor induction [53]. However, the protocol was lengthy, lasting over 70 days, and induction of otic placode cells, defined by expression of early otic progenitor marker PAX2, was extremely limited. This translated into low sensory cell induction during later stage culture, and only MYO7A was evaluated as a hair cell marker. Additionally, stereocilia-like protrusions were not observed in all experiments.

Ronaghi et al also pursued a guided differentiation model of human ESC differentiation, treating with WNT inhibitor and TGF-β antagonist along with IGF-1 to promote ectodermal induction during the first fifteen days of culture, and a combination of sustained FGF activation along with short periods of WNT activation and BMP inhibition and subsequent activation during days 15-21 to guide induction of otic progenitor markers. Maintenance in decreasing concentrations of knockout serum replacement (KSR) over the subsequent twenty days in culture led to the induction of cells expressing hair cell markers ATOH1 and MYO7A. This protocol did not require co-culture with embryonic chicken utricle cells; the authors purported the KSR treatment successfully substituted this, and that withdrawing KSR over time led to upregulation of hair cell markers. However, the hair cell marker expression was relatively low, implying low efficiency of hair cell induction despite a somewhat robust otic progenitor population initially observed.

Recently, Lahlou et al investigated the effects of Notch pathway modulation in monolayer otic differentiation from human iPSCs, finding that application of a Notch inhibitor enhanced expression of otic progenitor markers

and led to an increase in expression of hair cell markers MYO7A, ATOH1, and POU4F3 [54]. This culture system was adapted from the protocol described in Chen et al [51], and did not require co-culture or culture in conditioned medium. Similar to Ronaghi et al, induction of non-neural ectoderm and pre-placodal ectoderm was observed prior to otic induction [55]. The same group subsequently published a study describing a monolayer otic differentiation culture from human PSCs that boasted an enriched otic sensory progenitor population, through the early dual application TGF-β inhibitor and Wnt inhibitor and subsequent addition of Wnt agonist [56]. This protocol yielded an increase in the PAX2+ cell population compared to previously published methods [51, 56] and led to the induction of MYO7A+/POU4F3+ hair cell-like cells.

While these studies elucidated strategies for the induction of cells expressing generic hair cell markers such as MYO7A and ATOH1, which are expressed in both cochlear and vestibular hair cells, it is important to note that specific hair cell identity (cochlear vs. vestibular) was not defined. Additionally, although several studies employed 3D culture to the extent of embryoid body formation [44, 45], none of these studies exhibited the degree of organization observed in our 3D inner ear organoid cultures, which yield sensory-cells and supporting cells arising concurrently in a self-organized manner. This complexity is lacking in the derived cell populations from previously described studies.

Recently, Jeong et al published a study proposing a mechanism for the generation of inner ear organoids containing cochlear hair cell-like cells from human ESCs and iPSCs [57]. This study employed a 3D culture method in which

human ESCs or iPSCs are co-cultured on mitotically inactivated mouse embryonic fibroblasts prior to the formation of aggregates. Aggregate generation occurred in 96-well low adhesion plates, and a series of small molecule treatments, including dual BMP/SB and LDN/FGF treatment as outlined in the Koehler et al mouse ESC organoid study [48], were performed. Jeong and colleagues highlighted the additional inclusion of Rho-kinase inhibitor Y-27632 and 2-mercaptoethanol until culture day 8 [57]. Aggregates were cultured for up to 90 days, with derived otic vesicles observed by culture day 20, comprised of cells expressing otic progenitor markers PAX2, SOX2, and SOX9. By day 36, expression of F-ACTIN and stereocilia marker ESPIN were observed, and TEM revealed kinocilia and microvilli-like protrusions on cells within the derived otic vesicles. qPCR analysis confirmed expression of hair cell markers ATOH1 and MYO7A at this time point.

Derivation of cochlear-specific cell types was reportedly indicated by expression of outer hair cell markers PRESTIN and Oncomodulin (OCM), and a lack of expression of type II vestibular hair cell marker CALB2 [57]. However, OCM is also present in mouse vestibular hair cells [58], and its presence in human hair cells—either cochlear or vestibular—has not been documented. Curiously, some derived MYO7A+ cells also expressed vestibular supporting cell marker Otopetrin-1 (OTOP1). Morphological phenotypes were unclear, with observations of a cylindrical cell morphology potentially indicative of type II vestibular hair cells or cochlear outer hair cells, and a bulbous cell morphology, which may indicate either type I vestibular hair cells or cochlear inner hair cells.

Hair bundles with stereocilia were observed in some organoids, some of which included a kinocilia, indicative of vestibular hair cell types, and some of which were arranged in a step-wise fashion, indicative of a cochlear hair cell phenotype [57]. Additionally, nerve endings were observed, that appeared with either “button-like” or calyx terminals, which may indicate type I hair cells (vestibular) or cochlear cell types. Further functional characterization revealed that uptake of FM1-43FX dye, a styryl pyridinium dye that is often used to assess the presence of hair cell mechanotransduction channels [59], occurred in the derived cells. However, the functional analysis in this study did not give information with respect to the electrophysiological phenotype of the derived hair cells. Previous studies performed on mouse and human inner ear organoids generated from our group confirmed an electrophysiological phenotype similar to that observed in the native mouse utricle [19, 20, 22].

Overall, this study is the first in the previously discussed literature to assert derivation of cochlear cell types specifically, as opposed to cells co-expressing generic hair cell markers such as MYO7A and ATOH1. However, although expression of OHC-specific marker PRESTIN was observed, the analysis and interpretation of additional phenotypic hallmarks were less clear.

Single-cell RNA-sequencing analysis of the inner ear

RNA sequencing (RNA-seq) is a powerful tool to evaluate total gene expression within a population of cells. The recent advent of single-cell RNA-sequencing (scRNA-seq) has allowed for the evaluation of the distribution of

gene expression across a population of individually assessed cells. This technique may serve to inform reprogramming or guided differentiation studies by identifying novel markers within a culture system at key time points during development that have not previously been interrogated. Before discussing several landmark scRNA-seq studies of the inner ear, I will first detail the technology.

In scRNA-seq, transcriptomes of thousands of individual cells are generated simultaneously with the ability to trace gene expression data back to each individual cell. This technique differs from bulk RNA-seq, wherein the average gene expression patterns of a pooled cell population are assessed. Bulk RNA-seq is considered suitable for the assessment of a relatively homogenous cell population, whereas scRNA-seq serves as a powerful tool to assess transcriptional differences among a heterogeneous cell population, allowing for the potential to uncover cell-type specific markers within a specific tissue type or cell population.

The earliest scRNA-seq study was published by Tang and colleagues [60], detailing the sequencing of a single mouse blastomere. Technological advances soon allowed for more efficient single-cell analyses within the next several years, with the development of microfluidic, droplet-based platforms allowing for the sequencing of thousands of cells from a single sample [61]. There are several commercially available droplet-based scRNA-seq platforms, including the Fluidigm C1 system and 10X Genomics Chromium system. Both of these

platforms follow a similar method for generation of single-cell transcriptomes, described as follows (for reviews, see [61, 62]).

First, the desired cell population is isolated from a target tissue. Cells may be subjected to fluorescence activated cell sorting (FACS) in order to isolate a desired population by use of antibody staining or a fluorescent reporter. The single-cell solution is then loaded into a microfluidics chamber, where cells are individually combined into an oil-based droplet containing a barcoded bead (Figure 5a). The bead is coated in primers that bind to the poly[A] tails of mRNA, and contain molecular barcodes unique to each individual bead, as well as unique molecular identifiers (UMIs) that are specific to each primer (Figure 5b). The barcode allows for tracing of all the mRNAs back to an individual cell, whereas the UMIs allow for identification and quantification of each individual mRNA molecule [63]. Cells are lysed in order to capture RNA, and cDNA is generated from the mRNA via reverse transcriptase. cDNA is then amplified by PCR. The cDNA from each individual cell may then be pooled for subsequent sequencing.

scRNA-seq has been employed in analysis of the inner ear. A landmark paper from Burns and colleagues used scRNA-seq analysis in order to assess cells of the inner ear sensory organs from the neonatal mouse inner ear [64]. This study employed FACS to isolate sensory and non-sensory cell types from the cochlea and vestibular organs and assessed their transcriptomes. This analysis revealed candidate markers specific to sensory populations of the cochlea and vestibulum, as well as supporting cell types from both areas.

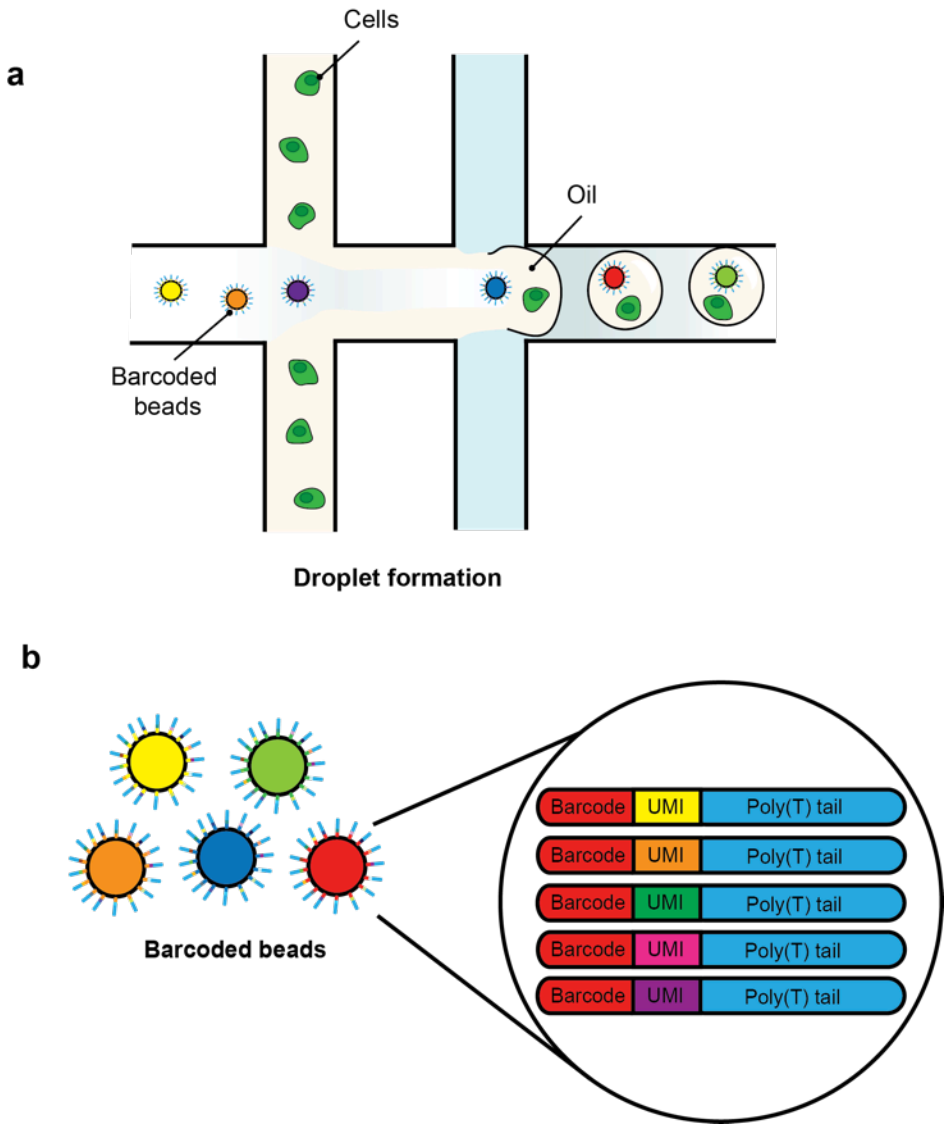

Figure 5: Droplet-based single-cell RNA-sequencing.

(**a**) In a microfluidics chamber, single cells are combined with individual barcoded beads within oil droplets. (**b**) Each bead contains barcoded primers unique to that individual bead, along with unique molecular identifiers (UMIs) to trace individual transcripts. A poly(T) tail allows for binding to the poly(A) tails of mRNA.

The study described in this dissertation employs scRNA-seq to assess transcriptional profiles of inner ear organoids cultured according to our previously published otic differentiation protocol [19], and those additionally exposed to SHH pathway modulation during otic vesicle maturation. This novel work thus far represents the earliest use of scRNA-seq analysis in human inner ear organoids.

The role of Sonic hedgehog signaling in inner ear development

The otic induction studies described previously explored modulation of key signaling pathways found to be involved in induction of otic cell types, including FGF and Notch signaling. However to date, SHH signaling pathway modulation has not been explored as a potential inducer of cochlear cell types in a PSC model of inner ear development, despite the key role of SHH in development of the cochlea. The following section will detail the SHH pathway, and its role in dorso-ventral patterning of the otic vesicle and subsequent cochlear development.

Sonic hedgehog signaling pathway

The Hedgehog (HH) family of secreted proteins function diversely, with roles in patterning and cell fate specification during development, and maintenance and proliferation of cell populations during adulthood (for review, see [65]. HH was first identified as a result of genetic screens in *Drosophila melanogaster* [66]. Three mammalian homologues were later identified: SHH, Indian hedgehog (IHH), and desert hedgehog (DHH). Of these homologues, SHH

is the most widely expressed, and has been implicated in patterning of the early neural tube, limb development, and in development of the inner ear [65]. IHH, which has partial redundancy with SHH, has been shown to regulate bone and cartilage development [67], while DHH functions in germ cell development in the testis [68] and peripheral nerve sheath formation [69, 70].

HH proteins undergo several processing events prior to secretion in the cell, including an autoproteolytic cleavage to form an N-terminal signaling peptide and a C-terminal fragment with no known signaling activity [71]. The N-terminal signaling peptide is modified further by the addition of a cholesterol molecule and palmitoyl moiety. In vertebrates, the HH signaling pathway is associated with the primary cilium, a microtubule-based protrusion found on the cell surface [72]. The HH receptor is a transmembrane protein called Patched-1 (PTCH1). PTCH1 inhibits another transmembrane protein, Smoothened (SMO), in the absence of HH binding, and prevents SMO from entering the primary cilium. When HH ligand binds PTCH1, SMO is able to move into the primary cilium and interact with the glioma-associated oncogene (GLI) family of transcription factors, comprising GLI1, GLI2, and GLI3, which serve as transcriptional mediators of SHH signaling (Figure 6).

GLI2 and GLI3 play dual roles in activation and repression of target genes (for review, see [73]). Bi-functional transcriptional activity is attributed to a C-terminal activation domain and N-terminal repressor domain. GLI1, which contains only a C-terminal activation domain, functions solely in transcriptional activation. Preferential cleavage of GLI2 and GLI3 leads to translocation of either

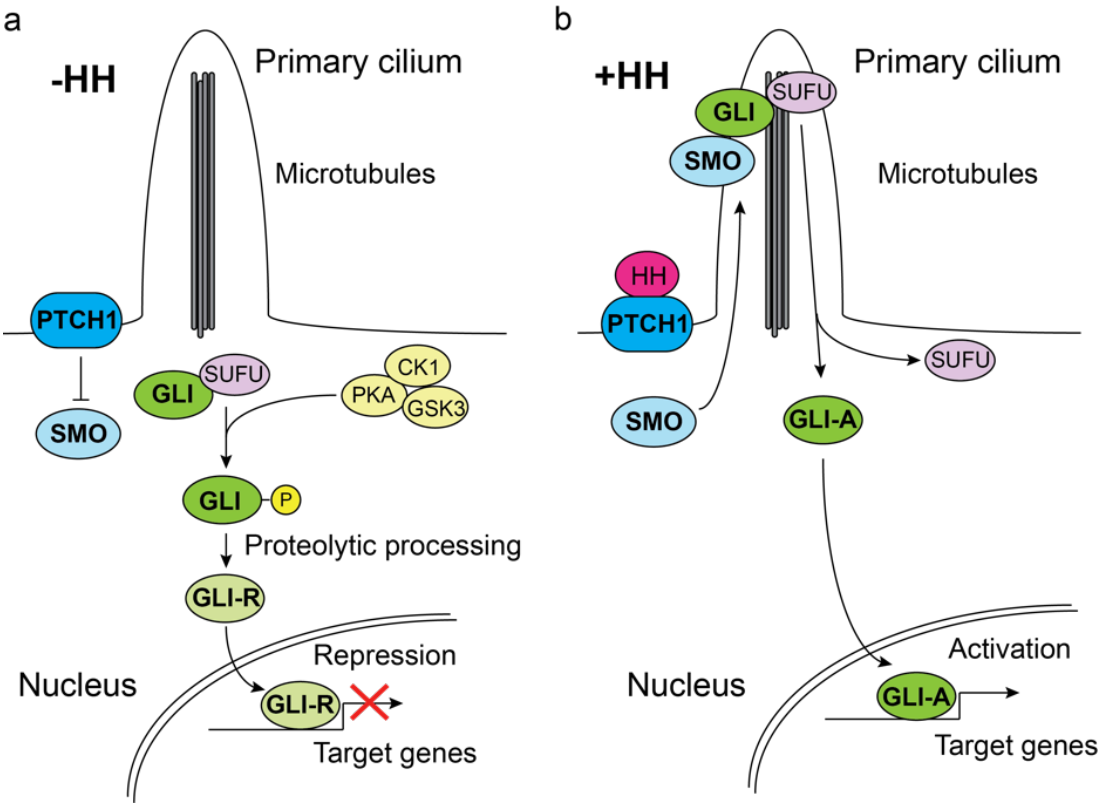

Figure 6: Hedgehog signaling pathway.

(**a**) In the absence of Hedgehog (HH), PTCH1 inhibits SMO. GLI transcription factors are bound to Suppressor of Fused (SUFU) and are susceptible to phosphorylation by PKA, CKI, and GSK3 kinases. Phosphorylated GLI undergoes proteolytic processing to its repressor form (GLI-R) which translocates into the nucleus and inhibits transcription of SHH target genes. (**b**) In the presence of HH, active SMO moves into the primary cilium and interacts with the GLI-SUFU complex. GLI, maintained in its full-length, activator form (GLI-A), dissociates from SUFU and enters the nucleus to activate transcription of HH target genes.

full-length (activator) or truncated (repressor) forms into the nucleus to bind GLI responsive genes and either initiate or suppress transcription [73].

Dorso-ventral patterning of the otic vesicle

SHH signaling has been shown to play an essential role in patterning of the otic vesicle and subsequent cochlear development [29, 31, 74]. During development, SHH emanating from the floor plate and notochord functions in establishing the dorsal-ventral (DV) axis of the otic vesicle [29, 31] (Figure 7a). As stated previously, the vestibular organs arise from the more dorsal portion of the otic vesicle, whereas the cochlea emerges as an outcropping of the ventral-most region of otic vesicle (Figure 7b). Additionally, neurogenic cell types derive from the antero-ventral region of the otocyst [29]. Precise gene expression patterning of these domains is necessary for proper development of the inner ear structures.

A study investigating the role of SHH in otic specification in found that otic vesicle induction occurred in SHH knockout mouse embryos, but subsequent morphogenesis of inner ear structures was significantly disrupted [29]. Otic vesicle induction typically occurs by E9.5 in mice, with formation of inner ear structures completed by E15.5. Paint-fill analysis of inner ear structures at E15.5 revealed aberrant morphology in SHH null mutants, with only partially formed posterior and anterior semicircular canals and a loss of lateral canal formation. A corresponding loss of sensory cell formation was observed in the vestibular

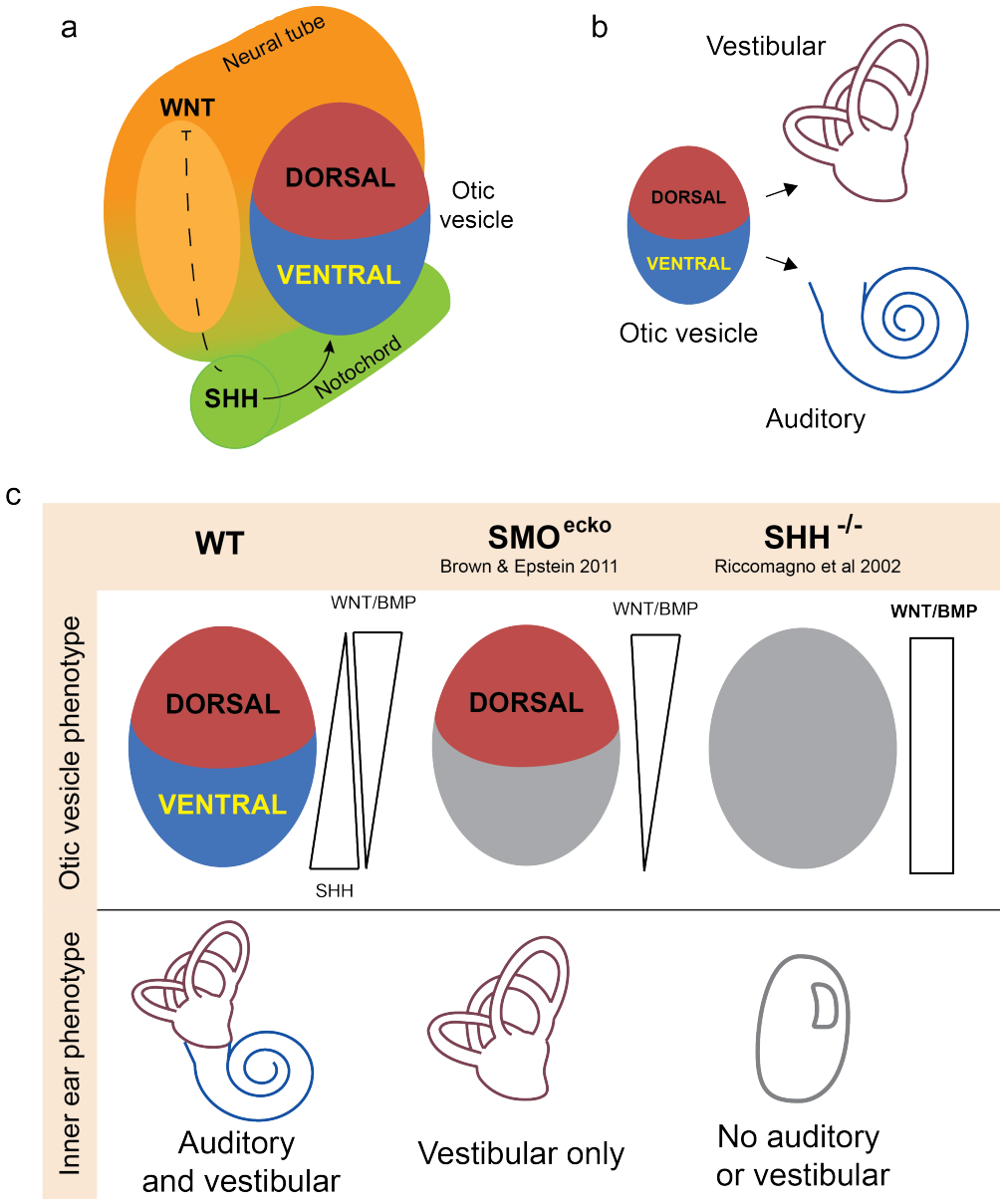

Figure 7: SHH signaling in inner ear development.

(**a**) SHH in the developing otic vesicle. SHH plays a direct role in ventral gene expression, and an indirect role in dorsal gene expression through modulation of WNT and BMP signaling from surrounding tissues. (**b**) The dorsal otic vesicle gives rise to the vestibular system, whereas the ventral-most region of the otic vesicle gives rise to the auditory organ, the cochlea.(**c**) Summary of Brown & Epstein (2011) and Riccomagno et al (2002) in which conditional inactivation of SMO in the inner ear leads to vestibular morphogenesis only with a lack of cochlear formation, whereas SHH deletion disrupts inner ear morphogenesis.

organs, with disrupted formation of the semicircular canals, as well as the utricular and saccular maculae. Additionally, the cochlear duct and endolymphatic ducts failed to form in these embryos, with maintenance of an otic vesicle-like morphology observed at the ventral-most region at E15.5, indicative of a potential halt in developmental progression at the otic vesicle stage.

This lack of cochlear formation following loss of SHH signaling led the investigators to evaluate the expression of markers of the ventral otic vesicle that precede cochlear development. Expression of homeobox transcription factors Otx1 and Otx2 was disrupted, with severely reduced Otx1 expression observed along with a lack of Otx2 expression. Additionally, transcription factor Pax2, which is expressed initially in the otic placode and then temporally restricted to ventromedial otic vesicle, was observed at E8.5, but expression was absent in the otic vesicles of E9.5 SHH knockout embryos. Further evaluation revealed ventral expansion of dorsal marker Dlx5 [29].

Interestingly, the cochleovestibular ganglion failed to form in SHH knockout embryos [29]. A neuroprogenitor population expressing inner ear neural marker Neurod1 was observed in the ventral otic vesicle, but minimal delamination of these neural precursors was observed, and the cochleovestibular ganglion was absent in E14.5 embryos.

This study indicated a potential role for SHH in ventral patterning of the otic vesicle. However, the complete loss of SHH during embryonic development obscured whether the observed inner ear phenotype in these embryos was due to a loss of direct action of SHH signaling on the inner ear, or as an indirect effect

of the loss of SHH acting to regulate signaling pathways from surrounding tissues. A subsequent study from the same group sought to answer this question by generating a mutant mouse in which SHH pathway effector SMO is conditionally inactivated in the developing otic epithelium. In this way, SHH signaling is still present and acting on the surrounding tissues, but is unable to act directly on the inner ear. In these SMO otic epithelium conditional knockout (SMO^{ecko}) mice, vestibular structures appeared to form in a wild-type manner, while cochlear morphogenesis did not occur [31] (Figure 7c). Examination of dorsal and ventral patterns of gene expression in the otic vesicles of these embryos showed that dorsal gene expression was maintained in the absence of SHH signaling, whereas ventral gene expression was disrupted [31].

Within our inner ear organoid model, small molecule treatments recapitulate early stage signaling cues involved in the specification of otic tissues. However, otic vesicle stage induction has not been closely analyzed, nor has the patterning phenotype at this *in vitro* developmental time point been assessed. The studies by Riccomagno and colleagues [29] and Brown & Epstein [31] have defined a role for SHH signaling in ventral specification of the otic vesicle, and additionally highlighted transcriptional profiles of the dorsal and ventral domains established in the developing otic vesicle. A study from Durruthy-Durruthy and colleagues detailed scRNA-seq analysis of cells from the mouse otocyst and early neural lineage, identifying a discrete cluster expressing ventral markers Lfng and Pax2, and another expressing dorsal markers Dlx5 and Oc90 [75]. A recent study by Roccio et al has additionally corroborated dorsal

and ventral marker expression in humans by performing gene expression analysis on human fetal inner ear tissue [76]. Expression of key dorsal and ventral markers has not been evaluated within our model, and therefore, it was unknown whether this dorso-ventral polarity is established within our model. The subsequent study seeks to address this knowledge gap.

Research aims

The primary goals of this project are to evaluate the gene expression phenotype of otic vesicle stage human stem cell-derived inner ear organoids and to investigate SHH signaling as a potential means to specify ventral otic derivatives within this *in vitro* model. The subsequent research sought to answer two key questions about inner ear organoid development:

1) What underlies the apparent commitment to a vestibular sensory fate within this model?

2) What factors may be applied in order to bias differentiation of otic progenitors toward a cochlear fate?

Derived sensory hair cells within our model exhibit a vestibular phenotype only, thereby representing only one aspect of the inner ear sensory system. The differentiation of cochlear cell types *in vitro* remains a goal in order to enhance the utility of this model as a platform for drug design, toxicity studies, and modeling of disorders related to hearing. To date, dorsal and ventral identity has not been characterized in human stem cell-derived otic vesicles. I hypothesize that bias toward a vestibular fate in derived sensory hair cells may be due to a

dorsal gene expression phenotype of the early derived otic vesicle (Figure 8). The prolonged application of WNT agonist CHIR99021 in our differentiation protocol may underlie this, given the role of WNT signaling in dorsal patterning of the otic vesicle [30]. Furthermore, I hypothesize that precise activation of SHH signaling, known to play a role in ventralization of the otic vesicle, may promote induction of ventral gene expression in the derived otic vesicles, which may bias differentiation toward ventral otic derivatives, particularly cochlear cell types, within the human inner ear organoid model.

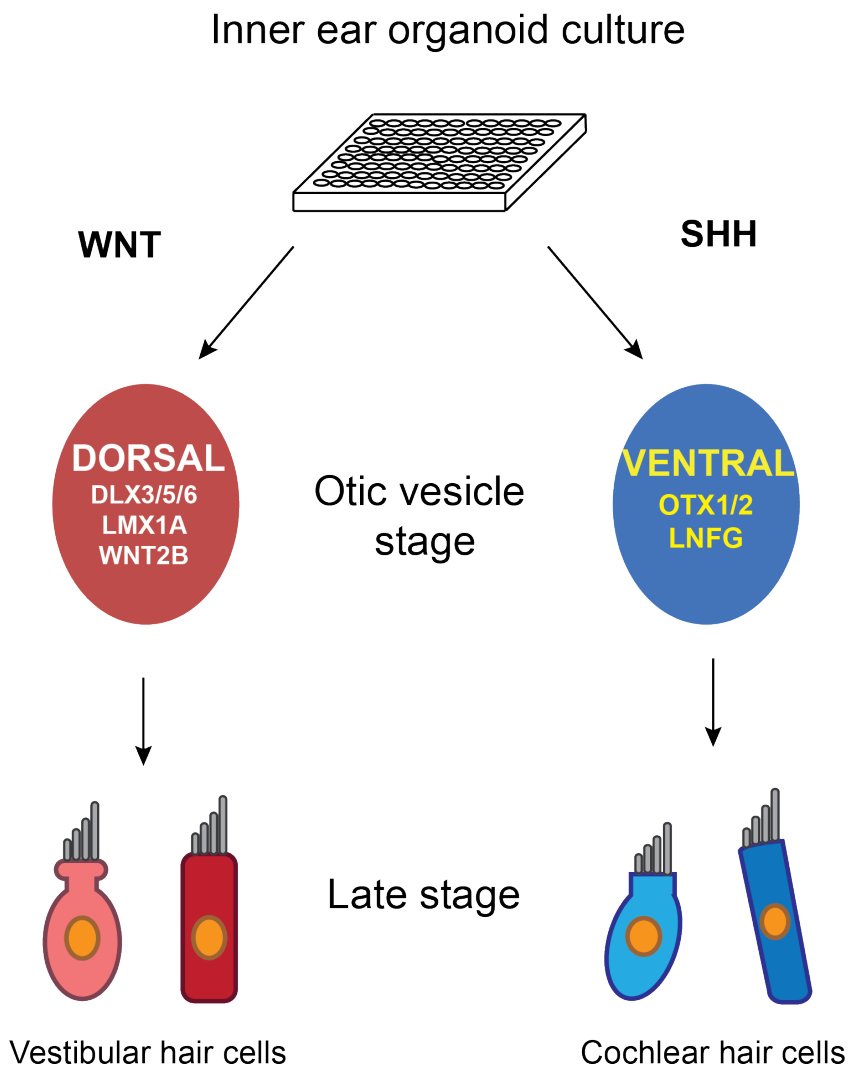

Figure 8: Hypothesis.

This study investigates the hypothesis that vestibular bias in the inner ear organoid culture model is due to a dorsalized phenotype of the early derived otic vesicle, typified by expression of dorsal genes (several candidate markers listed here). Furthermore, modulation of SHH signaling in early stage culture may promote expression of ventral markers, subsequently biasing differentiation toward a cochlear fate.

CHAPTER TWO: MATERIALS AND METHODS

Embryonic stem cell culture

WA25 human ESCs were obtained from WiCell. This feeder-free cell line does not require a mouse embryonic fibroblast feeder layer to maintain pluripotency. ESCs were maintained as described [19]. Prior to passaging, 1 mL Dulbecco's phosphate buffered saline (DPBS) without Calcium and Magnesium (Thermo Fisher Scientific, cat. no. 14-190-250) containing 1% recombinant human vitronectin (Thermo Fisher Scientific, cat. no. A14700) was added to the desired number of wells of a 6-well multi-dish (Thermo Fisher Scientific, cat. no. 14-832-11) and left at room temperature for one hour under sterile conditions in a biosafety cabinet. For passaging, cells were dissociated in 0.5 mM Ethylenediaminetetraacetic acid (EDTA) solution for 2-5 minutes at 37C, or until visible spaces appeared between cells on the outer edges of colonies, but prior to colonies lifting from the surface of the dish. While cells incubated in EDTA solution, vitronectin solution was aspirated from the new multi-dish and 2 mL of Essential 8 Flex (E8f) medium (Gibco, cat. no. A2858501) containing 100 µg/mL Normocin (Invivogen, cat. no. ant-nr-1) and RevitaCell supplement (Gibco, cat. no. A26445-01) at a concentration of 1:100 was added to each well. Following EDTA incubation, EDTA solution was aspirated from the treated cells. 1 mL E8f medium containing Normocin and RevitaCell supplement was then immediately added to the cells. Cells were "washed" from the surface of the plate by pipetting medium up and down, with care taken not to introduce bubbles into the solution. A desired volume of cells was then pipetted into the wells of the new 6-well plate

already containing medium. The plate was gently agitated by hand to spread cells evenly across the wells, and subsequently stored at 37C. Cells were maintained in E8f medium containing RevitaCell supplement for the first 24 hours after passaging. At one day post-passaging, medium was aspirated and replaced with E8f medium containing Normocin only. Cells were passaged upon reaching ~70-80% confluency or every 4-5 days, and maintained at 37C in 5% CO_2.

For the studies described herein, *PAX2*-2A-nGFP and *ATOH1*-2A-GFP human ESC reporter lines were additionally used. These cell lines contain green fluorescent protein (GFP) reporter cassettes driven by expression of otic progenitor marker PAX2 (*PAX2*-2A-nGFP cell line) or hair cell marker ATOH1 (*ATOH1*-2A-GFP cell line). The *PAX2*-2A-nGFP reporter cassette additionally contained a nuclear localization signal, so that GFP expression is observed in the nucleus. Reporter ESCs were maintained under the same parameters as WA25 human ESCs. Both reporter lines were previously established using CRISPR-Cas9 genome editing in WA25 human ESCs; generation of the *ATOH1*-2A-GFP human ESC reporter line was reported in [19].

Signaling molecules and recombinant proteins

During otic differentiation of human ESCs, recombinant Human FGF-2 (bFGF) (Peprotech, cat. no. 100-18B) was used to activate FGF signaling in early stage culture [77]. Small molecule TGF-β inhibitor,SB431542 (Stemgent, cat. no. 04-0010-05), and small molecule BMP pathway inhibitor LDN-193189 (Reprocell, cat. no. 04-0074-02), were additionally applied during early stage culture

(additional details in the following section). CHIR99021 (Stemgent, cat. no. 04-0004-02), a small molecule GSK3 inhibitor [16, 78-80], was employed as a Wnt pathway agonist. Purmorphamine (Stemgent, cat. no. 04-0009), a small molecule agonist for SHH pathway effector SMO [81], was applied for SHH pathway activation.

Inner ear organoid differentiation

Human PSCs were cultured to the formation of inner ear organoids as described [19]. Briefly, cells were aggregated in 96-well low adhesion V-bottom plates (Gel Company, cat. no. LCV96) in E8f medium containing Normocin and Y-27632 ROCK inhibitor (Stemgent cat. no. 04-0012-02) and placed at 37C in in 5% CO_2. After two days of culture, stem cell aggregates were transferred to 96-well low adhesion U-bottom plates (Thermo Fisher Scientific, cat. no. 174925) in chemically defined medium (CDM) (see Table 1 for ingredients) containing 2% Matrigel Growth Factor Reduced Basement Membrane Matrix (Corning, cat.no. 354230), SB-421542 (10 μM), and bFGF (4 ng/mL). After a subsequent four days of incubation, an additional 25 uL of CDM containing bFGF at 250 ng/mL (25 ng/mL final concentration) and 1 μM LDN-193189 (200 nM final concentration) was added to each well of the 96-well plate. Following an additional four days of culture, 25 uL of CDM containing WNT agonist CHIR99021 (CH) at a concentration of 18 μM (3 μM final concentration when added to the pre-existing volume of 125 uL medium per well) was added to each well. After an additional 3-4 days in culture,, aggregates were transferred to 100mm tissue culture dishes

Table 1: Organoid maturation medium (OMM) components

Component	Manufacturer	Catalog no.	Volume
Advanced DMEM/F12	Thermo Scientific	12634028	24.5 mL
Neurobasal	Thermo Scientific	21-103-049	24.5 mL
GlutaMax	Thermo Scientific	35-050-061	500 uL
B27 without Vitamin A	Thermo Scientific	12587010	500 uL
N2 supplement	Thermo Scientific	17502-048	250 uL
2-mercaptoethanol	Thermo Scientific	21985-023	90 uL
Normocin	Invivogen	ant-nr-1	100 uL

Table 2: Chemically defined medium (CDM) components

Component	Manufacturer	Catalog no.	Volume
Bovine serum albumin	Sigma-Aldrich	A1470-10G	0.25 g
F-12 + GlutaMax	Thermo Scientific	12634028	24.7 mL
IMDM + GlutaMax	Invitrogen	31980030	24.7 mL
Chemically defined lipid concentrate	Invitrogen	11905-031	500 uL
Insulin	Sigma-Aldrich	I9278-5ML	35 uL
Transferrin	Sigma-Aldrich	T8158-100MG	37.5 uL
1-thioglycerol	Sigma-Aldrich	M1753-100ML	2 uL
Normocin	Invivogen	ant-nr-1	100 uL

First described in Koehler et al, 2017 [19]

(Fisher Scientific, cat. no. 08-772B) in organoid maturation medium (OMM) (see Table 2 for ingredients) containing 1% Matrigel and CH (3 μM). On culture day 15, OMM was aspirated and replaced with OMM containing Matrigel + CH (3 μM) with a 1:1 volume of OMM containing no additional supplementation. Aggregates were transferred on culture day 18 to new 100 mm dishes in OMM containing no additional supplementation and maintained at 37C with weekly medium changes. Aggregates may be maintained in this manner for >150 days [19].

For studies with SHH pathway agonist Purmorphamine (PUR), aggregates were transferred to 100 mm plates on day 11-12 of culture and grown in OMM containing 1% Matrigel and CH (3 μM) (designated “CH” condition) or with OMM containing CH (3 uM) plus PUR (1 μM, except as specified) (designated “CH+PUR” condition) for four subsequent days of culture. On culture day 15, medium was aspirated completely and fresh OMM containing Matrigel and CH or CH+PUR was added to the plates with a 1:1 volume of OMM containing no additional supplementation. On day 18, aggregates were transferred as per the conventional protocol into OMM containing no additional small molecule treatments.

Quantitative PCR

For qRT-PCR experiments, total RNA isolation from whole aggregates or sorted cell populations greater than 500,000 cells was performed using the RNeasy Plus Mini Kit (Qiagen, cat. no. 74134). Dissociated and sorted cell populations less than 500,000 cells underwent RNA isolation using the RNeasy Micro Kit (Qiagen, cat. no. 74004) suitable for small cell populations. cDNA was

generated using the Omniscript RT Kit (Qiagen, cat. no. 205111). For qRT-PCR, PowerUp SYBR Green Master Mix was utilized. Samples were run in technical triplicate, with L27 used as a reference gene for normalization. qRT-PCR experiments were run on a Bio-Rad CFX96 Touch platform, and Bio-Rad CFX96 software was used to generate analysis. For a list of qPCR primers used, see Table 3.

Immunohistochemistry

For immunohistochemical analysis, aggregates were collected and fixed in 4% paraformaldehyde for 30 minutes (if collected at a timepoint ≤day 40) or 1 hour (if collected at a timepoint >day 40) at room temperature on a rotating table. Aggregates derived from human reporter ESCs were protected from light while undergoing fixation to avoid quenching of fluorescent signal. After fixation, aggregates were washed three times in 1X phosphate buffered saline (PBS; Gibco, cat. no. 10010049). Fixed aggregates were treated with 15% and 30% sucrose solutions for one hour each in serial, and then embedded in tissue freezing medium (Fisher Scientific, cat. no. 15-183-13), frozen at -20C for 30 minutes to 1 hour, and stored at -30C until sectioning. Cryoblocks were sectioned into 12-15 μm sections using a Leica CM1850 Cryostat microtome. Each slide prepared for immunohistochemistry typically contained 5-10 cryosections representative of 5-10 aggregates embedded together (for samples collected ≤day 30) or 3-4 aggregates embedded together (for samples collected ≥day 30).

Table 3: qRT-PCR primers

Gene	**Primer set**
L27	Forward: CGTGAAGAACATTGATGATGGC Reverse: GCGATCTTCTTCTTGCCCAT
PAX2	Forward: TCAAGTCGAGTCTATCTGCATCC Reverse: CATGTCACGACCAGTCACAAC
KI67	Forward: CTGACCCTGATGAGAGTGAGGG Reverse: TCTCCCCTTTTGAGAGGCGT

For fluorescent antibody staining, cryosections were blocked for 1 hour in PBS solution containing 0.1% Triton X-100 (Sigma-Aldrich, cat. no. 93443) and 10% normal goat serum (Vector Laboratories, cat. no. S-1000). Primary and secondary antibody incubation occurred in PBS solution containing 0.1% Triton X-100 and 3% goat serum. Following blocking, cryosections were incubated in primary antibody solution for 1 hour at room temperature, or at 4C overnight (see Table 4 for list of primary antibodies used). Slides were then washed in PBS three times, 10 minutes per wash on an agitator at room temperature, covered to protect from light. Cryosections were then incubated with secondary antibody solution containing Alexa fluor-conjugated secondary antibodies for 1 hour at room temperature. Slides then underwent three 10-minute washes in PBS at room temperature, protected from light. Cryosections were fixed with Prolong Gold Antifade Reagent with DAPI (Fisher Scientific, cat. no. P-36931) for nuclear staining.

Imaging was performed using a Nikon TE2000 or Leica DMi8 inverted fluorescent light microscope. For Leica imaging, images were taken in Z-stacks and subjected to 3D deconvolution and projection.

Fluorescence-activated cell sorting

Fluorescence-activated cell sorting (FACS) was used to assess *PAX2*-2A-nGFP+ expression in control and treated PAX2 reporter human ESC-derived aggregates, and to isolate the GFP+ cell population for downstream analysis. For sorting, a desired number of aggregates were collected and pooled in one well of

Table 4: Primary antibodies

Name	Vendor	Cat. no.	Host	Dilution
PAX2	Abnova	H00005076-M01	Mouse	1:100
PAX8	Abcam	AB97477	Rabbit	1:100
SOX2	BD Pharmingen	561469	Mouse	1:100
SOX10	eBioscience	14-5923-82 (20B7)	Mouse	1:50
FBXO2	Santa Cruz	sc-398111	Mouse	1:25-1:50
KI67	BD Pharmingen	550609	Mouse	1:100
GFP	Thermo Fisher	A-11120	Mouse	1:100
MYO7A	Proteus	256790	Rabbit	1:100
DLX3	Santa Cruz	sc-514094	Mouse	1:100
OTX2	R&D Systems	AF1979	Goat	1:20
NEUROD1	R&D Systems	AF2746-SP	Goat	1:50
LMOD3	Proteintech	14948-1-AP	Rabbit	1:50
TUJ1	Abcam	AB78717	Rabbit	1:100

a 24-well Nunclon Sphera Dish (Thermo Scientific, cat. no. 12-566-433) and washed three times with DPBS. Dissociation solution was prepared, consisting of DPBS containing 0.5X Accumax (Innovative Cell Technologies, cat. no. AM105), 1X TrpLE Select (Fisher Scientific, cat. no. 50-591-353), and 0.5 mM EDTA. 1 mL of dissociation solution was added to the aggregates. The 24-well plate was then placed at 37C. Aggregates were gently triturated by pipetting with P1000 and P200 pipets (set to maximum volume) every 15 minutes for 1 hour, and imaged at the 30-minute and 60-minute mark to assess dissociation. Imaging was performed using a Nikon TE2000 inverted microscope. Dissociated cells were then run through a Falcon 100 μm mesh cell strainer (Fisher Scientific, cat. no. 08-771-19) and 40 μm mesh cell strainer (Fisher Scientific, cat. no. 07-201-430) in succession. Dissociation to a single cell solution was confirmed by imaging. Viability was then assessed by staining with Trypan Blue (Thermo Fisher Scientific, cat. no. 15250061). A 1:1 volume of Trypan Blue and cell solution were combined in a 1.5 mL microcentrifuge tube, and 10 uL of the combined solution was loaded to each side of an Invitrogen Countess Cell Counting Chamber Slide (Fisher Scientific, cat. no. C10228). Cell count and viability were determined using a Countess II Automated Cell Counter (Thermo Fisher Scientific).

Dissociated cells were then spun down in a tabletop centrifuge for 3 minutes at 200 g and re-suspended in 1 mL FACS wash. FACS wash consisted of DBPS with 1% BSA (Sigma, cat. no. A1470-10G) and 1 mM EDTA. The dissociated cell volume was then run through a Falcon 5 mL round bottom test

tube with cell strainer cap (Corning, cat. no. 352235) with an additional 1 mL of FACS wash in order to remove cell clumps. 25 uL of propidium iodide (Thermo Fisher Scientific, cat. no. P3566) diluted in PBS was added directly to the cells prior to sorting for dead cell exclusion.

Cells were sorted on a BD FACSAria SORP (BD Biosciences) at the Indiana University School of Medicine flow cytometry core. Aggregates derived from WA25 human ESCs lacking a fluorescent reporter cassette were dissociated in parallel with *PAX2*-2A-nGFP aggregates and used as negative fluorescence controls for FACS. With respect to gating strategy, forward scatter height versus forward scatter area was used to identify single cells and exclude doublets and cell clumps. Forward scatter area versus side scatter area was used to identify the cell population and exclude debris. Finally, propidium iodide was assessed to eliminate dead cells, and plotted against FITC to identify the live GFP+ cell population. Cells were sorted into DPBS containing 1% BSA and placed on ice until processing.

Generation of dot plots from FACS experiments and further analysis of quantitative data from FACS was performed using FlowJo flow cytometry analysis software (https://www.flowjo.com).

Single-cell RNA-sequencing

For scRNA-seq studies, *PAX2*-2A-nGFP human ESCs were subjected to the inner ear differentiation protocol [19], subjected to either treatment with CH alone or dual CH+PUR treatment during culture day 11-18, and collected on

culture day 20. WA25 ESC-derived aggregates were cultured in parallel with the reporter aggregates, received the same treatments, and were collected at the same timepoint to serve as negative controls for FACS. Aggregates were dissociated for FACS as described in the previous section. For each scRNA-seq population, typically 30-50 aggregates per condition were collected and pooled into a single well of a 24-well plate, as described for FACS; triplicate wells were prepared for sorting (90-150 aggregates total to yield a single population for scRNA-seq). Cells were sorted to isolate the *PAX2*-2A-nGFP+ cell population, and brought to the Center for Medical Genomics at Indiana University School of Medicine for subsequent processing.

scRNA-seq experiments were conducted using the Chromium single cell 3' system (10X Genomics, Inc) and the NextSeq500 sequencer (Illumina, Inc). The single cell suspension obtained via FACS was first counted on the Countess II Automated Cell Counter to determine cell number, cell viability, and cell size. If the assessed viability was higher than 85%, the appropriate number of cells was loaded onto a multiple-channel micro-fluidics chip compatible with the Chromium Single Cell Instrument (10X Genomics) with a targeted recovery of 10,000 cells. The version 2 single cell reagent kit (10X Genomics) was used, including gel beads containing barcoded oligonucleotides for tracing transcripts to their cell of origin, and reagents for reverse transcriptase. After individual cells were captured into oil droplets containing the barcoded gel beads, cells underwent lysis and cDNA was synthesized and amplified. cDNA was subsequently used to prepare a library for sequencing on the Illumina Nextseq500. A custom program was

utilized, wherein 26 base pairs of cell barcode and UMI sequence and 98 base pairs were generated.

To process raw sequence data, CellRanger 2.1.0 software (http://support.10xgenomics.com/) was used. Briefly, bcl2fastq (https://support.illumina.com/) was utilized in CellRanger to demultiplex raw base sequence calls generated from the sequencer into sample-specific FASTQ files. RNAseq aligner STAR was then used to align the FASTQ files to the human reference genome (GrCH38). Gene expression levels were quantified for each cell based on reads of individual unique molecular indices (UMIs); replicates of the same transcript shared the same UMI. Filtered gene-cell barcode matrices were generated by CellRanger for further analysis. The Seurat package in R (https://satijalab.org/seurat) was used for subsequent analysis, including unsupervised clustering and the integration of multiple datasets for comparative analysis. Here, datasets generated from CH and CH+PUR treated populations were integrated for comparative analysis. For day 20 analysis, each condition was performed in triplicate. For time course analysis comparing day 15 and day 20 CH+PUR treated populations, a single day 15 CH+PUR scRNA-seq dataset was generated.

Additional plots were generated using Loupe Cell Browser software (10X Genomics). Loupe software is capable of interrogating gene expression targets in single populations, but cannot perform comparative analysis. Loupe generated plots are indicative of single datasets that have not undergone integrated normalization.

Statistical analysis

Statistics were conducted using Prism 7 Software (https://www.graphpad.com/scientific-software/prism/). For comparison of two groups, student's t-test was applied. One-way ANOVA was applied for comparisons of more than two groups, with Dunnett's multiple comparison test applied as a post hoc test. Significance was determined as $p<0.05$.

CHAPTER THREE: RESULTS

Validation of inner ear organoid differentiation

I first sought to validate inner ear organoid generation using human WA25 ESCs (Figure 9), as the formation of stem cell aggregates in 3D culture and subsequent differentiation of inner ear tissue serves as the foundation for this study. Morphological hallmarks of inner ear organoid development were observed as described in [19], including initial embryoid body formation (Figure 9a), a thickening and ruffling of the outer epithelium by day 12 (Figure 9e), and the appearance of presumptive “otic pits” by culture day 15 (Figure 9f). Inner ear organoids were observed in late stage culture as either embedded (Figure 9h) or protruding (Figure 9i) spherical structures visible on the surface of the aggregates.

Protein expression analysis coincided with previous observations that otic placode and vesicle induction occurs in human stem cell-derived aggregates between days 12-18 [19], with co-expression of transcription factors PAX8 and SOX2 indicative of an early otic progenitor phenotype, observed by day 18 (Figure 10a-c). Late stage immunohistochemical analysis validated the development of cells co-expressing hair cell marker MYO7A and SOX2 by culture day 60 (Figure 10d-f), indicative of a derived hair cell population. A SOX2+/MYO7A- cell population was also observed co-localizing with the derived hair cells, indicative of a supporting cell-like phenotype.

Taken together, 3D stem cell aggregates subjected to the inner ear differentiation protocol produced otic vesicles at early stages of culture, and were

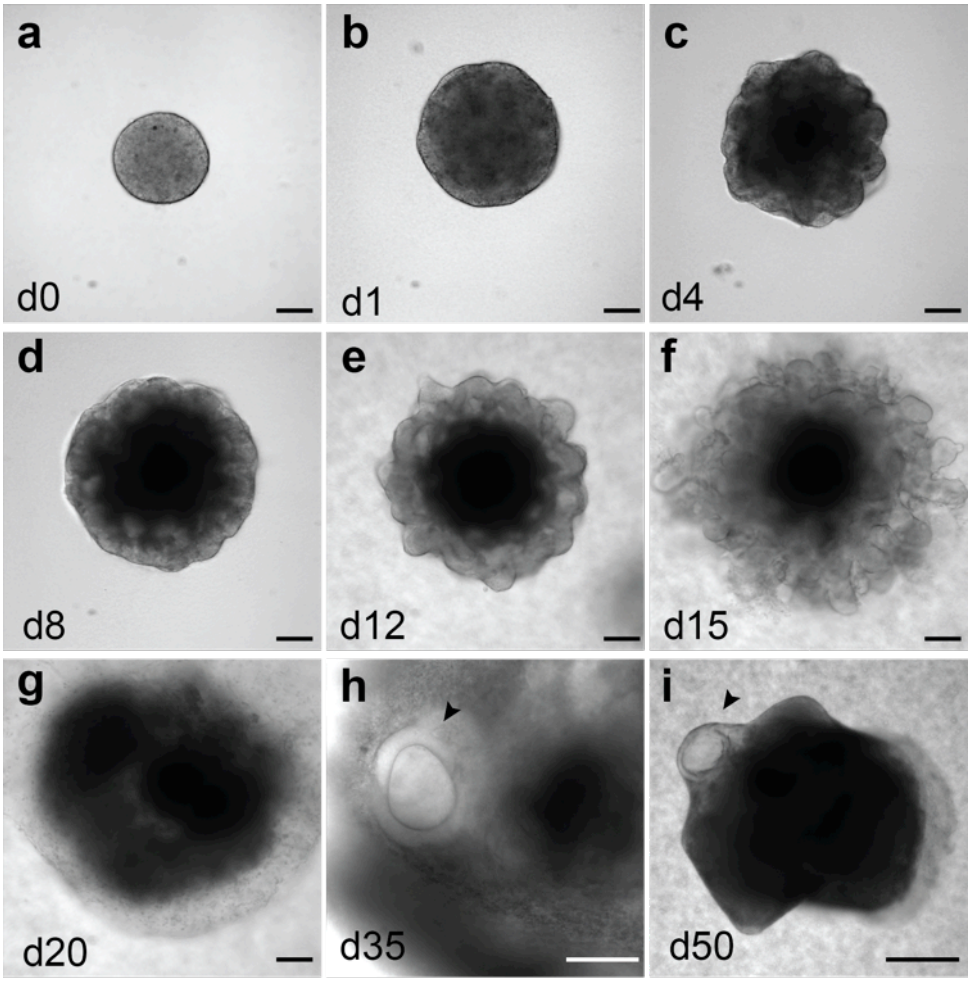

Figure 9: Morphological progression observed in inner ear organoid culture.

Stem cells were aggregated and treated with a series of small molecules during the first 8 days of culture to guide epithelium formation (**a-d**). A ruffled outer epithelium was visible by day 12 (**e**). Early otic vesicles pinch off from the surface of day 15 (**f**) aggregates and internalize by day 20 (**g**). Embedded (**h**) and protruding (**i**) organoids (arrowheads) may be observed in later stage cultures. Scale bars = 100 μm.

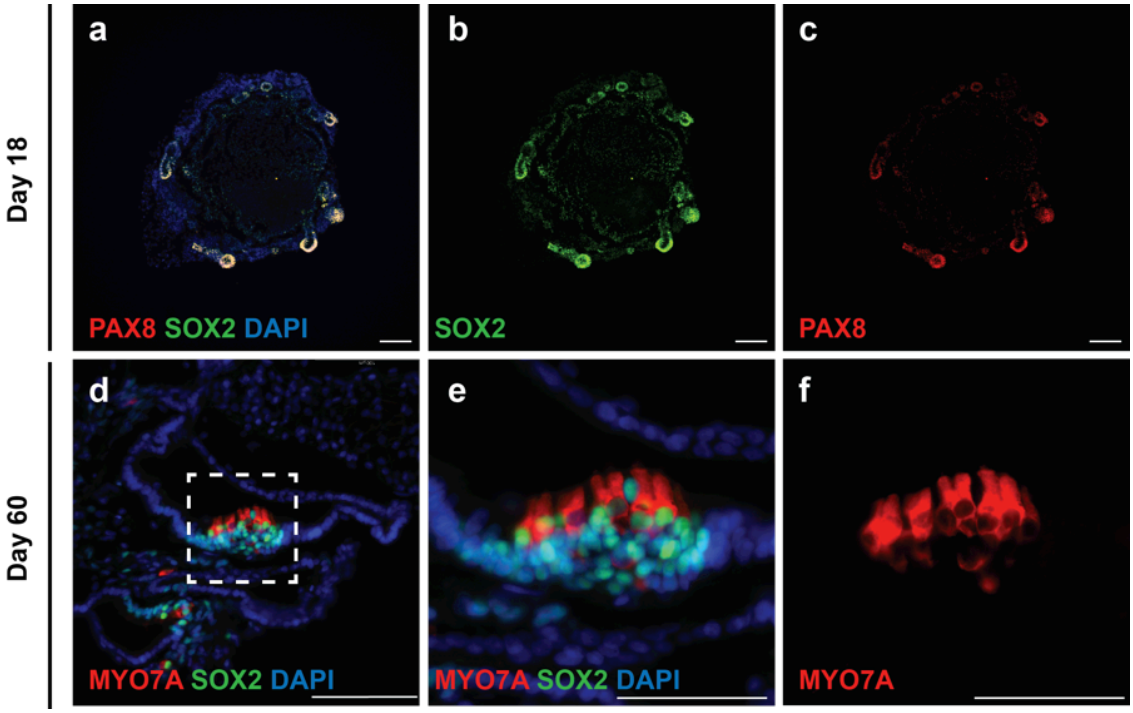

Figure 10: Immunohistochemistry of early and late stage inner ear organoids confirms expression of markers of otic development.

(**a**) Merged expression of early otic markers PAX8 and SOX2 in day 18 inner ear aggregates. Panels (**b**,**c**) illustrate Individual expression of SOX2 (**b**) and PAX8 (**c**). (**d**) Expression of SOX2 and hair cell marker MYO7A in a late stage inner ear organoid. MYO7A/SOX2 co-expression is indicative of a hair cell phenotype. Some SOX2+ cells lack expression of MYO7A, indicative of a non-sensory supporting cell-like phenotype. Dashed box indicates area seen in (**e**). (**f**) MYO7A+ cells exhibit a hair cell-like morphology. Scale bars = 100 μm (**a**-**d**), 50 μm (**e**,**f**)

capable of producing hair cell-like cells in long-term culture. This model appeared reproducible and suitable for the planned investigation. The majority of emphasis for the subsequent study will be placed on timepoints surrounding the induction of the derived otic vesicle (day 12-30) prior to the formation of hair cells, which are typically first observed in culture between day 40 to day 60 [19].

PAX2-2A-nGFP reporter line allows for monitoring the development of derived otic progenitors

In order to assess the patterning phenotype of human ESC-derived otic vesicle stage aggregates, I wanted a tool to track and isolate this developing population in live cultures. This spurred an investigation into possible candidate markers to employ as an otic reporter. Paired box 2 (PAX2) is a transcription factor that is highly expressed in the developing mammalian inner ear [82-84]. Pax2 knockout mice exhibit disrupted cochlear development, with rudimentary cochlea formation but arrested cochlear growth observed during early stage development [84]. PAX2 mutations in humans have been associated with renal-coloboma syndrome, a condition that impacts kidney and optic development. Sensorineural hearing loss has also been reported in patients with this mutation [85, 86].

PAX2 has previously been shown to be expressed in early stage human inner ear organoids, localizing in derived otic vesicle regions [19],. PAX2 protein expression has additionally been observed in organoids cultured for >60 days. Given the inner ear-specific expression of PAX2 previously reported *in vivo* [84,

87], and corroborated in our human inner ear organoid model, PAX2 appeared to be an excellent marker to validate the formation of early otic progenitors in culture, track the induction of this cell population in live aggregates, and isolate this population for downstream analysis. Therefore, we chose to employ a reporter line targeting *PAX2* that was generated using CRISPR/CAS9 genome editing in WA25 human ESCs. This reporter line contained a 2A-nGFP sequence targeted to the *PAX2* stop codon. Inclusion of a 2A linker sequence allows for bi-cistronic expression from a single mRNA [88], meaning that GFP expression is driven by native PAX2 expression, but results in separate translation of PAX2 and GFP, rather than the generation of a *PAX2*-GFP fusion protein. The GFP cassette additionally contained a nuclear localization signal, meaning the reporter line expresses GFP localized to the nucleus (nGFP).

PAX2-2A-nGFP reporter human ESCs were cultured according to our inner ear differentiation protocol [19] and monitored for the induction of GFP expression using fluorescent imaging of live cultures. The earliest instance of *PAX2*-2A-nGFP expression was observed on culture day 12 (Figure 11), with expansion of the *PAX2*-2A-nGFP+ cell population observed over the next several days in the protruding presumptive “otic pit” regions of the derived aggregates, leading to the formation of easily identifiable GFP+ vesicles.

Immunohistochemical analysis revealed that GFP expression overlapped completely with expression of endogenous PAX2 protein at all time points

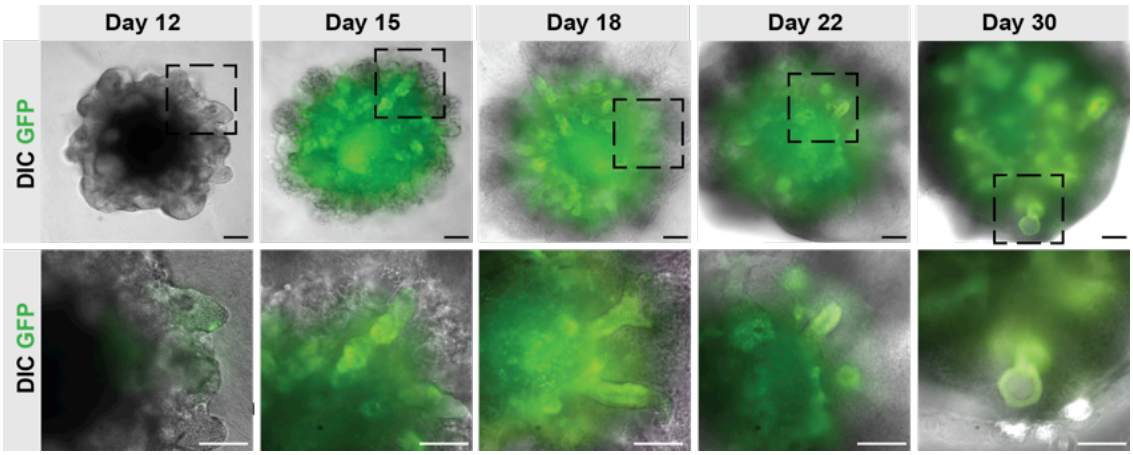

Figure 11: Live imaging of *PAX2*-2A-nGFP aggregates.

DIC and FITC imaging show structural morphology and induction of GFP+ cell population in *PAX2*-2A-nGFP human ESC derived aggregates. Dashed boxes indicate area in higher magnification shown in the lower set of panels. The earliest induction of GFP was observed in the aggregate outer epithelium on culture day 12, with expansion of the signal observed over time. Scale bars = 100 µm.

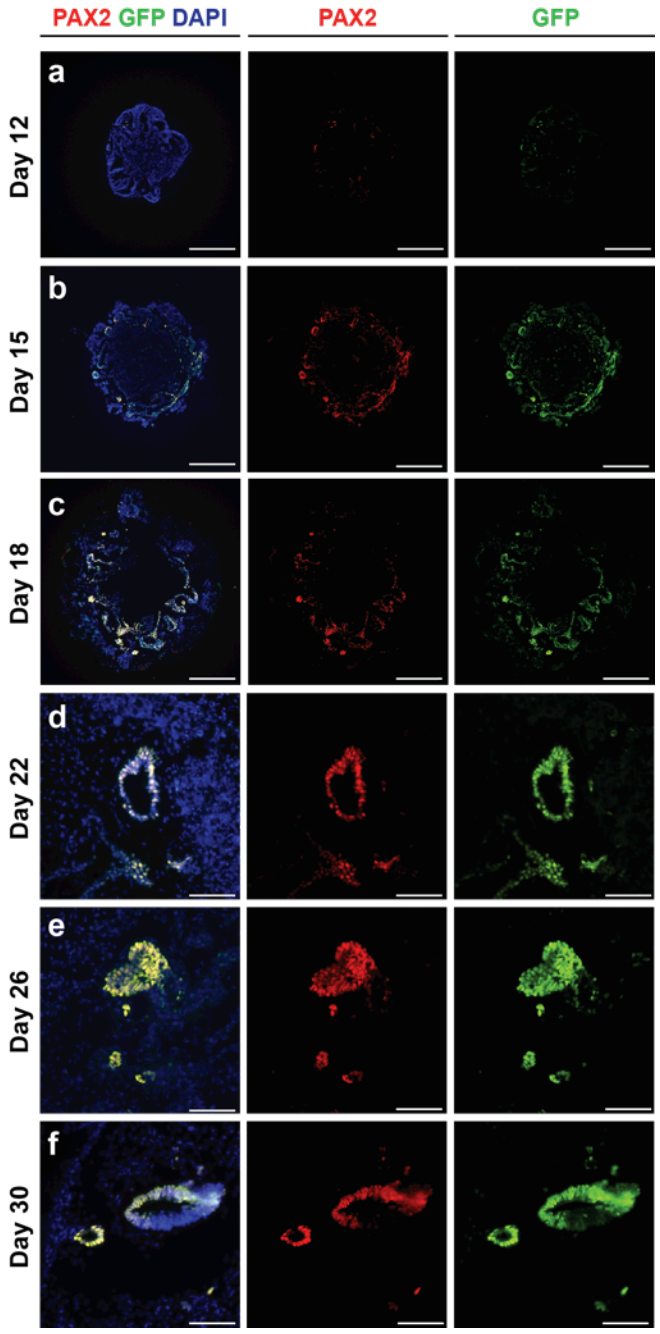

Figure 12: PAX2 and GFP expression overlaps completely in *PAX2*-2A-nGFP aggregates.

All time-points assessed exhibit overlap of PAX2 and GFP expression. PAX2 and GFP expression is low at culture day 12 (**a**) but expands in the outer epithelium of aggregates by culture day 15 (**b**) and 18 (**c**). (**d**-**f**) illustrate PAX2+/GFP+ otic vesicles during day 22 – day 30 of culture. Scale bars = 100 μm (**a**-**c**), 50 μm (**d**-**f**)

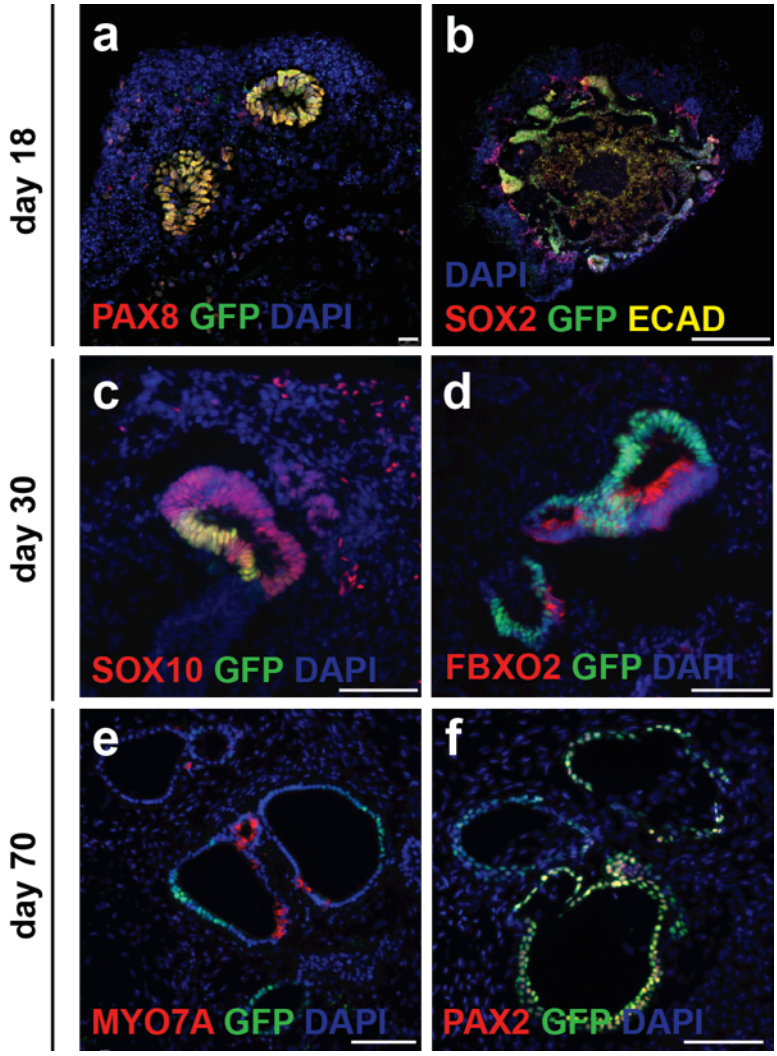

Figure 13: Expression of otic markers supports otic identity of *PAX2*-2A-nGFP+ cell population.

Immunohistochemical analysis of early stage otic markers PAX8 (**a**), SOX2 and ECAD (**b**) show localization with GFP in vesicle-like structures in day 18 aggregates. Panels **c-d** illustrate co-localization or co-expression of *PAX2*-2A-nGFP with SOX10 (**c**) and FBXO2 (**d**) in day 30 aggregates. (**e**) GFP localizes to vesicles with MYO7A+ putative hair cells in day 70 cultures. (**f)** PAX2 and GFP overlap is also observed in late stage cultures. Scale bars = 75 μm (**a**), 500 μm (**b**), 100 μm (**c**-**f**)

surveyed from day 12 to day 30 (Figure 12). Evaluation of additional early otic markers at culture day 18, including PAX8, SOX2 and E-cadherin (ECAD) (Figure 13a-b) showed co-expression with *PAX2*-2A-nGFP. Expression of otic markers SOX10 and FBXO2 (Figure 13c-d) showed either co-localization or co-expression within *PAX2*-2A-nGFP+ vesicles, further supporting the otic identity of this GFP+ cell population. Late stage immunohistochemical analysis showed localization of *PAX2*-2A-nGFP to vesicles containing cells expressing hair cell marker MYO7A (Figure 13e). Additionally, late stage analysis showed that PAX2 expression overlapped with expression of GFP (Figure 13f).

Having demonstrated the validity of this otic progenitor reporter line, these cells will serve as a tool to evaluate SHH pathway modulation in inner ear organoid culture.

SHH pathway modulation in early stage inner ear organoids

SHH has been shown to be indispensable for proper cochlear morphogenesis [29, 31]. SHH loss-of-function studies revealed disrupted morphogenesis of both vestibular and auditory inner ear structures, a phenotype attributed to aberrant expression of dorsal genes and a lack of ventral gene expression in the developing otic vesicle. A study in which the SHH downstream effector SMO was conditionally inactivated in the mouse otic epithelium revealed that vestibular organ development was maintained following loss of SHH pathway activation in the inner ear; however, the cochlea failed to form in these embryos [31]. This was attributed to a loss of expression of PAX2 and OTX2 in

the ventral otic vesicle, while wild-type expression of dorsal-specific marker DLX5 was maintained [31]. I hypothesize that activation of SHH signaling in early stage inner ear organoid culture will promote expression of ventral otic genes within the derived cell population.

To induce SHH pathway activation in the inner ear organoid model, Purmorphamine (PUR), a well-established small molecule agonist for SHH pathway effector Smoothened (SMO) [81, 89, 90], was selected. Aggregates were initially subjected to treatment with 1 μM PUR at day 11-12 of culture and maintained in medium containing PUR for an additional 6 days. During this time period, aggregates subjected to our previously published protocol are treated with WNT pathway agonist CHIR99021 (CH) to guide otic vesicle induction [19]. Morphological hallmarks associated with otic vesicle induction in inner ear organoids were not observed in PUR-treated aggregates, including the ruffling of the outer epithelium characteristic of presumptive otic pit formation during early stage culture (Figure 14). Instead, a condensed morphology with a darkened inner core was observed in these aggregates. Additionally, aggregates treated with PUR appeared not to express *PAX2*-2A-nGFP when assessed by live fluorescent imaging (Figure 14a). Pilot qRT-PCR analysis confirmed decreased expression of PAX2 in aggregates receiving PUR only compared to those treated with CH at this timepoint (Figure 14b). Taken together, these data indicated that treatment with PUR alone appeared insufficient to guide the formation of otic vesicles. For that reason, in subsequent PUR experiments, aggregates received

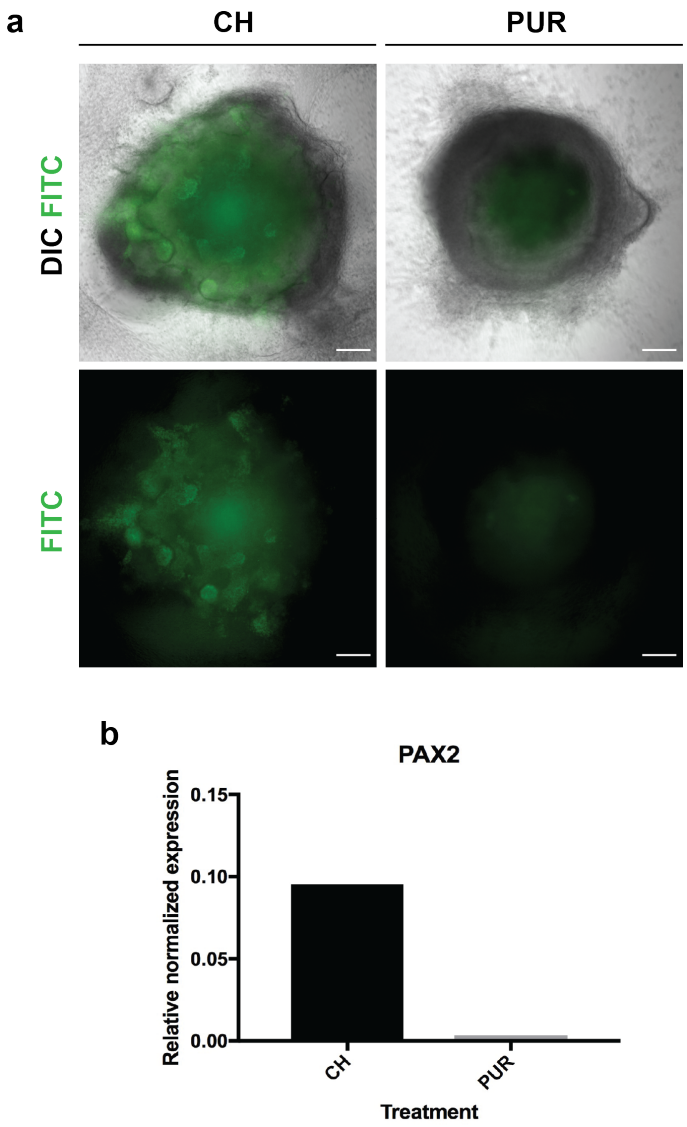

Figure 14: Purmorphamine treatment alone fails to induce presumptive otic vesicles.

(**a**) *PAX2*-2A-nGFP human ESC-derived aggregates treated with Wnt agonist CH from culture day 11-18 exhibit *PAX2*-2A-nGFP+ vesicle-like structures by culture day 18. Aggregates treated with PUR alone during this time period do not exhibit *PAX2*-2A-nGFP+ vesicles. Scale bars = 100 μm (**b**) Pilot qRT-PCR analysis of PAX2 expression in day 18 *PAX2*-2A-nGFP ESC-derived whole aggregates treated with CH or PUR only from day 11-18 (20 pooled aggregates per condition).

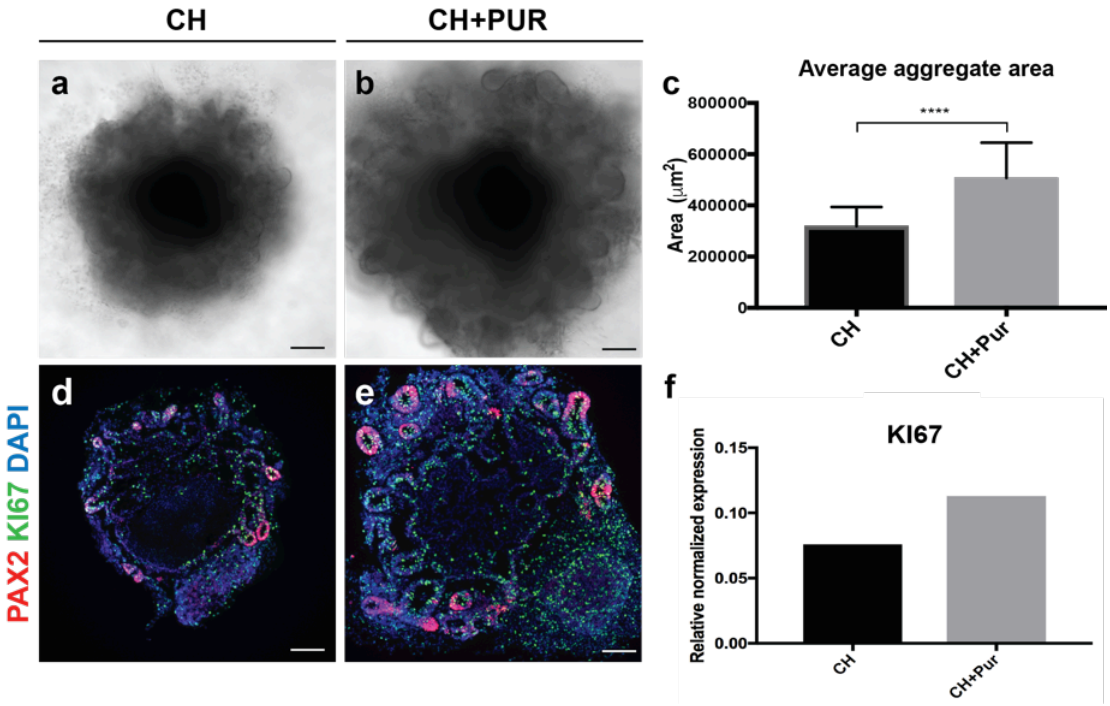

Figure 15: Size phenotype observed in CH+PUR treated aggregates.

(**a-b**) DIC images of day 18 WA25 aggregates receiving CHIR treatment alone (**a**) or CHIR + Purmorphamine (**b**). (**c**) Size comparison data between CH and CH+Pur aggregates showing average area. **** indicates indicates significance, p-value >0.0001 (n= 18 aggregates per condition, 3 independent experiments). Error bars indicate SD. (**d-e**) PAX2 and KI67 expression in CH (**d**) and CH+PUR (**e**) aggregates. (**f**) Pilot qRT-PCR analysis indicating relative normalized expression of KI67 in CH and CH+PUR whole aggregates. Scale bars = 100 μm.

dual CH and PUR treatment (indicated as CH+PUR) to ensure otic vesicle induction.

A size phenotype was observed following dual CH+PUR treatment beginning on day 11-12 of culture and spanning the period of otic vesicle formation (up to day 18 of culture). CH+PUR treated aggregates grew significantly larger than control aggregates treated with CH alone (Figure 15a-b). Immunohistochemical analysis confirmed the appearance of PAX2+ vesicles in CH+PUR treated aggregates, shown on day 18 (Figure 15e). Expression of proliferation marker KI67 (KI67) appeared more abundant in CH+PUR treated aggregates; a similar trend was observed in preliminary qRT-PCR analysis (Figure 15f). The size phenotype may be reflective of the mitogenic role of the SHH signaling pathway [71].

Dose response analysis was performed in order to assess the optimal concentration of PUR treatment (Figure 16). *PAX2*-2A-nGFP derived aggregates were treated with a consistent concentration of CHIR (3 μM, as reported in [19]), and increasing concentrations of PUR, ranging from 0.5-4 μM. GFP expression was observed in live cultures during the period of otic vesicle induction (day 11-18). Aggregates treated with 0.5-2 μM PUR exhibited relatively typical morphology and patterns of *PAX2*-2A-nGFP expression (Figure 16a). However, a sharp decrease in culture quality was observed in aggregates treated with 4 μM PUR, with cellular debris noted surrounding the aggregates during the treatment period. Additionally, PAX2 expression in aggregates treated with 4 μM PUR appeared diffuse and dim, with little evidence of PAX2+ vesicles observed in live

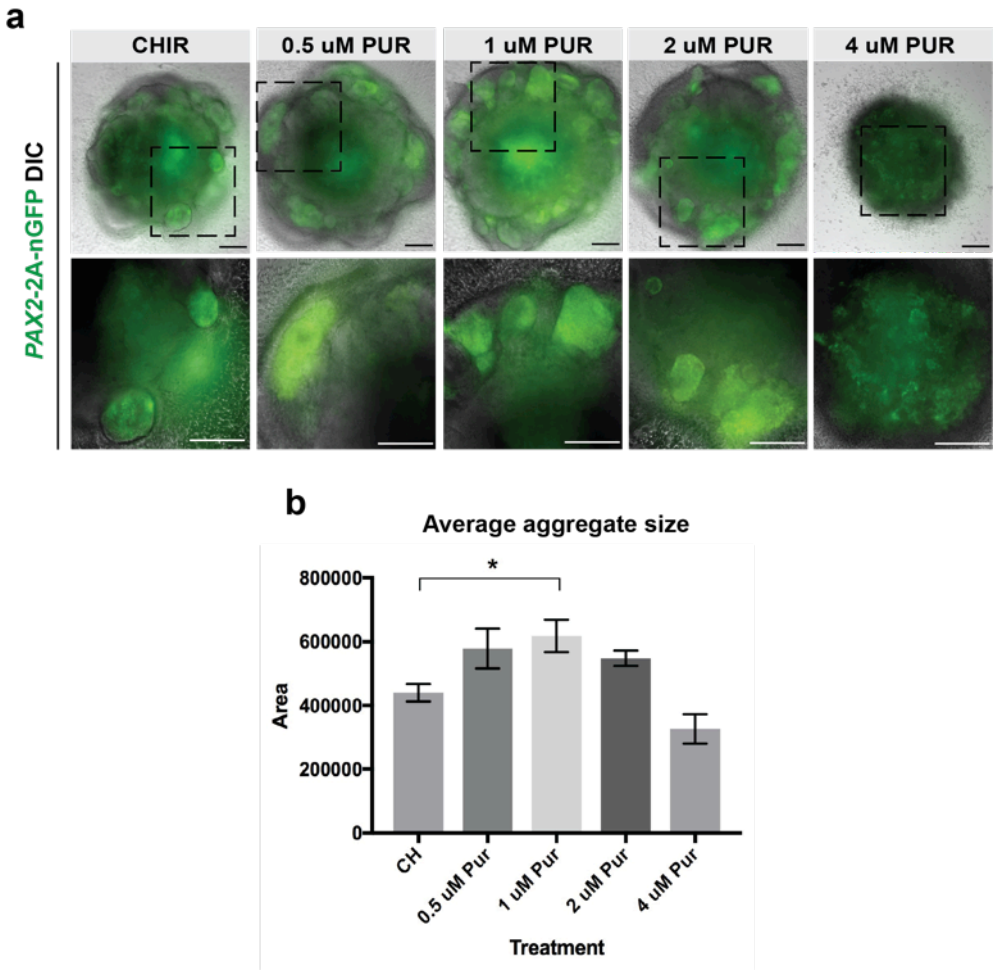

Figure 16: Purmorphamine dose response.

(**a**) DIC/FITC imaging of *PAX2*-2A-nGFP human ESC-derived aggregates. Dashed boxes indicate area of magnification seen in lower panels. Scale bars = 100 μm (**b**) Average aggregate area per treatment, n= 18 aggregates per condition from 3 independent experiments. * indicates significance, p-value = 0.0366. Error bars indicate sem.

cultures (Figure 16a). With respect to aggregate size, aggregates receiving 1 μM PUR were significantly larger in area than those receiving CH alone (p=0.0366, n=18 aggregates, 3 independent experiments) (Figure 16b), supporting previous results obtained comparing size in CH treated and CH+PUR (1 μM) treated WA25 human ESC-derived aggregates (Figure 14c). Concentrations of 0.5, 2, and 4 μM PUR did not exhibit a significant size difference compared to aggregates treated with CH alone (Figure 16b). A concentration of 1 μM PUR was ultimately selected for subsequent analysis.

Isolation and FACS analysis of *PAX2*-2A-nGFP+ derived cell populations

One challenge of the inner ear organoid model is the heterogeneous nature of the stem cell derived aggregates; non-otic cell types routinely emerge alongside the otic cell population. In order to accurately assess the gene expression phenotype of the otic population, it was necessary to optimize a strategy for dissociation and FACS of *PAX2*-2A-nGFP human ESC-derived aggregates to isolate the *PAX2*-2A-nGFP+ population (Figure 17). There have been no previously published methods for the dissociation of stem cell-derived inner ear organoids. Extensive troubleshooting ultimately led to the modification of a method from Herget and colleagues [91], who dissociated chicken vestibular sensory epithelia for flow cytometry using an enzymatic cocktail consisting of AccuMax Cell Dissociation solution (Cell Technologies, Inc.), trypsin, and EDTA. Herget et al found that incubation of dissected vestibular sensory epithelia in enzyme solution for 7 minutes at 37C, with gentle mechanical dissociation after 3

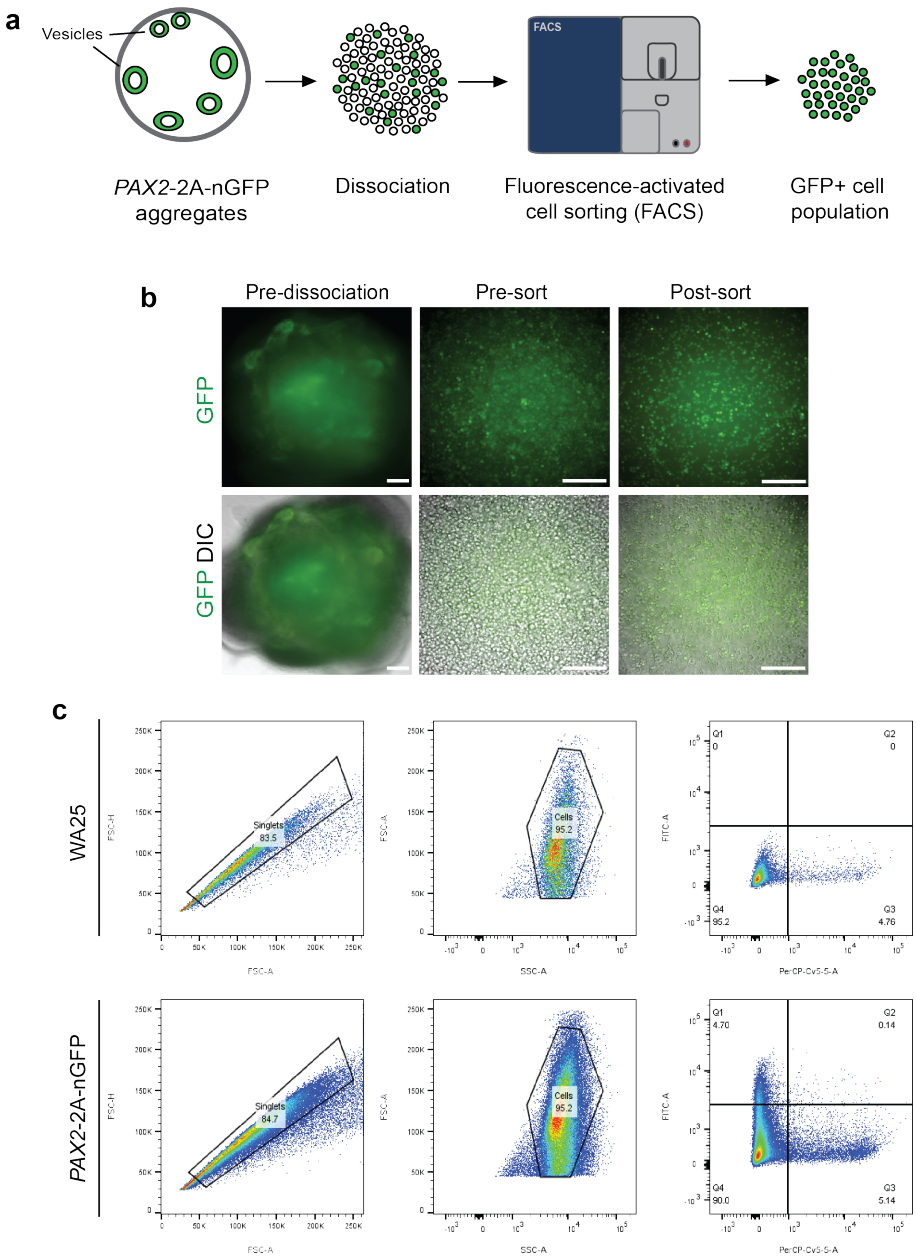

Figure 17: Fluorescence-activated cell sorting of *PAX2*-2A-nGFP aggregates allows for isolation of GFP+ cell population.

(**a**) Schematic describing strategy for analysis of *PAX2*-2A-nGFP aggregates. (**b**) DIC and FITC imaging shows Day 20 *PAX2*-2A-nGFP aggregate prior to dissociation (left panels), post-dissociation (middle) and post-sort (right). Scale bars = 100 µm (**c**) Representative dot plots illustrating gating strategy for WA25 negative fluorescent control cells (top panels) and *PAX2*-2A-nGFP sorted cell population (bottom panels). FITC axis represents GFP. Propidium iodide stain, indicated by PerCP-Cy5-5-A axis, was included for dead cell exclusion.

minutes of incubation, led to efficient dissociation and generation of a single-cell suspension [91].

The aggregates subjected to the human ESC inner ear differentiation protocol required a substantially longer incubation time for dissociation. For pilot dissociation experiments, aggregates collected were collected day 18-25 and placed in dissociation solution consisting of 0.5X AccuMax, 1X TrypLE, and 0.5 mM EDTA. Time course analysis was performed to evaluate the optimal length of time for incubation, using viability as assessed by trypan blue staining and formation of a single-cell solution as a measure of efficacy (data not shown). The optimal dissociation conditions for FACS of human stem cell-derived inner ear aggregates comprised a one-hour static incubation at 37C with periodic gentle mechanical trituration. This method maintained adequate cell viability as assessed by propidium iodide staining during sorting (Figure 17c).

FACS was performed on day 20 *PAX2*-2A-nGFP human ESC-derived aggregates treated with either CH or CH+PUR during otic vesicle induction (Figure 18a), with WA25 timepoint-matched aggregates used as a GFP negative control. Analysis at day 20 revealed a trend toward an increased *PAX2*-2A-nGFP+ population in the CH+PUR treated group compared to aggregates treated with CH alone (Figure 18b), although the difference was not statistically significant across three replicates.

Altogether, we established a method for dissociation and FACS of otic vesicle stage inner ear organoids and demonstrated the ability to isolate

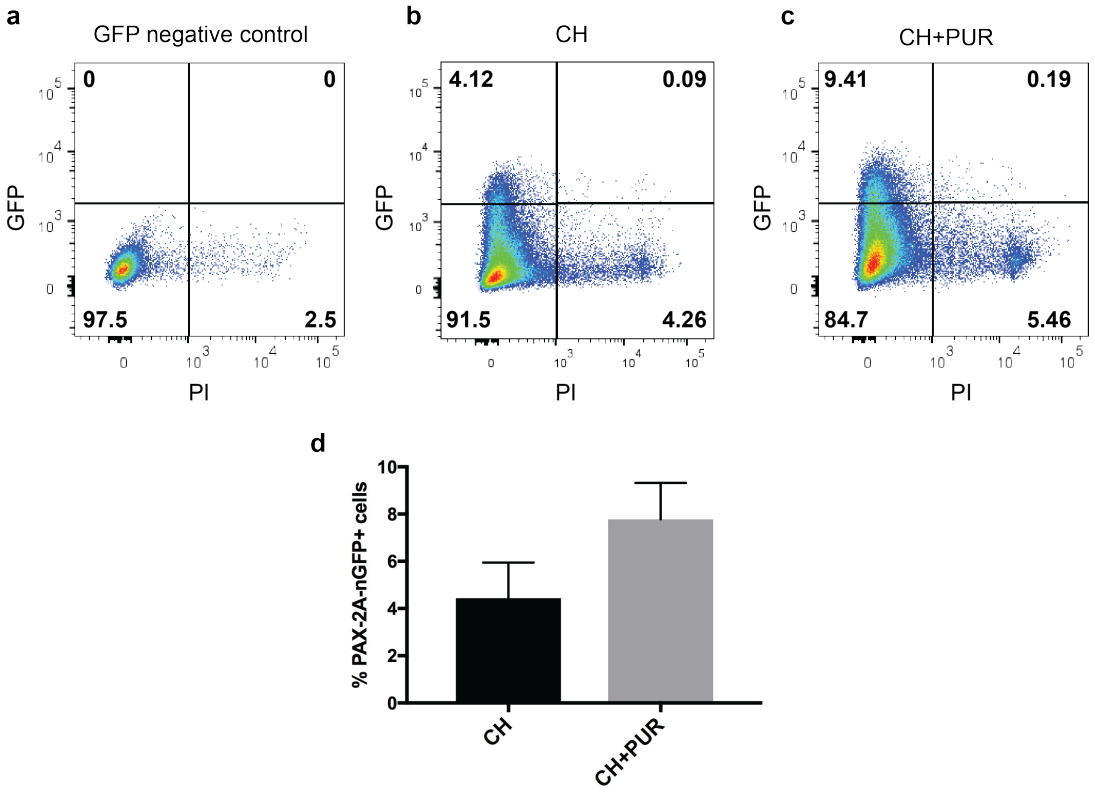

Figure 18: Fluorescence activated cell sorting of CH and CH+PUR treated aggregates.

Representative dot plots of *PAX2*-2A-nGFP FACS, indicating sorted cell populations from WA25 aggregates prepared as a negative control for GFP expression (**a**), aggregates receiving CH treatment alone (**b**), and aggregates receiving CH+PUR treatment (**c**). Percentage of *PAX2*-2A-nGFP expression indicated in upper left quartile. Panel (**d**) indicates the average percentage of GFP+ cells per condition, n=3 biological replicates per condition (indicative of aggregates from three independent cultures prepared for three individual FACS experiments per treatment group).

PAX2-2A-nGFP+ presumptive otic progenitors. This method will be further employed for subsequent transcriptomic analysis of CH and CH+PUR treated aggregates.

Evaluation of control and treated cell populations via single-cell RNA-sequencing

Having successfully isolated *PAX2*-2A-nGFP+ cells from early stage inner ear organoids, our next goal was to analyze the gene expression profile of sorted cell populations. Expression of dorsal and ventral inner ear patterning markers has not previously been evaluated within the inner ear organoid model. Single-cell RNA-sequencing (scRNA-seq) was performed at day 20, a timepoint following otic vesicle induction, to determine whether a dorsalized phenotype is present in control treated (CH) aggregates, potentially underlying the vestibular bias in subsequent hair cell differentiation, and whether SHH pathway modulation may promote ventralization and lead to induction of cochlear cell types.

scRNA-seq platforms have evolved greatly in recent years, increasing in high-throughput capability [61]. For the scRNA-seq experiments described here, the 10X Chromium 3' single-cell platform was utilized. *PAX2*-2A-nGFP derived aggregates were treated with either CH or CH+PUR from day 11 to day 18 and monitored for induction of *PAX2*-2A-nGFP. Aggregates were collected on day 20 of culture and sorted to isolate the *PAX2*-2A-nGFP population. The GFP+ cells were then subjected to scRNA-seq. Each treatment group was replicated three times, for a total of six individual scRNA-seq datasets. Variation was observed

from sample to sample within each treatment group with respect to number of cells read, as well as with respect to the expression of certain individual markers. scRNA-seq analysis provides only a snapshot of cells at the time they were isolated, so some natural variation is to be expected. However, results presented here for specific genes of interest were consistent across replicates unless otherwise specified. The following passages will detail processing and quality control analysis of one representative sample set.

To process each cell population following scRNA-seq, quality control analysis was performed using Seurat [92, 93]. Cell filtering was applied based on the number of genes expressed per cell and the number of mitochondrial genes present. High mitochondrial gene content may be indicative of poor cell quality [94]. For the first CH control population processed, cells with unique gene counts greater than 5,500 and less than 1,000 were filtered out, along with cells that displayed greater than 6% mitochondrial gene expression (Figure 19). These filtering metrics eliminated 0.014% of the cell population from subsequent analysis, reducing the data set from 6967 cells to 6866 cells. The same approach was used to filter the first CH+PUR dataset, excluding 0.011% of the total cell population, thereby reducing the initial sample size of 8798 cells to 8693 cells after filtering. For all replicate samples, consistent quality control metrics for filtering and processing were applied.

Data was then normalized via a global-scaling normalization method in Seurat; gene expression measurements for each cell were normalized by the

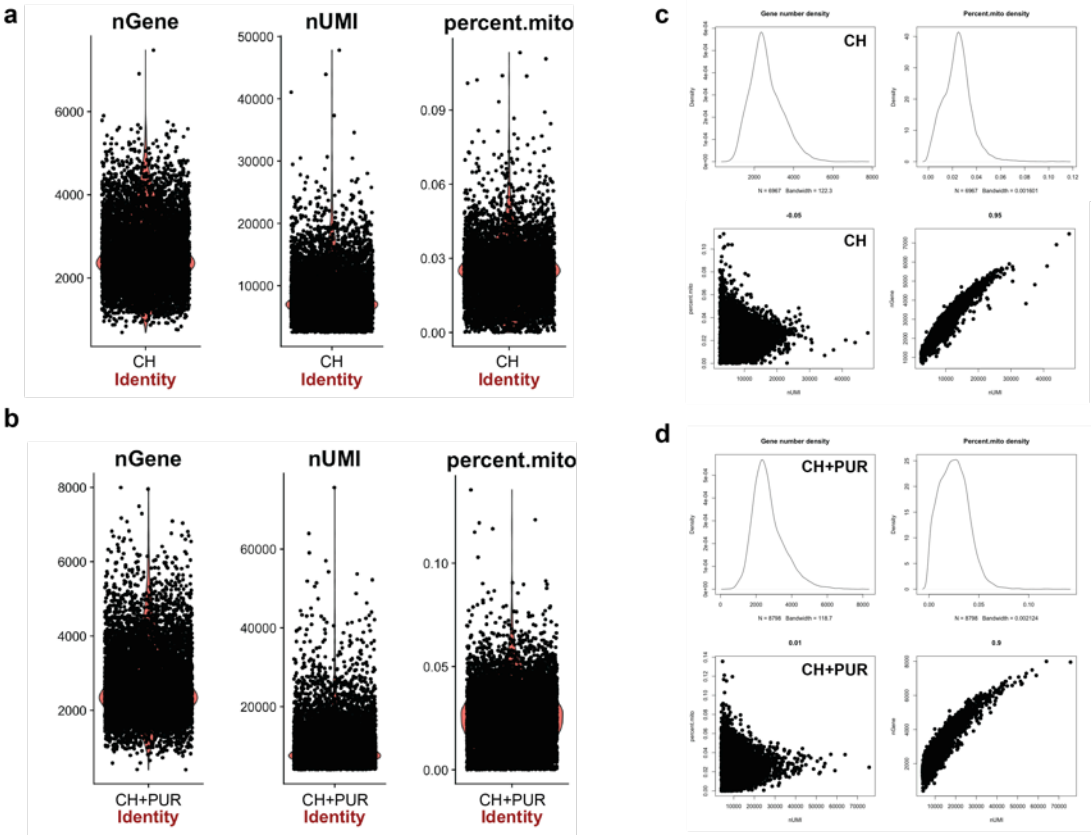

Figure 19: Quality control analysis of CH and CH+PUR treated *PAX2*-2A-nGFP+ 'cell populations.

(**a-b**) Dot plots indicating the number of genes expressed, number of UMI counts, and percentage of mitochondrial genes expressed in the evaluated cell populations for representative CH (**a**) and CH+PUR (**b**) treated cell populations. (**c-d)** Plots illustrating the gene number density and percentage of mitochondrial gene density for CH (**c**) and CH+PUR (**d**) treated cell populations.

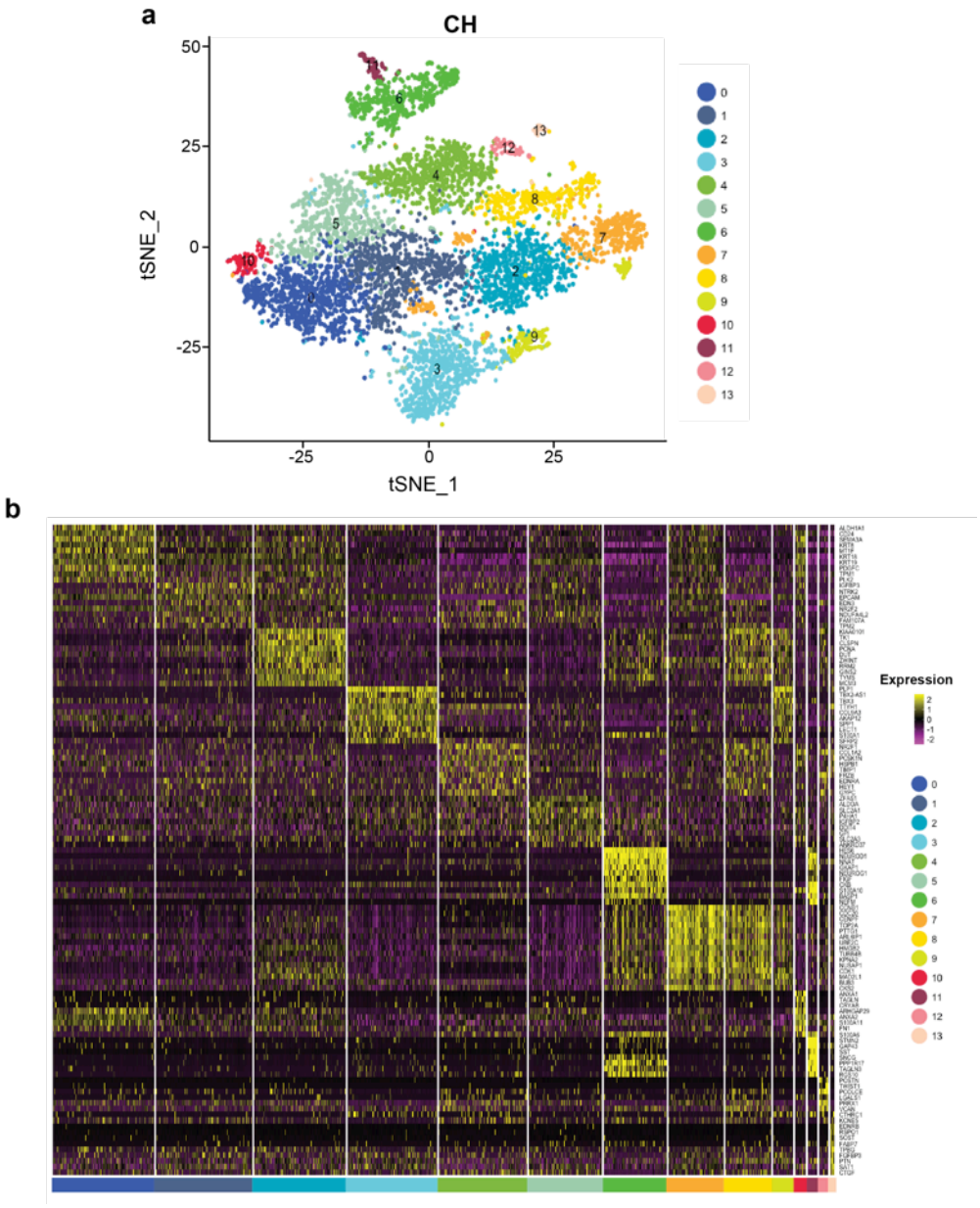

Figure 20: Clustering of CH treated single-cell population.

(**a**) Clustering analysis distinguished 14 individual clusters of differential gene expression (numbered 0-13) in the CH treated sorted cell population. (**b**) Heatmap illustrating differential gene expression among the 14 clusters.

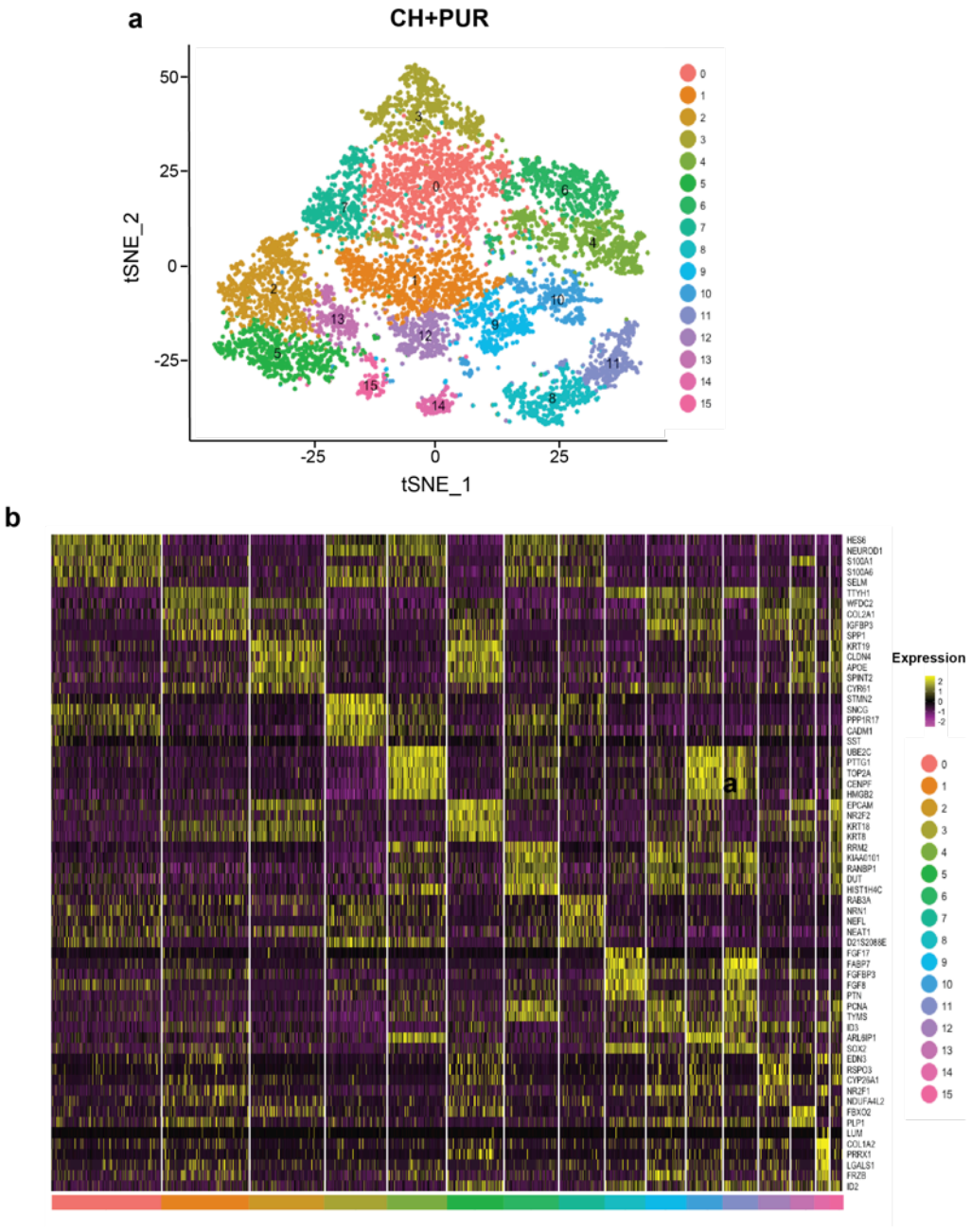

Figure 21: Clustering of CH+PUR treated single-cell population.

(**a**) Clustering analysis distinguished 16 individual clusters of differential gene expression (numbered 0-15) in the CH+PUR treated sorted cell population. (**b**) Heatmap illustrating differential gene expression among the 16 clusters.

total expression, multiplied by a scaling factor of 10,000 and log-transformed. Highly variable genes were then identified for downstream analysis. For the CH dataset, 1609 variable genes were identified (Figure 20). Principle component analysis (PCA) was performed, and a graph-based clustering approach was applied to visualize the data. Non-linear dimensional reduction visualized via t-distributed stochastic neighbor embedding (tSNE) revealed 14 clusters of differential gene expression within the CH dataset. 1668 variable genes and 16 clusters were identified for the CH+PUR dataset (Figure 21) using the same clustering and visualization method.

Evaluation of dorso-ventral patterning markers

The goal of this scRNA-seq analysis was to evaluate the patterning phenotype of early derived otic progenitors in control conditions (CH) and in cells additionally exposed to SHH pathway agonist PUR (CH+PUR) to determine whether control cells exhibit a more dorsalized phenotype, and whether SHH pathway modulation may increase expression of ventral otic markers. Comparative analysis of the two datasets was performed in order to evaluate differential expression of markers of interest between the two treatment groups. In particular for my analysis, focus was initially placed on markers of otic development, SHH pathway component expression, and dorsal and ventral otic vesicle patterning markers. Figure 4, featured in CHAPTER ONE: INTRODUCTION, lists key markers of otic induction, many of which were evaluated among the scRNA-seq datasets.

For comparative analysis, CH and CH+PUR datasets were combined and filtered according to previous mentioned quality control metrics, including mitochondrial gene and total gene expression. Integrated analysis was then performed, in which the pooled datasets were clustered by PCA and visualized via tSNE (Figure 22). Fifteen clusters of differential gene expression were identified for the combined population. Genes of interest were individually evaluated and will be discussed further below.

Otic marker expression observed in PAX2-2A-nGFP+ populations

We first assessed the expression of otic markers among the cell populations of both treatment groups. PAX2 is expressed in otic progenitors of the developing inner ear, but has also been observed in other areas during development, including the central nervous system and kidney [83, 95]. Therefore, we wanted to confirm the presence of an otic population within the isolated *PAX2*-2A-nGFP+ cells. Coinciding with the observations from our immunohistochemical analysis of *PAX2*-2A-nGFP aggregates, both CH and CH+PUR sorted cell populations exhibited expression of otic markers PAX8, SOX2, SOX10, and FBXO2.

Figure 23 shows localization of these markers within both the CH and CH+PUR populations (Figure 23a-d). Between the two treatment groups, the percentages of cells expressing PAX8, SOX10, and FBXO2 were not significantly different (Figure 23e), though variation from marker to marker was observed. Only a small percentage of cells, 2.09±0.46% (±sem, n= 3 independent datasets

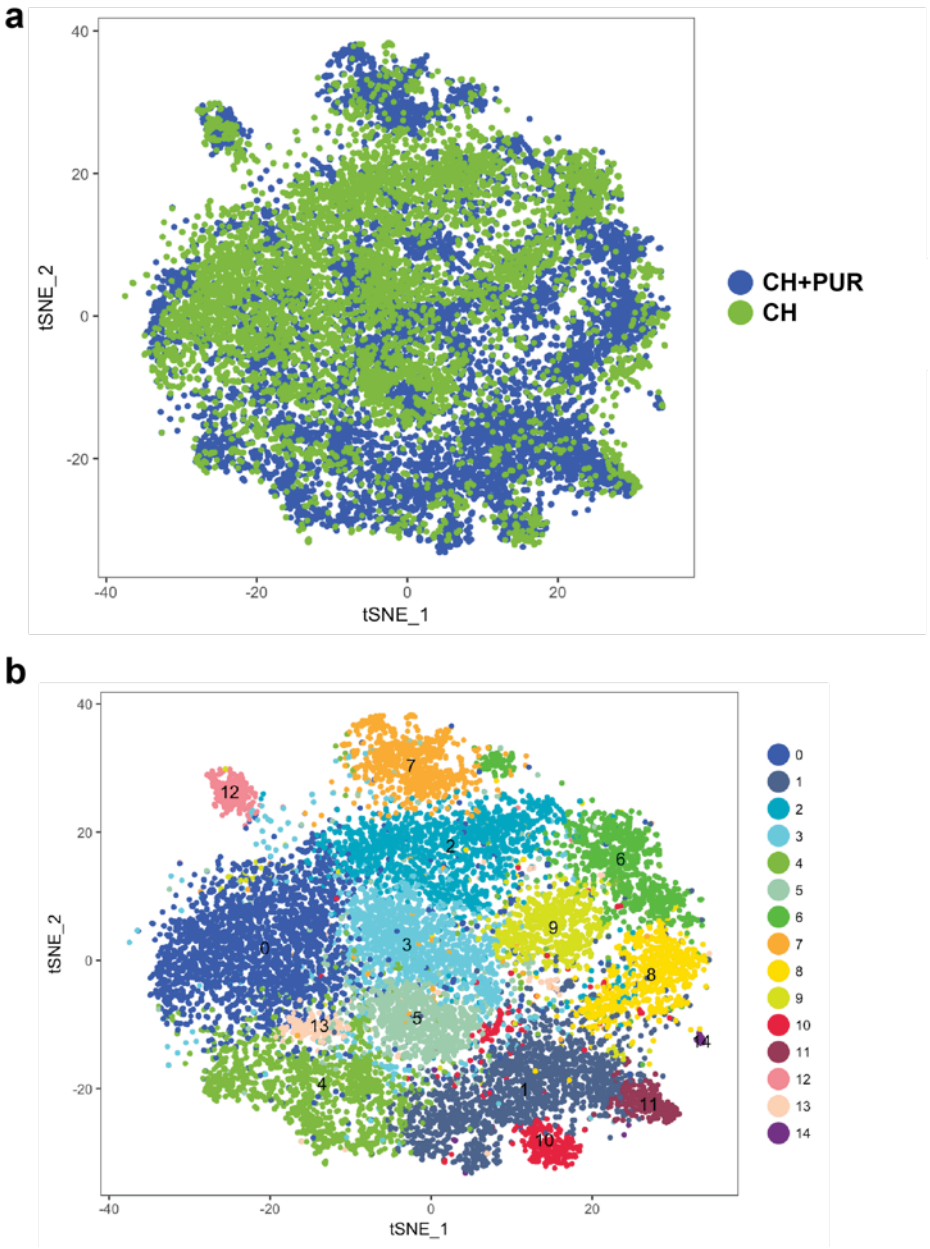

Figure 22: Integrated analysis of CH and CH+PUR datasets.

For comparative analysis, CH and CH+PUR datasets are pooled. Panel (**a**) depicts overlay of the two populations, with CH cells indicated in green and CH+PUR cells indicated in blue. Combined datasets were then subjected to PCA and projected via tSNE for differential clustering (**b**). For the integrated dataset, 15 individual clusters were observed (labeled 0-14).

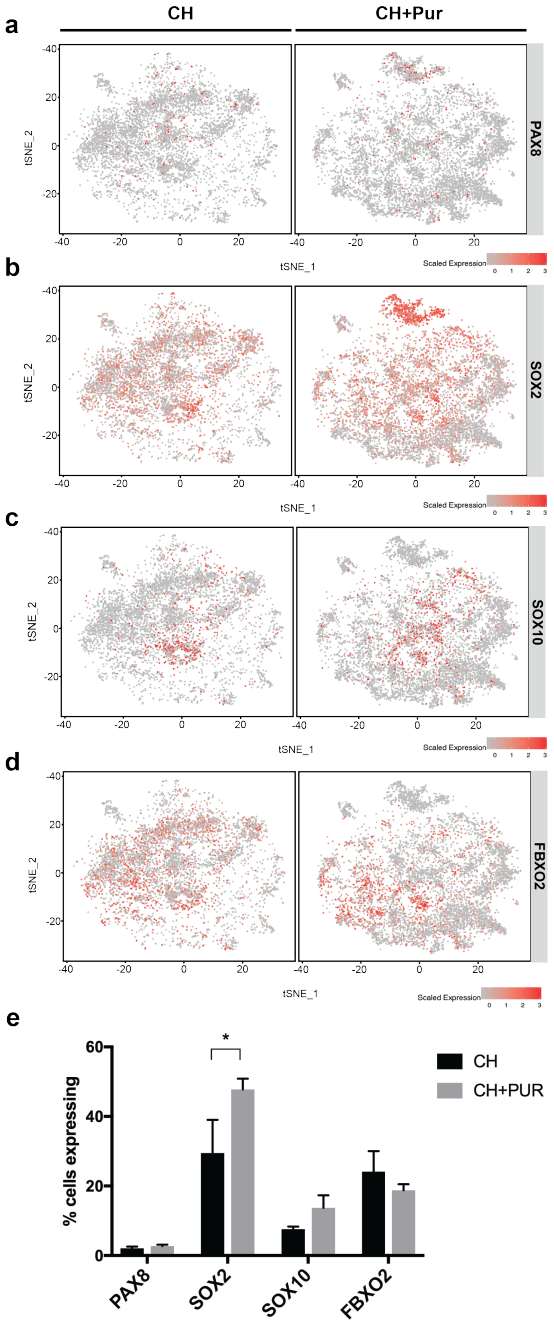

Figure 23: Otic marker expression in single-cell datasets.

Both CH and CH+PUR treated populations were observed to express markers of early otic development include PAX8 (**a**), SOX2 (**b**) SOX10 (**c**), and FBXO2 (**d**). Expression of these markers within the sorted *PAX2*-2A-nGFP+ populations supports an early otic progenitor phenotype within each treatment group. Panel (e) indicates the average percentage of cells expressing these markers across (3) replicate datasets per condition. Error bars indicate sem. * indicates significance, p=0.046.

per treatment group) in the CH treatment group and 2.64±0.25% in the CH+PUR treatment group, expressed otic placode marker PAX8 (Figure 23e). SOX10 was expressed in 7.57±0.73% of CH-treated cells and 13.74±3.59% of CH+PUR treated cells, whereas FBXO2 expression was observed in 24.14±5.90% of CH treated cells and 18.76±1.75% of CH+PUR treated cells. Notably, the percentage of cells expressing otic progenitor marker SOX2 was significantly different between the two treatment groups; SOX2 expression was observed in 29.47±9.53% of CH treated cells, and 47.75±3.14% of CH+PUR treated cells. It is important to note that SOX2 and FBXO2 may also be expressed in neural cell types [96-98].

Overall, single-cell analysis confirmed expression of mRNA for otic markers within both treatment groups, coinciding with our previous observations of protein expression of these markers in *PAX2*-2A-nGFP derived aggregates subjected to our inner ear organoid differentiation protocol (Figure 13). Of the otic markers evaluated, only SOX2 exhibited significant enrichment in the CH+PUR treated population.

Expression of SHH pathway components

We next sought to assess the expression of SHH pathway components within the CH and CH+PUR cell populations, to evaluate whether SHH signaling activation was occurring in the CH+PUR treated cultures. Patched1 (PTCH1) is the cell surface receptor for SHH, and is itself regulated by the SHH signaling pathway [99]. Figure 24 illustrates the localization of PTCH1 expressing cells

amongst the CH and CH+PUR treated populations (Figure 24a). The relative normalized expression of PTCH1 also appeared increased in the CH+PUR treated population, as did the number of cells expressing PTCH1 (Figure 24b). Quantitative analysis across three replicates revealed the percentage of cells expressing PTCH1 was significantly larger in the CH+PUR treated population compared to the population treated with CH alone (Figure 24d).

Evaluation of GLI1, a downstream SHH pathway transcription factor also regulated by SHH signaling [100], demonstrated expression in the representative CH+PUR treated population, but no expression in the CH treated population illustrated in Figure 24 (Figure 24c). However, GLI1 expression was observed in the CH treated populations of the two additional replicate datasets, so the lack of GLI1 expression in this CH dataset appeared to be sample-specific, and may be an artifact of library preparation and/or filtering. Across the three replicate datasets per treatment, GLI1 was expressed in 0.11±0.06% (±sem, n=3 replicates per condition) of CH treated cells, and 2.85±0.64% of CH+PUR treated cells. SHH pathway components SMO, GLI family zinc finger 2 (GLI2), and GLI family zinc finger 3 (GLI3), which are not directly regulated by SHH signaling, were shown to have comparable expression in both the CH and CH+PUR treatment groups (Figure 24d-f). The percentage of cells expressing each of these pathway components was not significantly different between the two treatment groups (Figure 24g). Overall, assessment of SHH pathway components appeared to indicate that GLI2, GLI3, and SMO were unaffected between the two treatment groups. However, SHH pathway-regulated PTCH1 did

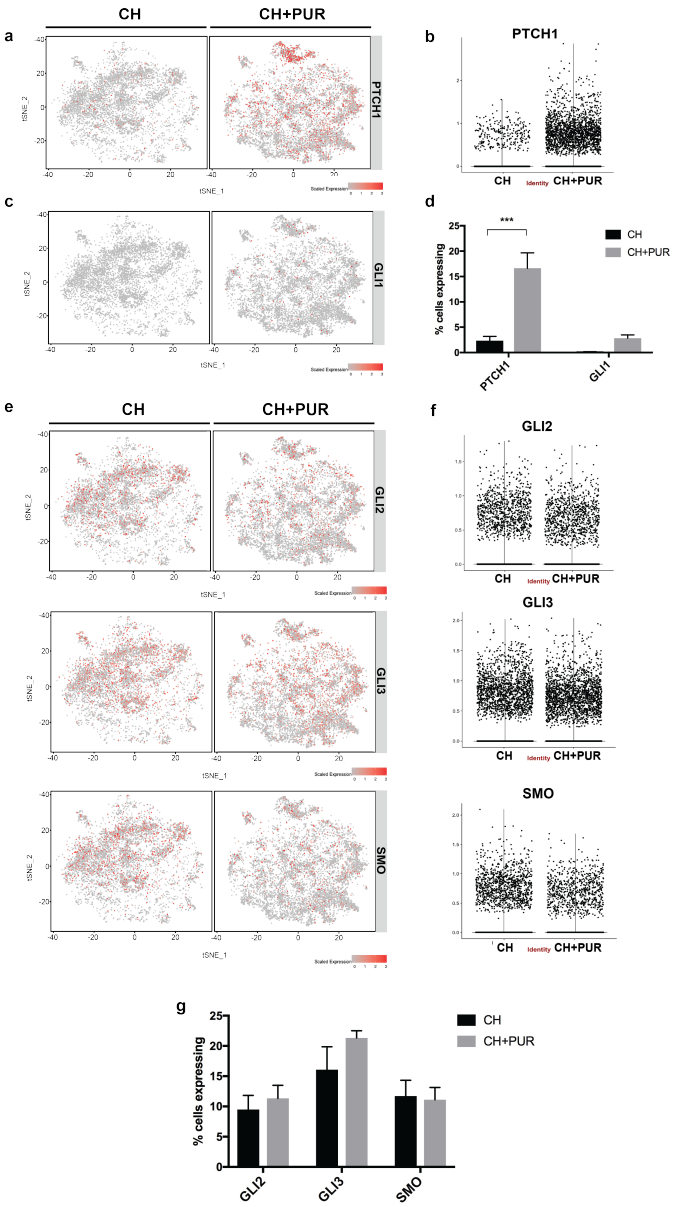

Figure 24: SHH pathway component expression.

(**a**) Comparative analysis revealed differential expression of SHH pathway component PTCH1. (**b**) Violin plots illustrating relative normalized expression of PTCH1 among the single-cell populations; each dot is representative of one cell. (**c**) Localization of GLI1 expression among both treatment groups. (**d**) Average percentages of PTCH1 and GLI1-expressing cells. n=3 replicate datasets per treatment group; error bars indicate sem, * indicates significance, p=0.0005. (**e**) Localization of other SHH pathway components whose expression is not dependent on SHH signaling, GLI2, GLI3, and SMO. (**f**) Violin plots illustrating relative normalized expression of GLI2, GLI3, and SMO. (**g**) Average percentages of GLI2, GLI3, SMO-expressing cells. n= 3 replicate datasets per treatment group, error bars indicate sem.

exhibit increased expression in the CH+PUR treated population, supporting SHH pathway activation following PUR treatment in inner ear organoid cultures.

Ventral patterning marker analysis

Several previously validated markers of the ventral otic vesicle, including LFNG, OTX1, and OTX2 [29, 31, 101], were evaluated in the CH and CH+PUR datasets to determine whether CH+PUR treatment enhances expression of ventral genes. Figure 25 illustrates the localization of each marker among the CH and CH+PUR populations among one set of representative samples (Figure 25a). Violin plots illustrate the relative normalized expression of each marker per treatment group (Figure 25b). Across three replicate datasets, a significantly higher percentage of cells expressing LFNG was observed in the CH+PUR treated population compared to those cells receiving CH alone, with 8.21±1.45% (±sem, n=3 replicates per condition) of CH+PUR treated cells expressed LFNG and 1.68±0.21% of CH treated cells expressing LFNG (Figure 25c). Additionally, a significantly higher percentage of CH+PUR treated cells expressed OTX1 (6.08±2.00%), compared to 0.77±0.39% of CH treated cells (Figure 25c). However, expression of ventral marker OTX2 was seen in a higher percentage of cells in the CH-treated group compared to CH+PUR, with 1.46±0.18% of CH-treated cells expressing OTX2, compared to 0.78±0.02% of CH+PUR treated cells, although the difference was not statistically significant across the triplicate datasets. Immunohistochemical analysis of OTX2 revealed the occurrence of both OTX2+ cells and GFP+/OTX2+ cells (Figure 26). The single-positive

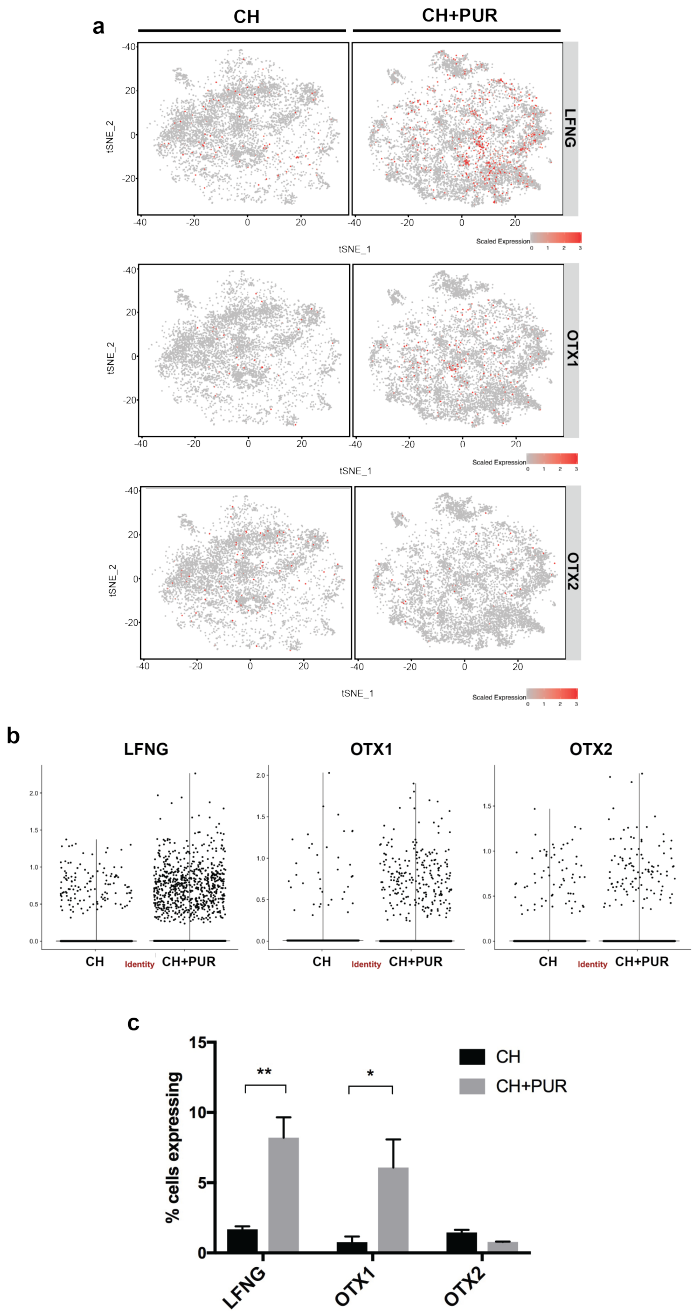

Figure 25: Ventral patterning marker analysis.

(**a**) Dot plots illustrating localization of ventral markers within each treatment group; datasets were normalized for comparative analysis. (**b**) Violin plots of candidate ventral genes LFNG, OTX1, and OTX2. Y-axis represents relative normalized expression. Each dot corresponds with a cell expressing the candidate gene. (**c**) Average percentage of cells expressing each marker; n= 3 replicate datasets per treatment group, error bars indicate sem, ** indicates significance, p=0.0022, * indicates significance, p= 0.01.

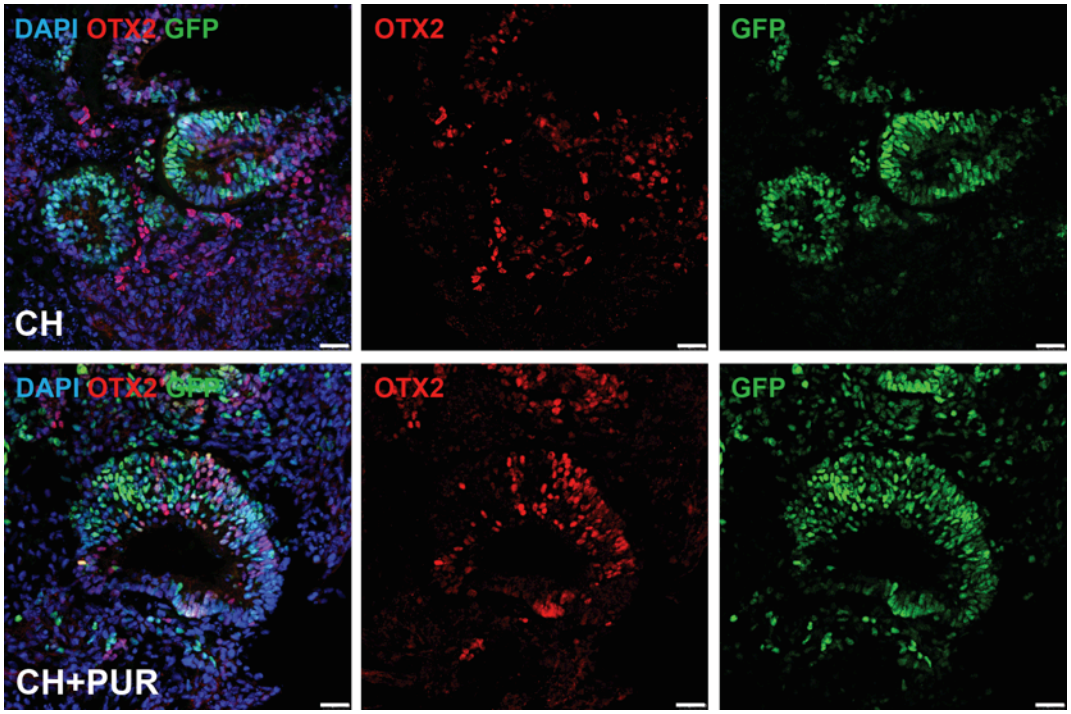

Figure 26: Immunohistochemical analysis of ventral marker OTX2 in CH and CH+PUR treated aggregates.

Staining for OTX2 and GFP in cryosections of early stage aggregates reveal localization of OTX2 in GFP+ vesicles. OTX2+/GFP+ cells are observed in both treatment groups, along with OTX2+/GFP- cells. Scale bars = 25 µm.

population was likely excluded due to FACS isolating *PAX2-2*A-nGFP+ cells only, and may not be representative of the total OTX2+ cell population co-localizing with GFP+ vesicles. *In vivo*, PAX2 and OTX2 expression does not overlap completely [84]; therefore, the OTX2+/GFP- population in the derived aggregates may still be representative of otic progenitors exhibiting a ventral phenotype.

Dorsal patterning marker analysis

Single-cell analysis was used to interrogate patterning markers of the dorsal otic vesicle, the region from which the vestibular organs arise. We first evaluated expression of distal-Less homeobox transcription factors DLX3, DLX5, and DLX6 (Figure 27), which are expressed in the dorsal otic vesicle [102]. Both DLX3 and DLX5 appeared to exhibit lower relative normalized expression in the CH+PUR treated group compared to cells treated with CH alone (Figure 27b). The percentage of cells expressing DLX5 was not significantly different between the two treatment groups, as was the case with DLX6 (Figure 27c). However, DLX3 was expressed in a significantly lower percentage of cells treated with CH+PUR compared to the CH treated population with expression observed in 5.45±1.02% (±=sem, n=3 replicate datasets) of CH+PUR treated cells compared to 17.27±4.17% of cells treated with CH alone (Figure 27c). The results with DLX3 were supported by immunohistochemical analysis, wherein DLX3 expression was observed co-localized in areas of GFP expression in CH treated aggregates, but not in CH+PUR treated aggregates (Figure 28).

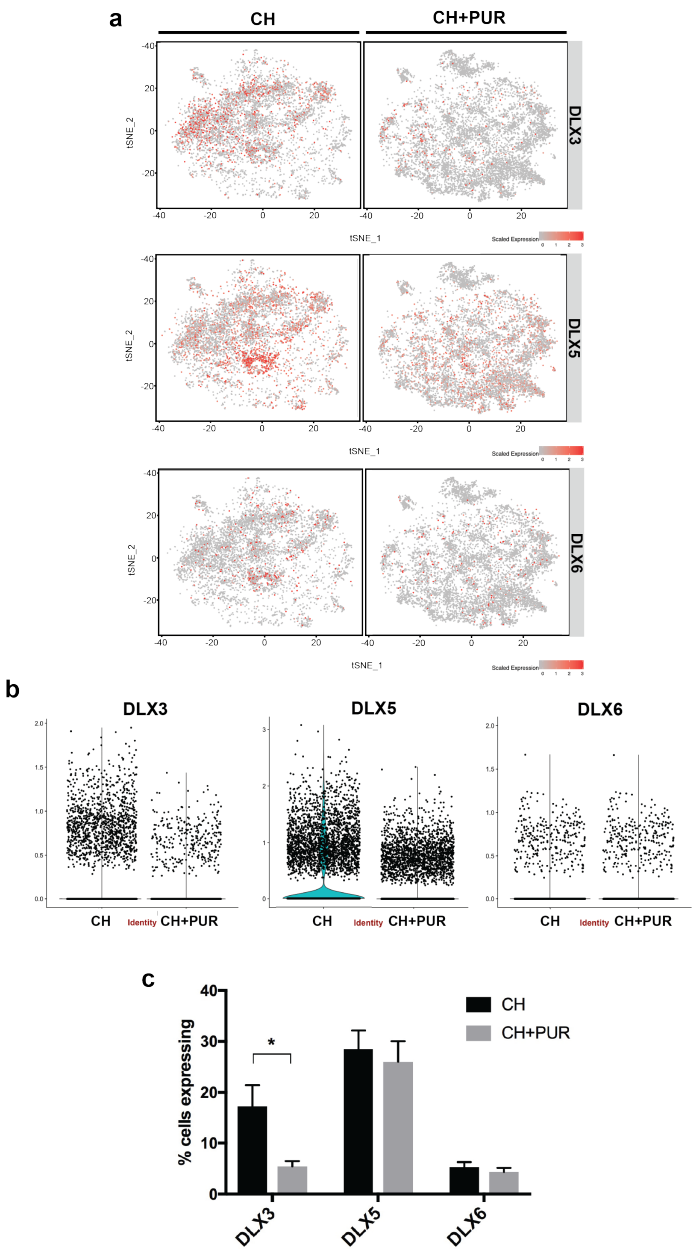

Figure 27: Expression of dorsal markers DLX3, DLX5 and DLX6 in CH and CH+PUR treated populations.

(**a**) Localization of dorsal markers DLX3, DLX5, and DLX6 within the CH and CH+PUR treated populations. Datasets have been normalized for comparative analysis. (**b**) Violin plots illustrating expression of DLX3, DLX5, and DLX6. Y-axis represents relative normalized expression. (**c**) Percentage of cells expressing DLX markers within the CH and CH+PUR datasets. Error bars indicate sem, * indicates significance, p= 0.0385.

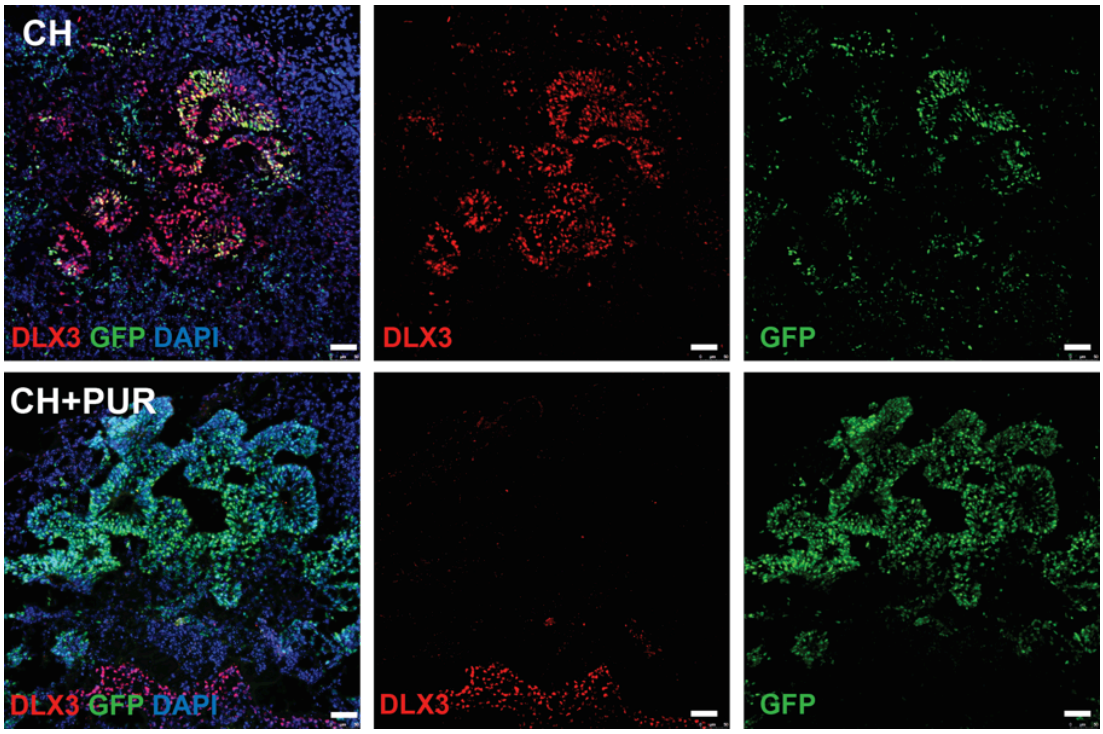

Figure 28: Immunohistochemical analysis of dorsal marker DLX3 in CH and CH+PUR treated aggregates.

Cryosections from CH and CH+PUR treated aggregates stained for DLX3 and GFP revealed co-localization of DLX3 with GFP+ areas in CH but not CH+PUR treated sections. A DLX3+/GFP- population was also observed. Scale bars = 50 µm.

Both populations also exhibited expression of dorsal markers LMX1A and WNT2B (Figure 29a). However, a significantly lower percentage of cells treated with CH+PUR expressed WNT2B, with 2.22±0.64% of CH+PUR treated cells expressing WNT2B, compared to 6.69±0.76% of cells in the CH treated population (Figure 29b). Additionally, a significantly lower percentage of CH+PUR treated cells expressed LMX1A, with 0.74±0.31% of CH+PUR treated cells exhibition LMX1A expression, compared to 5.80 ±1.63% of cells in the population receiving CH alone (Figure 29b). Relative normalized expression also appeared lower in the CH+PUR treated group compared to the CH treated group for both markers (Figure 29c).

Overall, these findings indicate a significant reduction in the incidence of select dorsal markers among the CH+PUR treated population, although the phenotype does not appear consistent across all dorsal markers examined.

Increased neural population observed in SHH pathway modulated cell population

During development, the cochleo-vestibular ganglion emerges from the antero-ventral region of the otic vesicle, initially observed as a population of cells expressing transcription factors NEUROG1 and NEUROD1 [103]. Interestingly, single-cell analysis revealed significantly higher expression of both neural factors among the CH+PUR treated population. Figure 30 illustrates the localization and relative normalized expression of NEUROD1 (Figure 30a) and NEUROG1 (Figure 30b) among the CH and CH+PUR treated populations.

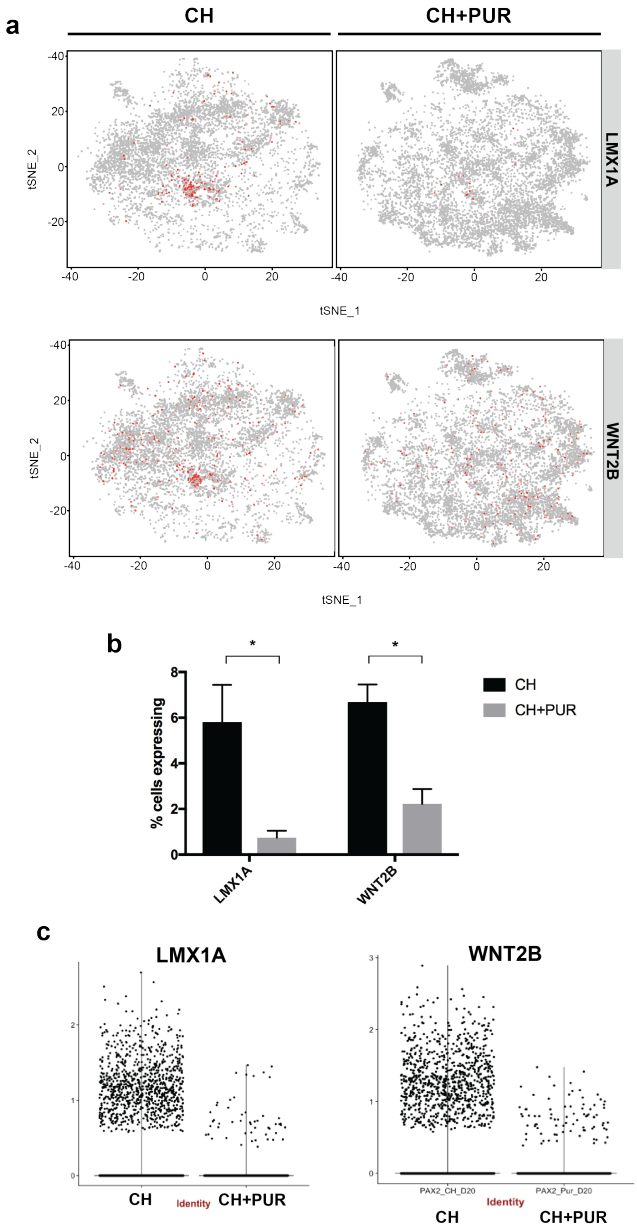

Figure 29: Evaluation of additional dorsal markers within the CH and CH+PUR sorted populations.

(**a**) Localization of dorsal markers LMX1A and WNT2B within the CH and CH+PUR treated populations. Datasets have been normalized for comparative analysis. (**b**) Average percentage of cells expressing LMX1A and WNT2B within the CH and CH+PUR datasets. Error bars indicate sem, * indicates significance, p=0.0124 (LMX1A), p=0.0234 (WNT2B). (**c**) Violin plots illustrating expression of LMX1A and WNT2B. Y-axis represents relative normalized expression.

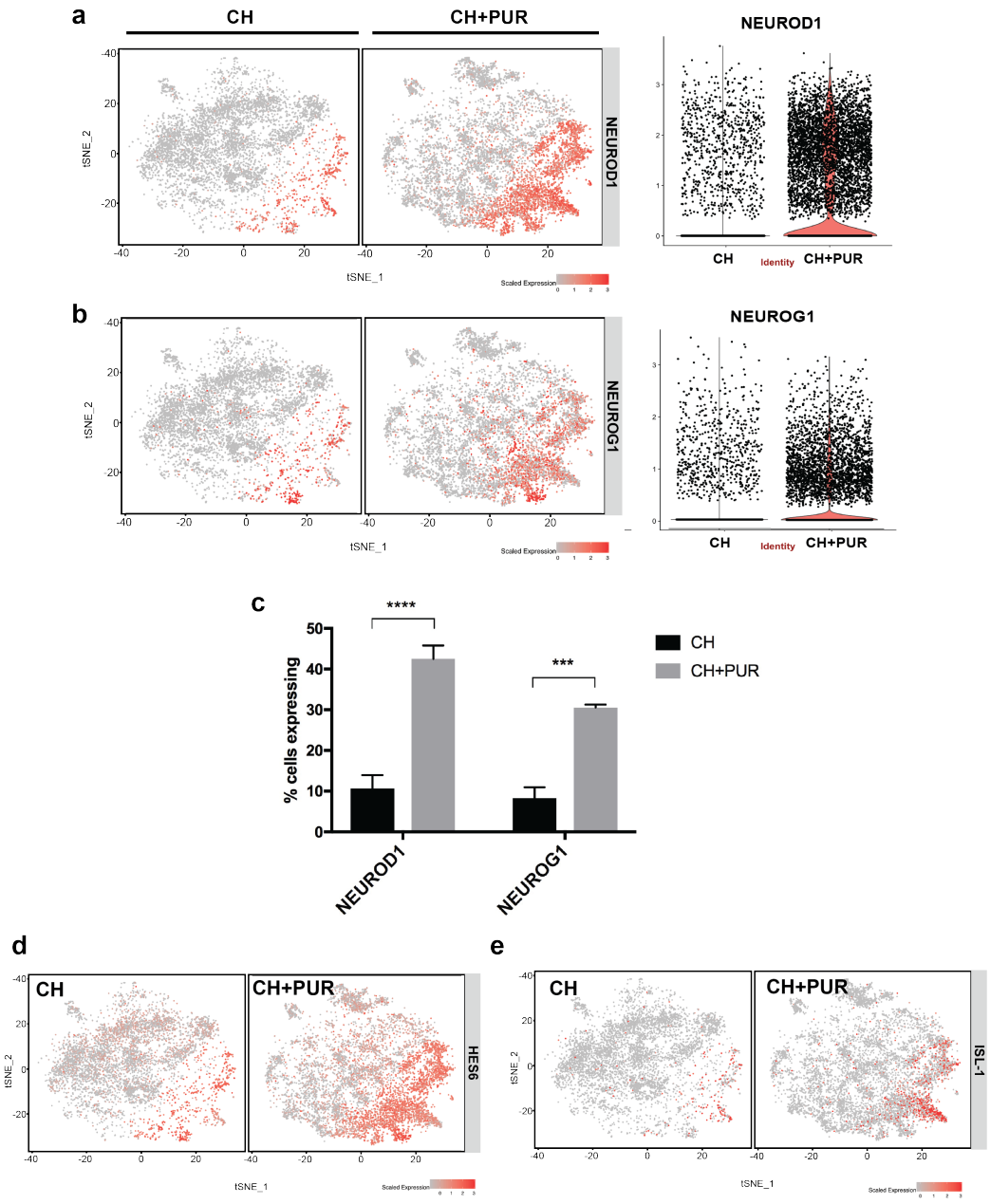

Figure 30: CH+PUR treated cultures exhibit an increased neural population.

Localization and relative normalized expression of inner ear neuroprogenitor markers NEUROD1 (**a**) and NEUROG1 (**b**). (**c**) Average percentage of cells expressing NEUROD1 and NEUROG1 (n= 3 replicates per treatment). Error bars indicate sem, **** indicates significance, p<0.0001, *** indicates significance, p=0.008 (**d**-**e**) Expression patterns of inner ear neural markers HES6 (**d**) and ISL-1 (**e**) in the CH and CH+PUR treated populations.

Among the CH+PUR population, 42.52±3.27% (±= sem, n= 3 replicate datasets per condition) of cells expressed NEUROD1 and 30.54±0.71% cells expressed NEUROD1, while the CH treatment group exhibited NEUROD1 expression in 10.67±3.27% of cells, and NEUROG1 expression in 8.30±2.67% of cells (Figure 30c).

In mice, Neurog1 expression precedes NeuroD expression in otic neural precursors, with Neurog1 observed at E9.0, and NeuroD induction observed by E9.5 [104]. Both the CH and CH+PUR cell populations exhibited a larger percentage of cells expressing NEUROD1 compared to NEUROG1. The CH and CH+PUR presumptive neural populations additionally contained cells expressing proneural markers HES6 (Figure 30d) and ISL-1 (Figure 30e). Cells exhibiting expression of these markers within the NEUROD1/NEUROG+ clusters mirror the phenotype of neuroblasts delaminating from the early otic vesicle [96, 105, 106].

Immunohistochemical analysis confirmed NEUROD1 protein expression in both CH and CH+PUR treated aggregates (Figure 31). Figure 31 illustrates the co-localization of NEUROD1 within *PAX2*-2A-nGFP+ vesicles in both treatment groups. NEUROD1+/GFP+ cells were observed within the vesicles. Both treatment groups additionally exhibited NEUROD1+/GFP- cells both within and surrounding the vesicles.

The expanded neural population observed in the CH+PUR cell population spurred interrogation of additional neural markers among the CH and CH+PUR scRNA-seq datasets. We previously observed the emergence of cells co-expressing neuronal markers TUBB3 (TUJ1) and POU4F1 between 20-30 days

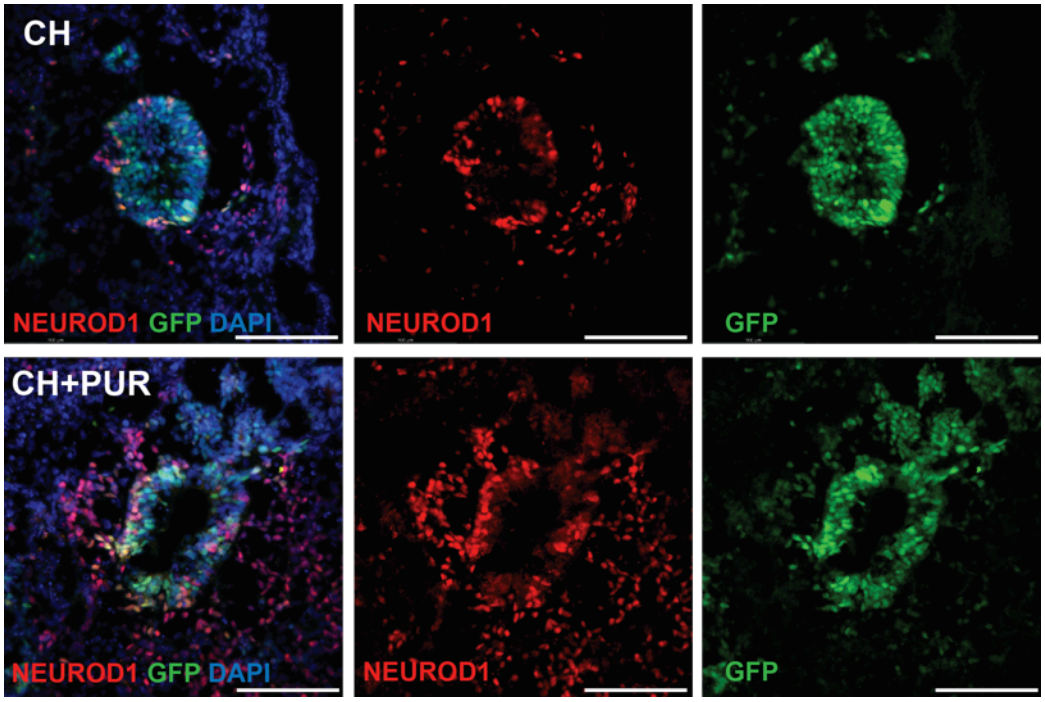

Figure 31: Immunohistochemical analysis of inner ear neuroprogenitor marker NEUROD1 in CH and CH+PUR treated aggregates.

Antibody staining for NEUROD1 confirms scRNA-seq observations of an increased NEUROD1 population in CH+PUR treated aggregates. A NEUROD1+/PAX2- population is also observed in both treatment conditions. Scale bars = 100 μm.

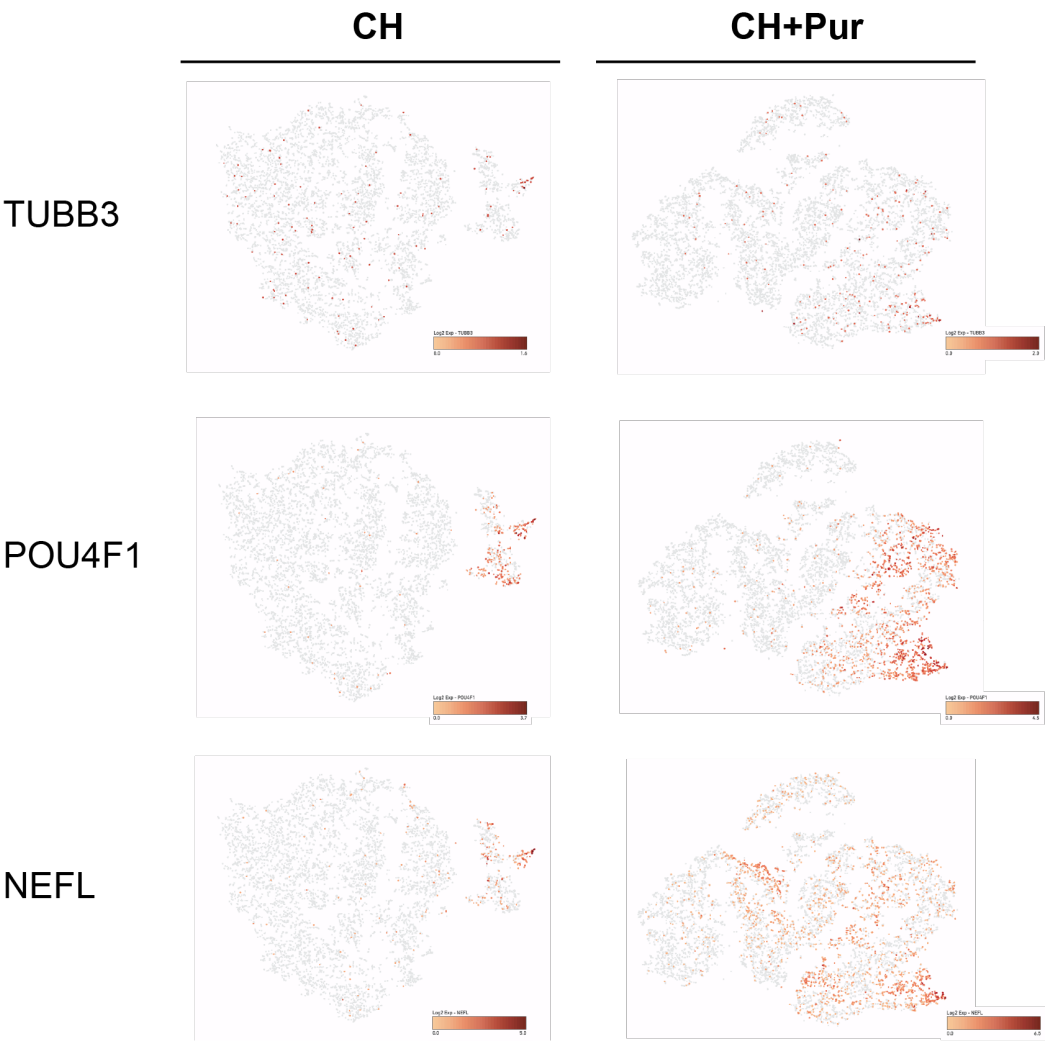

Figure 32: Additional neural marker expression in CH and CH+PUR treated populations.

Expression of neural markers TUBB3, POU4F1, and NEFL was observed in both CH and CH+PUR treated populations, with expanded expression of POU4F1 and NEFL observed in the CH+PUR treated cells. Scales indicate Log2 gene expression.

of inner ear organoid culture [19]. Single-cell analysis revealed that this population is evident in both CH and CH+PUR treated *PAX2*-2A-nGFP+ cells (Figure 32). Figure 32 depicts individual populations from representative CH and CH+PUR datasets. These plots were generated using Loupe Cell Browser software, and represent datasets that have not been integrated for comparative analysis. As such, quantitative observations cannot be made from these plots. Additional comparative analysis may be performed in order to facilitate quantitative analysis. Nonetheless, Figure 32 illustrates expression of both TUBB3 and POU4F1 among the CH and CH+PUR datasets. TUBB3-expressing cells are interspersed throughout the CH treated population, while POU4F1 exhibits highly restricted localization to a presumptive neural cluster. Within the CH+PUR treated population, TUBB3 is also exhibited across the population, while POU4F1 expression is robust and highly exhibited within the presumptive neural clusters. Additionally, expression of Neurofilament light chain (NEFL), a marker abundantly expressed in axons of the central nervous system (CNS) and peripheral nerves, appeared enriched in the CH+PUR treated population compared to cells treated with CH alone (Figure 32). Previously published immunohistochemical analysis revealed expression of NEFL in day 60-75 inner ear organoids [19]. This scRNA-seq analysis indicates the presence of this presumptive neural NEFL+ population in otic vesicle stage aggregates.

Due to the neuroprogenitor-like phenotype observed within the scRNA-seq datasets, we elected to examine the expression of markers indicative of vestibular ganglion or spiral ganglion development within the individual datasets.

Both the CH and CH+PUR populations exhibited expression of markers of vestibular ganglion development ONECUT1 and PCDH19 [107] (Figure 33). Within the CH treated population, ONECUT1+ cells appeared restricted to the NEUROD1/NEUROG1+ presumptive neural cluster, whereas expression of PCDH19 was observed both within and outside of this presumptive neural population. In the CH+PUR treated population, ONECUT1+ cells were observed among the presumptive neural population. Expression of PCDH19 was observed both within the presumptive neural population and elsewhere in the population as a whole (Figure 33).

Expression of SGN-associated markers SHOX2, INSM1, INSM2, and ST18 was additionally observed in both populations (Figure 34). In the CH treated population, expression appeared restricted to the presumptive neural clusters. In the CH+PUR population, robust expression of SHOX2 and INSM1 was observed, along with expression of INSM2 and ST18 in the expanded presumptive neural regions. BDNF expression was also seen in both treatment groups; this factor has been shown to be a key element for the development of synaptic connections between SGNs and sensory cells of the cochlea [104, 108].

Expression of these markers could be indicative of SGN and VGN precursors arising within the presumptive neural populations of both treatment groups, with more widespread expression observed in the CH+PUR treated population. Taken together, these data support a neural phenotype in both CH and CH+PUR treated cell populations reminiscent of progenitors of the cochleovestibular ganglion. Interestingly, cells expressing these markers appear

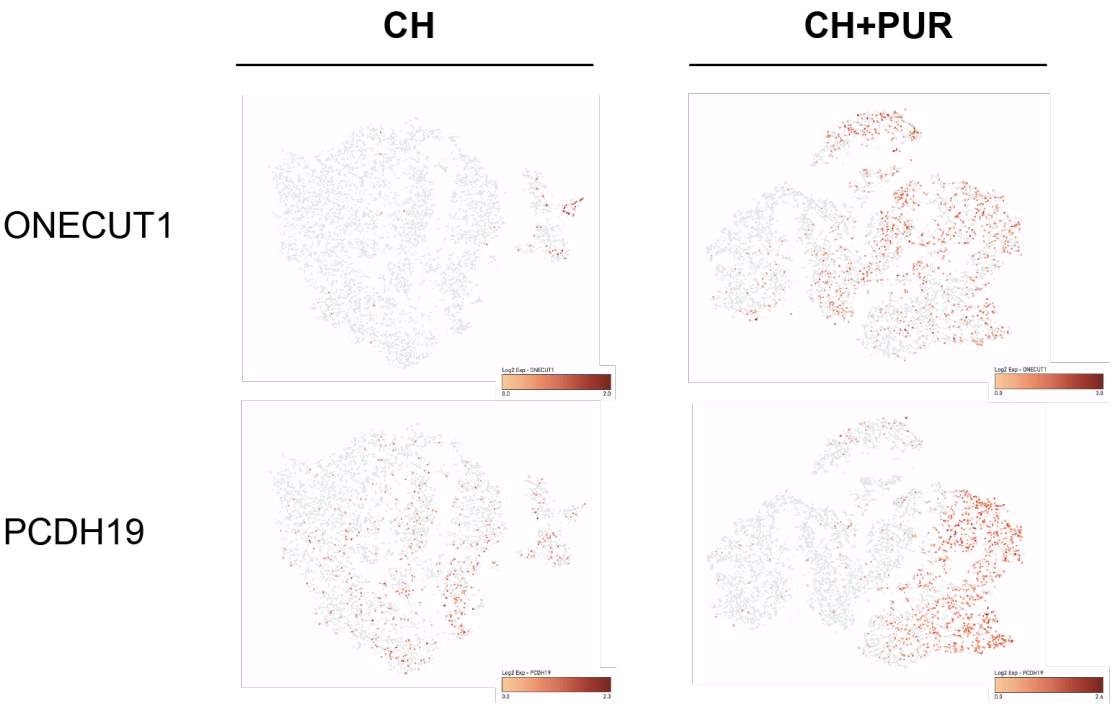

Figure 33: Markers of vestibular ganglion neuron development.

scRNA-seq analysis revealed expression of markers of vestibular ganglion neuron development, ONECUT1 and PCDH19, in both the CH and CH+PUR populations. Scales indicate Log2 gene expression.

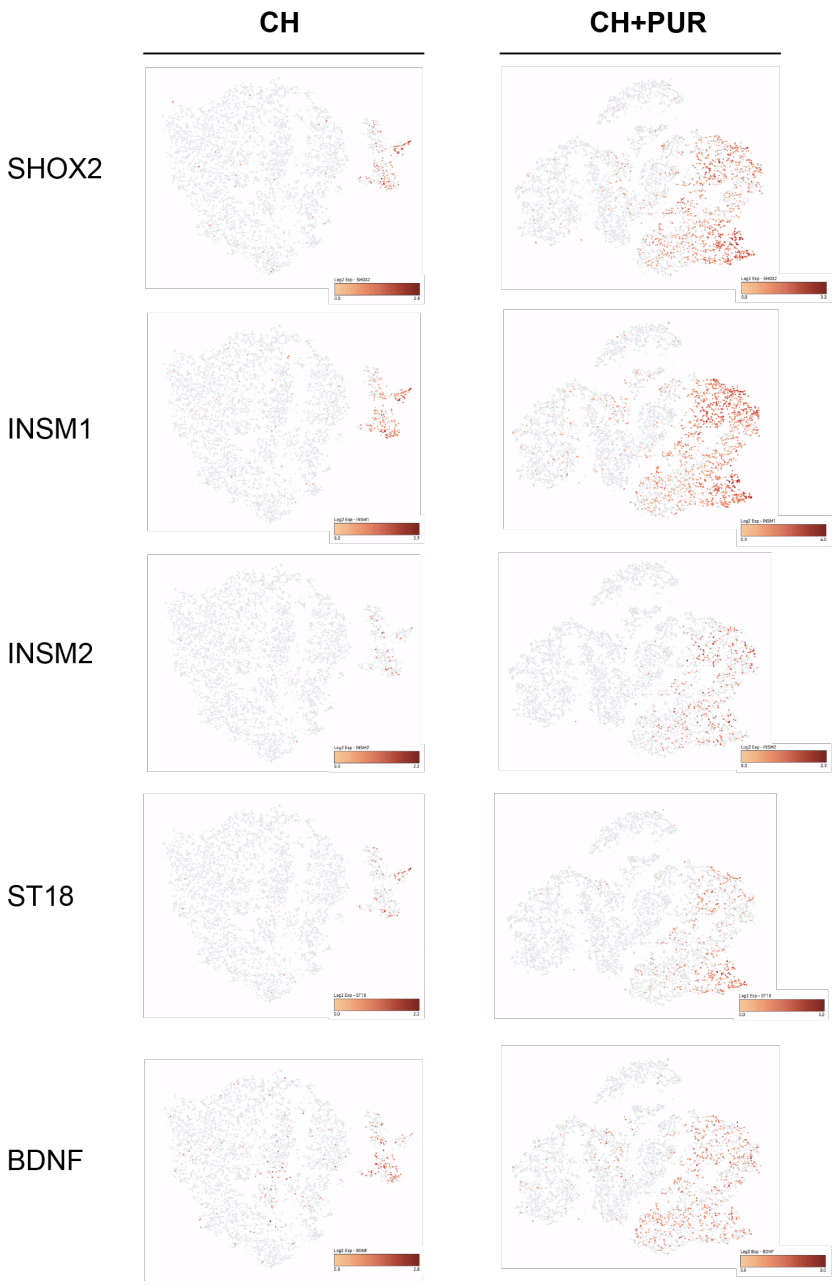

Figure 34: Markers of spiral ganglion neuron development.

Both CH and CH+PUR treated populations contained cells expressing spiral ganglion neuron markers SHOX2, INSM1, INSM2, and ST18. BDNF, a factor necessary for the development of connections between SGNs and cochlear hair cells, is also expressed. Scales indicate Log2 gene expression.

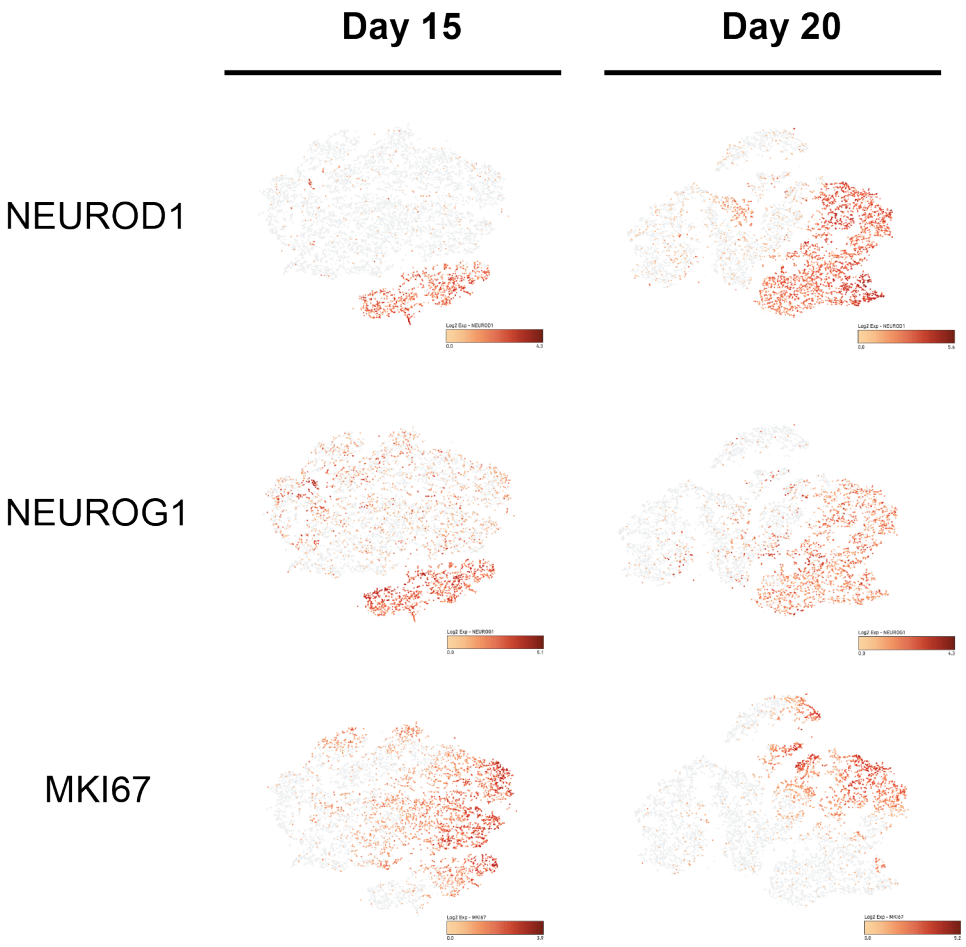

Figure 35: Temporal analysis of CH+PUR treatment.

scRNA-seq analysis of day 15 CH+PUR treated samples was performed for comparison with day 20 CH+PUR treated samples. Expansion of the NEUROD1 population was observed, along with restriction of NEUROG1 expression from day 15 to day 20. MKI67 expression also appeared downregulated between the two timepoints. Scales indicate Log2 gene expression.

enriched in the population receiving CH+PUR during otic vesicle formation, indicating that SHH pathway modulation in early stage culture may bias differentiation toward a neuroprogenitor rather than an epithelial fate.

Temporal gene expression changes in Purmorphamine treated cultures

Time course analysis was performed to track temporal expression of markers of inner ear development in response to SHH pathway modulation. *PAX2*-2A-nGFP aggregates were treated with CH+PUR on culture day 11 and collected on culture day 15. At this timepoint, *PAX2*-2A-nGFP+ cells are observed localized to presumptive otic pit regions extending from the surface of the aggregates (Figure 10). scRNA-seq was performed on sorted day 15 *PAX2*-2A-nGFP+ cells for comparison to a day 20 CH+PUR treated dataset. Preliminary analysis revealed an expansion of the NEUROD1+ population from day 15 to day 20 (Figure 35). Conversely, more widespread and robust NEUROG1 expression was observed throughout the population on day 15, becoming somewhat more restricted by day 20. There was also an apparent reduction in expression of cell cycle marker MKI67 from day 15 to day 20, indicating a potential decrease in proliferation between these two timepoints (Figure 35).

Late stage evaluation of Purmorphamine treatment

Preliminary late stage analysis was performed to assess the effects of dual CH+PUR treatment on late stage aggregates, with an emphasis on hair cell

differentiation, to evaluate if SHH pathway modulation impacts the derived hair cell population, in particular biasing differentiation toward a cochlear fate. While early stage CH+PUR treated aggregates appeared to exhibit a reduction in dorsal marker expression compared to aggregates treated with CH alone and an increase in the number of cells expressing ventral markers LFNG and OTX1, the neural phenotype was the more striking observation following CH+PUR treatment, compared to the more modest effects on dorso-ventral patterning. We evaluated late stage inner ear organoids (≥day 60) to see if this early stage phenotype impacted later stage development.

CH+PUR treatment was performed on early stage inner ear organoids cultured from human ESCs containing a GFP reporter for hair cell marker ATOH1 (previously described in [19]). *ATOH1*-2A-nGFP human ESC derived aggregates cultured long-term produce organoids containing GFP+ cells that co-express hair cell marker MYO7A [19]. Derived *ATOH1*-2A-nGFP+ cells were also reported to exhibit functional capability similar to that observed in the native mouse utricle [19].

While induction of *ATOH1*-2A-GFP+ cells was observed in CH+PUR treated aggregates, the derived sensory population appeared to be reduced in late stage CH+PUR treated aggregates compared to aggregates treated with CH alone (Figure 36). Quantitative analysis is necessary to confirm whether this perceived reduction in *ATOH1*-2A-GFP induction in late stage CH+PUR treated aggregates is significant.

Immunohistochemical analysis was performed to assess whether the derived hair cells in CH+PUR treated organoids exhibit a cochlear phenotype. Leiomodin 3 (LMOD3) is a marker specific to both inner and outer cochlear hair cells (Figure 37a), and is not expressed in vestibular sensory epithelia (Figure 37b). Immunohistochemical analysis showed that derived hair cells from both CH and CH+PUR-treated aggregates did not express LMOD3 (Figure 37d). A lack of expression of this specific and established marker of cochlear identity appears to indicate that derived hair cells arising in CH+PUR treated aggregates do not exhibit a cochlear phenotype. Further evaluation is necessary to confirm a vestibular identity of these cells.

Immunohistochemical analysis additionally confirmed expression of neural marker TUBB3 (TUJ1) in both CH and CH+PUR treated organoids (Figure 38). Further evaluation of this late stage neuronal population is currently underway to determine whether the observations of an expanded neural population in early stage CH+PUR treated cultures translate to a late stage phenotype.

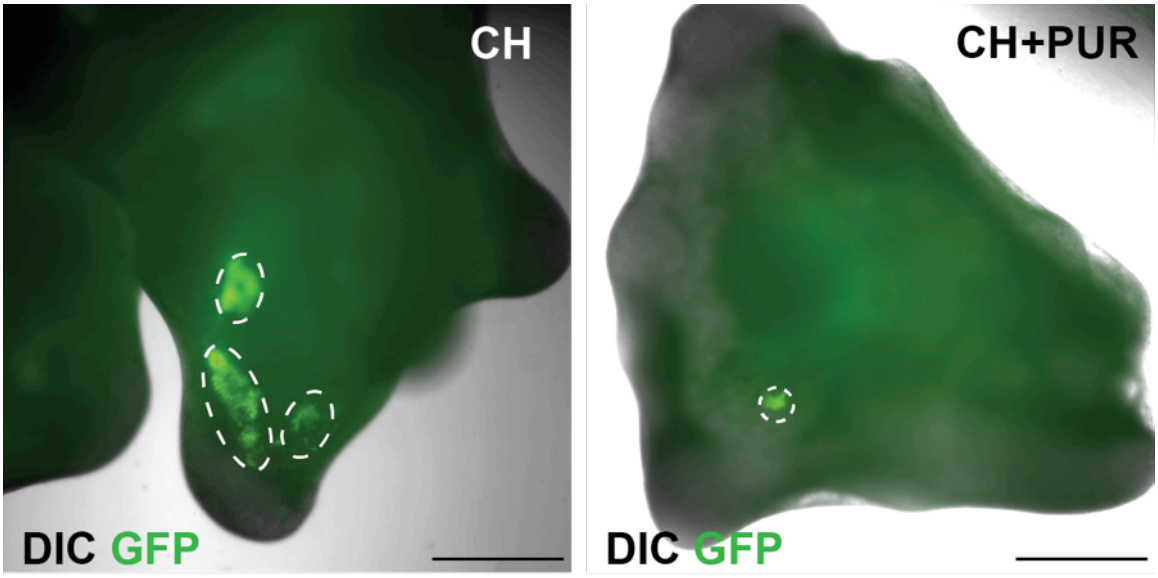

Figure 36: *ATOH1*-2A-GFP+ population appears reduced in late stage CH+PUR treated aggregates.

DIC/FITC overlay of live day 60 *ATOH1*-2A-GFP derived aggregates. Day 60 CH treated aggregate exhibiting three *ATOH1*-2A-GFP+ patches. CH+PUR treated aggregate exhibits one *ATOH1*-2A-GFP+ patch. Dashed lines indicate GFP+ cell populations. Scale bars = 500 µm.

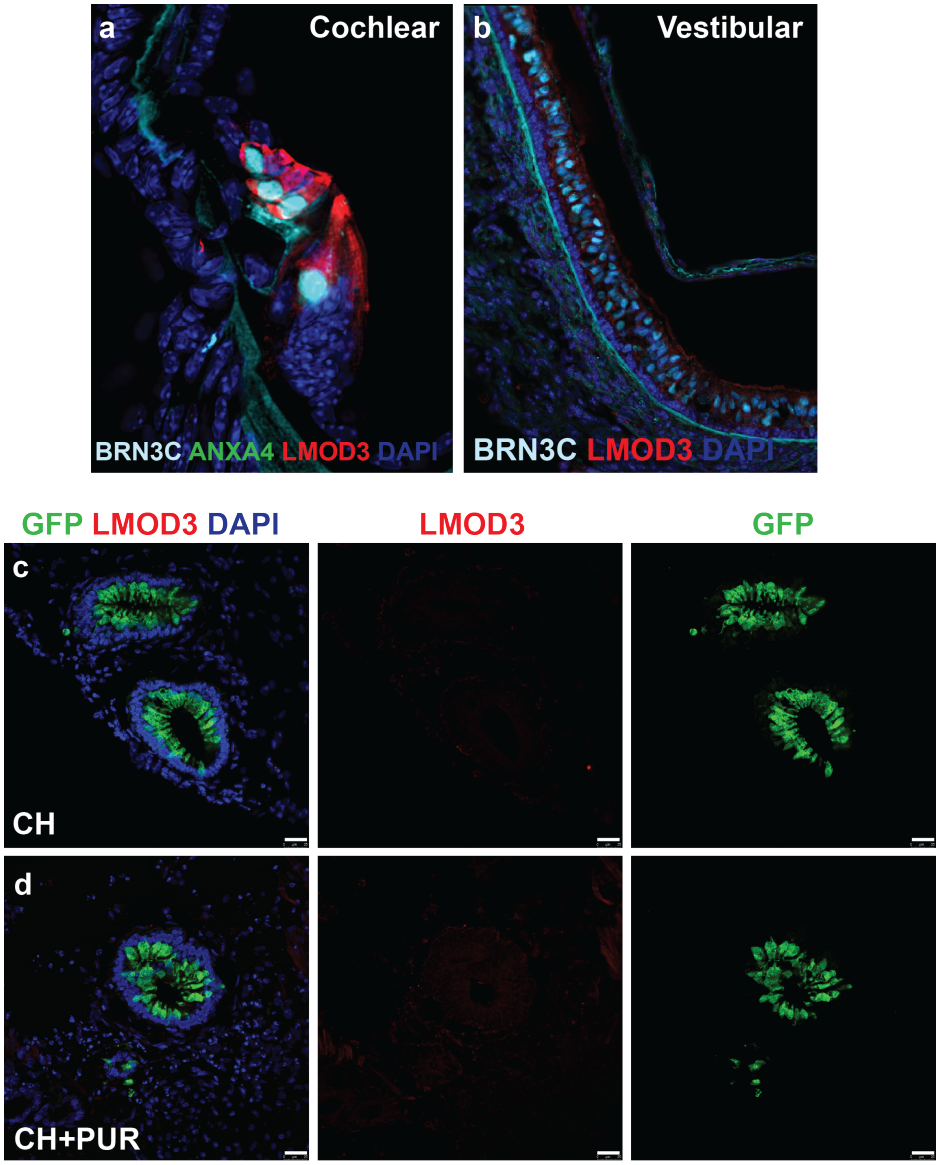

Figure 37: Late stage inner ear organoids do not express cochlear hair cell marker LMOD3.

(**a**) Cross section of P8 mouse cochlea, Robust LMOD3 expression observed in both inner and outer cochlear HCs.BRN3C and ANXA4 are generic hair cell markers expressed in both cochlear and vestibular hair cells. (**b**) Cross section of P8 mouse utricle. Utricular tissue lacks LMOD3 expression. (**c**) LMOD3 expression is not observed in Day 60 CH-treated *ATOH1*-2A-GFP aggregates. (**d**) Purmorphamine treated aggregates at the same time point are LMOD3^{-}. Scale bars = 25 µm.

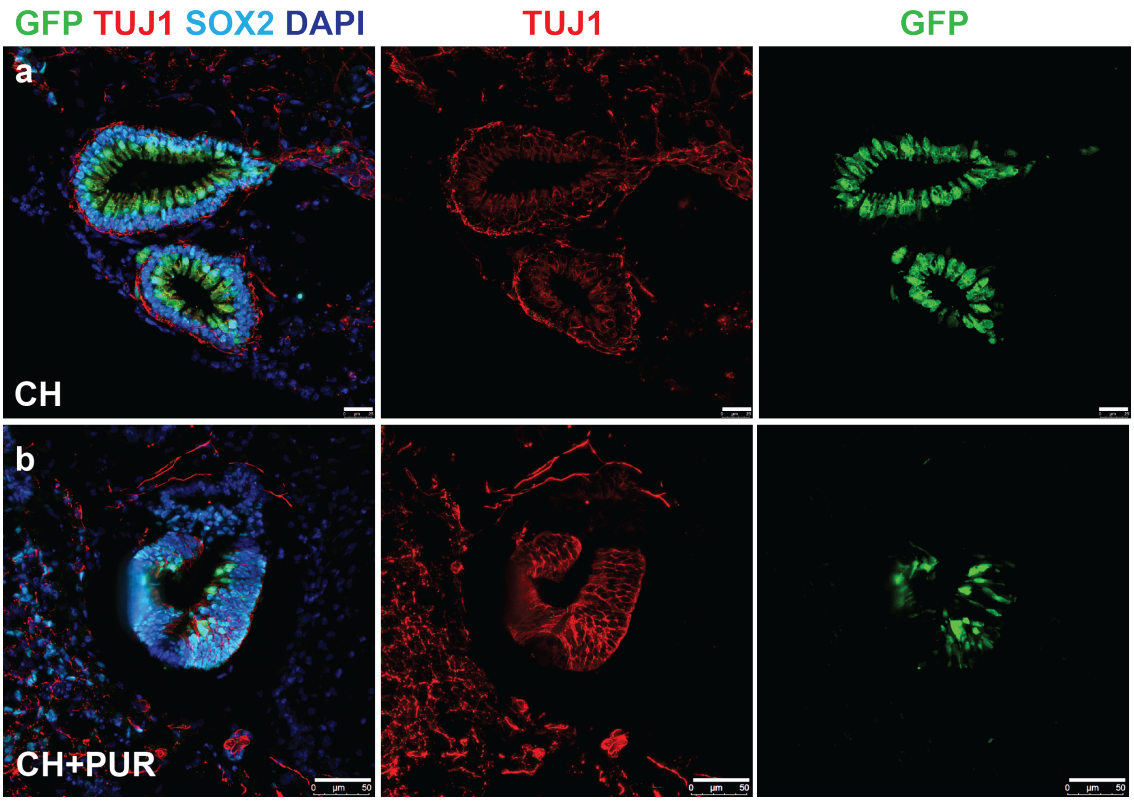

Figure 38: Late stage inner ear organoids express neural marker TUJ1.

GFP+/SOX2+ cells exhibit a hair cell-like phenotype in day 60 *ATOH1*-2A-nGFP hESC derived inner ear organoids in both CH (**a**) and CH+PUR (**b**) treated aggregates. TUJ1 expression is indicative of a neuronal population emerging in both treatment groups. Scale bars = 25 µm (**a**), 50 µm (**b**)

CHAPTER FOUR: DISCUSSION

Sensory cells of the mammalian inner ear are unable to undergo regeneration. Efforts have been made toward deriving inner ear sensory cells *in vitro.* The inner ear organoid model pioneered by Koehler et al (2017) uses human PSCs grown in 3D culture and treated with a timed series of signaling molecules to guide induction of otic tissue [19]. What results within this model are self-organized 3D structures bearing sensory hair cell-like cells that exhibit functional capability and bear a morphological and gene expression phenotype reflective of native vestibular hair cells. The goals of this dissertation were to investigate the source of the apparent vestibular bias within this model, and to evaluate a strategy for the induction of ventral otic derivatives, including cochlear cell types, *in vitro*. Focus was placed on the period of otic vesicle development, a time *in vivo* in which localized domains of gene expression are established that are crucial for subsequent development of the inner ear sensory structures. This study is the first to evaluate the patterning phenotype of human stem cell derived otic vesicles, and sheds light on the transcriptomic profile at this critical point of *in vitro* development. Furthermore, this work demonstrates that SHH pathway modulation induces changes in the patterning phenotype of the derived cell population, with the unexpected result of an expanded population reminiscent of neuroprogenitors of the cochleovestibular ganglion. This information may inform future inner ear organoid studies, and contribute to the realization of a more complete *in vitro* system of inner ear development.

Figure 39 summarizes the key findings of the study described in CHAPTER 3: RESULTS. In the following chapter, I will address these findings in the context of my two fundamental research questions.

What underlies the apparent commitment to vestibular fate within the inner ear organoid model?

In order to investigate the apparent vestibular bias within our inner ear model, we first employed a tool to isolate otic progenitors in early stage culture. The use of a *PAX2*-2A-nGFP human ESC reporter line served to surmount one of the challenges of the 3D inner ear organoid model: the heterogeneous nature of the stem cell-derived aggregates. While otic cell types develop in culture, the aggregates also contain an uncharacterized cell population that arises simultaneously. From a differentiation standpoint, these uncharacterized cells may make contributions to the aggregate “micro-environment” that are indispensable for otic induction. However, for evaluation of gene expression, this cell population may bias observations about the otic population. For example, dorsal otic marker DLX3 is seen to co-localize with PAX2 within inner ear aggregates; however, we have also observed a DLX3+/PAX2- population arising in the core region of the aggregates. DLX3 expression is not specific to otic cell types alone during development [109]. qRT-PCR analysis of whole aggregates would include this non-otic DLX3+ core population, and may skew the interpretation of DLX3 expression within the otic population. Therefore, a method

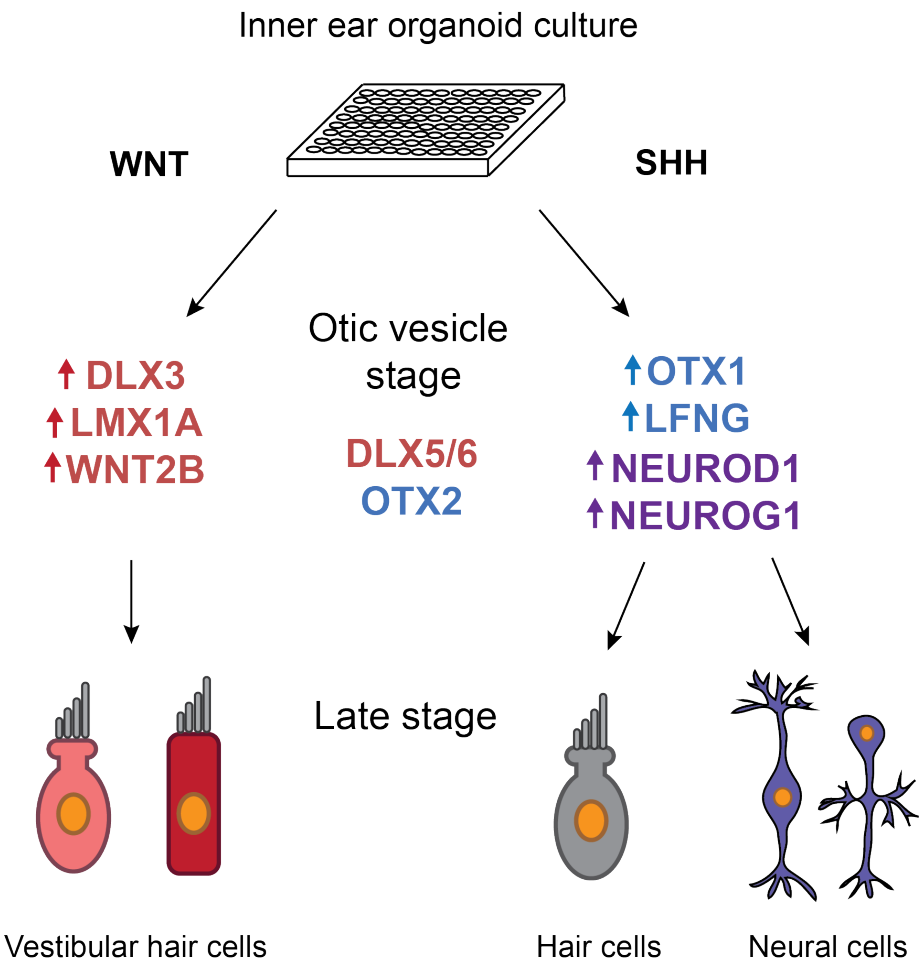

Figure 39: Summary of findings.

Analysis of cell populations exposed to either WNT agonist alone (left), or with the addition of SHH pathway modulation (right) revealed differential expression of dorsal patterning markers (indicated in red), ventral patterning markers (indicated in blue), and neuroprogenitor markers (indicated in purple). However, not all dorso-ventral patterning markers were differentially expressed between the two treatment groups. Preliminary late stage analysis has indicated that SHH pathway modulated aggregates do not give rise to hair cells exhibiting a cochlear phenotype, and that the derived hair cell population may be reduced at the expense of an increased neuronal population.

for purification of the presumptive otic population for gene expression analysis was desirable.

Using a *PAX2*-2A-nGFP human ESC reporter line allowed for monitoring and isolation of presumptive otic cells in live cultures. The first line of inquiry addressed was whether or not the *PAX2*-2A-nGFP+ cells arising in 3D inner ear culture were representative of derived otic progenitors. Many of the markers that define otic progenitors do not exhibit specificity solely to otic tissue; therefore it is necessary to compile and demonstrate expression of a battery of markers to support an otic phenotype. Rigorous immunohistochemical analysis of *PAX2*-2A-nGFP derived aggregates showed overlapping expression of *PAX2*-2A-nGFP with otic markers PAX2 and PAX8. However, PAX2 and PAX8 are both expressed in kidney progenitors during fetal development [110]. Further immunohistochemical analysis of the expression of otic markers SOX2, FBXO2, and SOX10 supported the otic identity of the *PAX2*-2A-nGFP+ cells. Additionally, dorsal otic markers DLX3 and DLX5 are not observed in the embryonic kidney [26], nor are ventral patterning markers OTX1 and OTX2 [101]. Immunohistochemical analysis confirmed expression of DLX3 and OTX2 coinciding with areas of *PAX2*-2A-nGFP expression, and scRNAseq analysis confirmed expression of all of these candidate markers among the isolated *PAX2*-2A-nGFP+ population, further supporting the otic identity of this population.

scRNA-seq analysis additionally allowed for the interrogation of multiple markers of otic development among the *PAX2*-2A-nGFP+ population that have previously proven difficult to evaluate due to limited availability of antibodies with

high specificity. With this analysis, we were able to evaluate for the first time the nature of the patterning phenotype within the derived early stage otic population. *In vivo*, the otic vesicle is patterned along a dorso-ventral axis in response to the action of graded signaling molecules, including WNT and SHH. Localized gene expression domains are key for proper morphogenesis of the inner ear sensory structures, with the vestibular system arising from a more dorsal region, and the cochlea arising from the ventralmost region.

Here, scRNA-seq analysis indicated mRNA expression of dorsal markers DLX3, DLX5, DLX6, LMX1A and WNT2B among the derived *PAX2*-2A-nGFP+ population in aggregates subjected to our established otic differentiation protocol, in which WNT agonist CHIR99021 (CH) is applied from day 11-18 in order to guide otic vesicle induction. These findings coincide with previously reported gene expression characterization of the dorsal otic vesicle [29-31, 76], and may support the hypothesis that vestibular bias may be due to a dorsalized phenotype of the early derived otic vesicles. This dorsalized phenotype may be the result of sustained exposure to WNT agonist CH during early stage culture, coinciding with the period of otic placode induction and subsequent otic vesicle formation. It is possible that dorsalization may be the result of a lack of sufficient ventralization signals in culture. However, it is important to note that expression of ventral genes OTX1, OTX2, and LFNG were also observed in CH-treated aggregates, albeit in a smaller percentage of cells than exhibited expression of dorsal markers.

In order to enhance expression of ventral genes, SHH pathway modulation was applied during culture, and will be discussed in the subsequent section, along with an expanded interpretation of dorsal gene expression in CH treated aggregates relative to those receiving SHH pathway modulation.

What factors may be applied in order to guide differentiation of otic progenitors toward a cochlear fate?

In this investigation, focus was placed specifically on SHH pathway modulation as a strategy for cochlear cell differentiation, due to the role of SHH in ventral patterning and subsequent cochlear induction [29, 31]. Alternate strategies for guiding cochlear development *in vitro*, including the investigation of additional signaling pathways, will be discussed more extensively in CHAPTER FIVE: FUTURE DIRECTIONS**.**

We found that dual treatment of CH and SHH pathway agonist PUR during early stage culture led to a size phenotype compared to control treated aggregates receiving CH alone, with the CH+PUR-treated aggregates growing significantly larger. This could be indicative of increased proliferation, which corresponds to the role of SHH as a mitogen [71]. Additionally, the trend toward an increased PAX2+ population in CH+PUR treated aggregates, as assessed by immunohistochemistry and FACS, may indicate enriched otic progenitor formation. This may be due to increased proliferation overall, or indicative of the promotion of ventralization in the derived aggregates, as PAX2 is initially broadly

expressed in the early otic epithelium but becomes restricted to the ventral domain during otic vesicle maturation [82].

scRNA-seq analysis provided insight into the transcriptomic profiles of isolated *PAX2*-2A-nGFP+ population subjected to CH+PUR treatment during otic vesicle development. We evaluated expression of PTCH1 and GLI1, SHH pathway components that are both regulated by the SHH signaling pathway [99, 100]. The CH+PUR treated population was found to contain a significantly larger population of cells expressing SHH receptor PTCH1 compared to cells treated with CH alone. The trend with respect to SHH pathway effector GLI1 was similar but not significant across three replicate datasets. In general, the observations between the two treatment groups appear to indicate that SHH pathway activation is occurring within the CH+PUR treated aggregates.

Single-cell analysis was additionally used to interrogate the patterning phenotype of the CH+PUR treated population. A significantly higher percentage of CH+PUR treated cells exhibited expression of ventral markers LFNG and OTX1 compared to cells treated with CH alone. Unlike LFNG and OTX1, ventral marker OTX2 appeared to be expressed in a higher number of cells in CH-treated samples compared to those treated with CH+PUR. It should be noted that while OTX1 and OTX2 exhibit overlapping expression in the *in vivo* otic vesicle, they does not overlap entirely [101]. Furthermore, OTX1 and OTX2 expression may be controlled by independent mechanisms. In a study from Riccomagno et al, inner ears of mice exhibiting ectopic expression of SHH in the dorsal region of the otic epithelium were evaluated to determine whether overexpression of SHH

is sufficient to ventralize the otic vesicle [29]. Expanded expression of several ventral markers into the dorsal otic vesicle was observed in these mice, along with a reduction in dorsal marker expression. However, OTX2 expression was unaffected by ectopic Shh signaling, maintaining localization to the ventralmost region of the otic vesicle. This finding implied that OTX2 may not be directly regulated by Shh, or that additional signals may be required in order to activate OTX2 expression. Within our scRNA-seq datasets, SHH pathway modulation did not appear to influence OTX2 expression. Taken with the observation that the overall number of OTX2-expressing cells is low in both treatment groups, it is possible that in both conditions a key signaling pathway may be missing in order to induce expression of OTX2.

In general, the percentage of cells expressing ventral markers LFNG and OTX1 was increased in the CH+PUR treated population compared to the CH population, but still modest, representing less than 9% of CH+PUR treated cells and less than 2% of CH treated cells for LFNG, and less than 6% of CH+PUR treated cells and less than 1% of CH treated cells for OTX1. These results appear to indicate that while CH+PUR treatment may induce a minor ventralization effect, it is not sufficient to induce a more robust gene expression phenotype across the population as a whole.

However, the observations with respect to dorsal markers appeared more substantial; there was a significant reduction in the number of cells expressing dorsal markers DLX3, WNT2B, and LMX1A in the CH+PUR treated population compared to the population treated with CH alone. The size of the population

expressing additional dorsal markers DLX5 and DLX6 was not significantly different between the two treatment groups; this observation will be addressed further in the context of late stage analysis. Nonetheless, the decrease in several key dorsal markers in the CH+PUR treatment group, taken together with the evaluation of ventral marker expression, may imply that SHH pathway modulation is sufficient to reduce dorsalization within the derived otic progenitor population to some extent, but insufficient to substantially increase expression of ventral genes.

The most striking finding within our analysis was the expansion of a neural progenitor population in the CH+PUR treated cells, indicated by a significantly higher percentage of cells expressing neuroprogenitor markers NEUROG1 and NEUROD1, which are found in precursors to cells of the cochleovestibular ganglion [104, 111, 112]. This was an unanticipated result, but coincides with the role of SHH pathway in neural patterning of the inner ear at this stage of development [29, 31]. Temporal analysis of day 15 and day 20 CH+PUR treated populations revealed a more robust NEUROG1+ population at day 15 compared to day 20, seemingly mirroring *in vivo* observations that NEUROG1 expression precedes NEUROD1 in developing inner ear neuroblasts [104]. Expansion of the NEUROD1-expressing population was observed from day 15 to day 20, further reflecting the *in vivo* progression of inner ear neural development [104, 111]. Comparative analysis of otic marker expression between the CH and CH+PUR populations additionally revealed that the CH+PUR population exhibited a significantly higher percentage of cells expressing transcription factor SOX2,

which is expressed in both sensory and non-sensory otic cell types, and functions in inner ear neurogenesis [96, 113].

Roccio and colleagues recently performed microarray analysis of microdissected SGNs from human fetal tissue at several time points [76]. Within our datasets, the stem cell derived presumptive neural populations of both treatment groups exhibiting expression of NEUROD1, NEUROG1, and neural marker ISL1 is similar to the phenotype observed in week 9 to week 11 human fetal SGNs [76]. Expression of additional neural markers POU4F1, TUBB3, and NEFL among the presumptive neural populations further supported a neural identity, while additional expression of markers of SGN and VGN development appeared to support an early neuronal phenotype specific to neurons of the inner ear. Expression of these markers appeared consistently expanded within the CH+PUR treated population compared to the CH-treated population, which exhibited a more restricted neural population. Altogether, these results indicate a presumptive neural population in both treatment groups similar to that of the neuroprogenitors that give rise to spiral and vestibular ganglion neurons. Additionally, the expanded neural population observed among the CH+PUR treated cells may indicate that SHH pathway modulation in early stage inner ear organoid culture serves to bias differentiation toward a neural as opposed to an epithelial fate.

Preliminary late stage analysis of SHH pathway modulated aggregates has indicated a decreased hair cell population compared to aggregates treated with CH alone during otic vesicle induction. It is possible that hair cell

differentiation has been minimized as a result of the expanded neuroprogenitor population at the otic vesicle stage in CH+PUR treated aggregates. Neural cell types have previously been observed within our culture model arising alongside the derived inner ear hair cell population [19]. However, this population has not yet been characterized to confirm whether these cells are representative of inner ear neurons, or indicative of other neural cell types. The observations of a neuroprogenitor population in early stage culture reminiscent of inner ear neuroblasts potentially provide support for otic identity in late stage neurons. Interrogation of SGN and VGN markers at the late stage of culture would be necessary to characterize this derived neural population. Additionally, quantitative analysis would be beneficial to confirm whether the early stage phenotype of an expanded neural population in CH+PUR treated aggregates correlates with an expanded neural population in late stage cultures.

It is important to note that the derived hair cells in CH+PUR treated cultures do not express cochlear hair cell marker LMOD3. Further analysis is necessary to confirm a vestibular phenotype in these cells, but this preliminary observation indicates that a cochlear identity has not been achieved as a result of our current SHH treatment paradigm. This could be owing to several possibilities. One potential reason may be related to the expression of dorsal markers DLX5 and DLX6 observed in both the CH and CH+PUR treated populations via scRNA-seq comparative analysis in early stage culture. Unlike the other dorsal markers surveyed, the percentages of cells expressing DLX5 and DLX6 were not statistically significant between the two treatment groups.

Notably, DLX5 was expressed in an average of 28% of CH treated cells and 26% of CH+PUR treated cells, exhibiting the highest representation of all the dorsal markers evaluated across both datasets. $Dlx5^{-/-}$/$Dlx6^{-/-}$ double mutant mice fail to form vestibular structures [114], and a similar effect is observed in $Wnt1^{-/-}$/$Wnt3a^{-/-}$ knockout mice, wherein no vestibular components arise, coinciding with a loss of Dlx5 and Dlx6 expression in the dorsal otic vesicle [30]. Expression of these dorsal markers therefore appears indispensable for vestibular structure formation. Our observations that the expression of DLX5 and DLX6 is unaffected by SHH pathway modulation raises the possibility that these factors may be more directly responsible for maintaining vestibular fate within our model than the other dorsal factors evaluated, including DLX3, WNT2B, and LMX1A, that did exhibit significant reduction following SHH pathway modulation. Riccomagno and colleagues demonstrated that DLX5 and DLX6 expression in the otic vesicle is dependent on Wnt signaling, but is regulated in larger context by the interplay between Wnt and Shh signaling pathways acting on the developing otocyst [30]. The concerted efforts of these two pathways in dorso-ventral patterning of the inner ear is complex, and it appears that each pathway may regulate markers of regional identity in different ways [115]. Within our model, the current CH+PUR treatment strategy may not accurately reflect the balance of signals needed to sufficiently reduce dorsalization and induce ventralization to an extent permissive to cochlear cell induction. Further strategies to refine this treatment, along with alternate strategies for cochlear cell differentiation, are discussed in CHAPTER FIVE: FUTURE DIRECTIONS.

Another possibility underlying the apparent vestibular bias within our model is that the current length of culture is simply insufficient to observe cochlear cell types. In human embryological development, formation of the vestibular organs and sensory populations occurs prior to cochlear development [76]. Cochlear hair cell differentiation occurs between weeks 11-12 in human development, with MYO7A+ cells observed in the vestibular sensory epithelium by weeks 8-9. A potential gap in the analysis of the CH+PUR treatment in human inner ear organoids is the time span—here, CH+PUR aggregates were cultured for up to 70 days only. Maintenance of inner ear aggregates in culture has previously been demonstrated for up to 150 days [19]. It is possible that culturing aggregates for a longer time period may lead to the induction of cochlear hair cells naturally, as cochlear hair cell induction succeeds vestibular hair cell development *in vivo*.

CHAPTER FIVE: FUTURE DIRECTIONS

This study has provided valuable insight into the gene expression phenotype of the presumptive otic progenitor population from early stage human ESC-derived inner ear organoids. Additionally, this work has shed light on the differential gene expression occurring in response to SHH pathway modulation within this model. SHH treatment was pursued as a potential strategy for inducing a patterning phenotype permissive to cochlear induction *in vitro*. While treatment with SHH pathway agonist PUR was shown to reduce expression of select markers local to the vestibular-yielding dorsal otic vesicle, upregulation of ventral genes was modest. More strikingly, a phenotype indicative of a neuroprogenitor population indicated that SHH pathway modulation in early stage inner ear organoid culture may bias differentiation toward a neural lineage at the expense of an epithelial lineage. Strategies to further investigate these findings, along with strategies to further enrich ventral gene expression and induce cochlear cell types, will be discussed in this chapter.

Improving efficiency of otic induction

One of the limitations of the human inner ear organoid system remains the efficiency of otic induction. FACS analysis has shown that generation of presumptive otic progenitors, as defined by *PAX2*-2A-nGFP expression, appears to be ~5% of the total cell population in conventionally treated aggregates (CH treatment from day 11-18). FACS of late stage *ATOH1*-2A-GFP aggregates stained for epithelial marker EPCAM (expressed in supporting and sensory cell

populations) yielded less than 4% of the total cell population, indicative of both sensory and non-sensory otic cells (data not shown). Treatment with SHH pathway agonist PUR increases the size of the *PAX2*-2A-nGFP+ population in early stage culture, but this appears to occur at the expense of late stage induction of sensory hair cells.

Optimization is necessary to increase the overall efficiency of otic induction and subsequent induction of sensory cell types within the inner ear organoid model. This will increase the utility of this system as a platform for high-throughput drug screening, drug design, or otic toxicity studies. A study from Wu et al investigated a strategy to reduce off-target cell types in an organoid model of human kidney development [116], wherein small molecule inhibition of BDNF receptor NTRK2 resulted in a 90% decrease in unwanted neuronal cell types observed in culture. A similar strategy may potentially be employed to improve efficiency of otic induction by reducing off-target differentiation; factors within the scRNA-seq datasets generated here may be identified and targeted with small molecule treatment in culture to decrease off-target cell induction and therefore lead to enriched otic differentiation.

Optimization of small molecule treatments during the first eight days of culture may also lead to increased otic induction. Successive inhibition of BMP and WNT pathways along with FGF activation has been shown to lead to the specification of the pre-placodal region [117]. Within our model, aggregates are treated with BMP inhibitor LDN and with FGF-2 on culture day 4 to this purpose. We have not explored the effects of additional WNT inhibition at this timepoint

[20, 118]. Adding WNT inhibitor within the first eight days of culture may lead to more efficient induction of the pre-placodal region, which may then lead to enriched otic induction at later stages of culture.

Toward cochlear differentiation

While SHH treatment was shown to induce changes in the patterning phenotype of early stage derived otic progenitors, late stage analysis did not confirm the induction of cochlear cell types. Proposed here are several potential strategies to continue the pursuit of cochlear induction within our inner ear model.

Fine-tuning SHH pathway modulation

In vivo, SHH is secreted from the floor plate and notochord and acts on the developing otic vesicle in a graded manner [115]. One of the limitations of treating aggregates with a small molecule agonist for SHH pathway activation is that it is a broad, untargeted treatment. A possible avenue of investigation would be to attempt to model the SHH gradient observed *in vivo* within the culture model. Embedding early stage aggregates in Matrigel and co-culturing with beads coated in PUR or another SHH pathway activator may serve to better mimic the *in vivo* environment, in which a gradient of SHH signaling acts on the developing otic vesicle. Enacting SHH treatment in a more nuanced manner may result in a phenotype reflecting both neural induction and ventralization. Furthermore, as opposing gradients of SHH and WNT act on the developing otic

vesicle *in vivo* [29, 30, 119, 120], it may be beneficial to co-culture with both SHH pathway and WNT signaling agonists in a regionalized manner.

Additionally, this study investigated the application of small molecule agonist PUR for SHH pathway activation in culture. Alternate small molecules for SHH signaling activation may be evaluated, including SAG and GSA-10 [121, 122], to determine whether the effects are specific to PUR treatment, or consistent with other small molecules. PUR, SAG, and GSA-10 all act as agonists for SHH pathway effector SMO. The application of SHH recombinant protein in culture may also be investigated, to evaluate the effects of eliciting SHH signaling activation via a different pathway component.

Additional pathway modulation

WNT signaling has been shown to function in specification of dorsal otic fates, contributing to the prevailing model that opposing gradients of WNT and SHH signals from the hindbrain are responsible for specification of dorsal and ventral gene expression domains within the developing otic vesicle [29, 30, 119, 120]. We have shown that aggregates that receive WNT agonist CH along with SHH pathway agonist PUR during the otic vesicle induction stage appear to express markers of the dorsal otic vesicle in a lower relative number of cells compared to aggregates receiving WNT modulation alone at the same stage. While SHH pathway modulation appears to induce a modest enrichment of ventral markers, it is possible that subsequent WNT inhibition following SHH pathway treatment may serve to further ventralize the derived otic vesicles.

Treatment with SHH pathway agonist PUR alone during otic vesicle induction appears to negatively impact otic vesicle formation. Therefore, initial treatment with WNT agonist appears to be indispensable for otic vesicle formation within this model. However, application of WNT inhibitor subsequent to CH+PUR treatment may allow for otic vesicle formation, but may further promote ventralization necessary for cochlear induction.

BMP signaling has additionally been implicated in dorsal patterning of the otic vesicle [115, 123]. The human inner ear aggregates are thought to exhibit a certain degree of endogenous BMP signaling, as evidenced by the variable BMP treatment necessary for non-neural ectoderm induction across different human pluripotent stem cell lines [19]. Aggregates of human WA25 ESCs do not require BMP treatment in early stage culture, whereas aggregates cultured from mND2-0 human iPSCs required BMP treatment in order to exhibit non-neural ectoderm induction [19]. It stands to reason that a degree of endogenous BMP signaling may be at play in otic vesicle stage culture as well, but this has yet to be assessed. Due to the contribution of BMP in dorsal otic vesicle patterning, it is possible that the introduction of BMP inhibition during otic vesicle induction *in vitro* may additionally serve to reduce dorsalization of the derived otic population, and thereby promote ventral otic fates.

The potential impact of the in vivo microenvironment

As in all *in vitro* studies, the contributions of the *in vivo* microenvironment cannot be ignored. It is possible that small molecule treatments alone, no matter

how nuanced the delivery, are insufficient for induction of cochlear cell types *in vitro*. The coordinated effects of signaling pathways *in vivo* may be so complex that the correct “cocktail” of signaling molecules cannot be fully comprehended for precise cochlear induction *in vitro*. Implanting derived otic progenitors into the embryonic mouse inner ear may provide the missing cues necessary for cochlear differentiation, and would further serve to validate the otic identity and differentiation capacity of these derived cells.

Assessing late stage neural identity

Further analysis to determine the identity of the late stage neural population in CH+PUR treated aggregates will be key to confirming whether the derived inner ear neuroprogenitor population observed in early stage cultures is capable of giving rise to cells of SGN and/or VGN identity. Previous efforts to derive inner ear neurons *in vitro* have employed stepwise differentiation methods driven by the manipulation of signaling pathways implicated in neural development [51, 124, 125]. Transient expression of Neurog1 [126], exposure to human fetal auditory neuron conditioned media [127], and co-culture with auditory neuron explants [128] have also been investigated as strategies for inner ear neuron differentiation. Among these studies, SHH signaling has been largely ignored as a strategy for auditory and vestibular neuron induction, and 2D culture has served as the prevalent format for differentiation. Our system offers the advantage of concurrently arising hair cell and neuronal populations, and a degree of self-organization that more closely mimics *in vivo* inner ear

development. The neuroprogenitor population identified within our early stage culture appears to be a promising foundation to support inner ear neural induction within our system. Immunohistochemical analysis of inner ear neural markers, as well as evaluation of the functional capability of this population through electrophysiological analysis, would be appropriate next steps to confirm the identity of the late stage derived neuronal population.

The presence of a verified inner ear neuron population within our model would serve to enhance the complexity of the system, thereby bolstering its applicability in future inner ear studies as a more complete representation of the native inner ear.

REFERENCES

1. Centers for Disease, C. and Prevention, *Identifying infants with hearing loss - United States, 1999-2007.* MMWR Morb Mortal Wkly Rep, 2010. **59**(8): p. 220-3.

2. Blackwell, D.L., J.W. Lucas, and T.C. Clarke, *Summary health statistics for U.S. adults: national health interview survey, 2012.* Vital Health Stat 10, 2014(260): p. 1-161.

3. Baharvand, H., et al., *Differentiation of human embryonic stem cells into hepatocytes in 2D and 3D culture systems in vitro.* Int J Dev Biol, 2006. **50**(7): p. 645-52.

4. Tian, X.F., et al., *Comparison of osteogenesis of human embryonic stem cells within 2D and 3D culture systems.* Scand J Clin Lab Invest, 2008. **68**(1): p. 58-67.

5. Edmondson, R., et al., *Three-dimensional cell culture systems and their applications in drug discovery and cell-based biosensors.* Assay Drug Dev Technol, 2014. **12**(4): p. 207-18.

6. Eiraku, M., et al., *Self-organizing optic-cup morphogenesis in three-dimensional culture.* Nature, 2011. **472**(7341): p. 51-6.

7. Nakano, T., et al., *Self-formation of optic cups and storable stratified neural retina from human ESCs.* Cell Stem Cell, 2012. **10**(6): p. 771-85.

8. Kadoshima, T., et al., *Self-organization of axial polarity, inside-out layer pattern, and species-specific progenitor dynamics in human ES cell-derived neocortex.* Proc Natl Acad Sci U S A, 2013. **110**(50): p. 20284-9.

9. Lancaster, M.A., et al., *Cerebral organoids model human brain development and microcephaly.* Nature, 2013. **501**(7467): p. 373-9.

10. Dye, B.R., et al., *In vitro generation of human pluripotent stem cell derived lung organoids.* Elife, 2015. **4**.

11. McCracken, K.W., et al., *Generating human intestinal tissue from pluripotent stem cells in vitro.* Nat Protoc, 2011. **6**(12): p. 1920-8.

12. Takasato, M., et al., *Kidney organoids from human iPS cells contain multiple lineages and model human nephrogenesis.* Nature, 2015. **526**(7574): p. 564-8.

13. Morizane, R., et al., *Nephron organoids derived from human pluripotent stem cells model kidney development and injury.* Nat Biotechnol, 2015. **33**(11): p. 1193-200.

14. Allison, S.J., *Developmental biology: Nephrogenesis in kidney organoids derived from human pluripotent stem cells.* Nat Rev Nephrol, 2015. **11**(12): p. 689.

15. Kunz-Schughart, L.A., et al., *The use of 3-D cultures for high-throughput screening: the multicellular spheroid model.* J Biomol Screen, 2004. **9**(4): p. 273-85.

16. Howes, A.L., et al., *3-Dimensional culture systems for anti-cancer compound profiling and high-throughput screening reveal increases in EGFR inhibitor-mediated cytotoxicity compared to monolayer culture systems.* PLoS One, 2014. **9**(9): p. e108283.

17. Dutta, D., I. Heo, and H. Clevers, *Disease Modeling in Stem Cell-Derived 3D Organoid Systems.* Trends Mol Med, 2017. **23**(5): p. 393-410.

18. Rossi, G., A. Manfrin, and M.P. Lutolf, *Progress and potential in organoid research.* Nat Rev Genet, 2018. **19**(11): p. 671-687.

19. Koehler, K.R., et al., *Generation of inner ear organoids containing functional hair cells from human pluripotent stem cells.* Nat Biotechnol, 2017. **35**(6): p. 583-589.

20. Koehler, K.R., et al., *Generation of inner ear sensory epithelia from pluripotent stem cells in 3D culture.* Nature, 2013. **500**(7461): p. 217-21.

21. Eiraku, M., et al., *Self-organized formation of polarized cortical tissues from ESCs and its active manipulation by extrinsic signals.* Cell Stem Cell, 2008. **3**(5): p. 519-32.

22. Liu, X.P., et al., *Functional development of mechanosensitive hair cells in stem cell-derived organoids parallels native vestibular hair cells.* Nat Commun, 2016. **7**: p. 11508.

23. Ekdale, E.G., *Form and function of the mammalian inner ear.* J Anat, 2016. **228**(2): p. 324-37.

24. Lim, R. and A.M. Brichta, *Anatomical and physiological development of the human inner ear.* Hear Res, 2016. **338**: p. 9-21.

25. Goldberg, J.M., A. Lysakowski, and C. Fernandez, *Morphophysiological and ultrastructural studies in the mammalian cristae ampullares.* Hear Res, 1990. **49**(1-3): p. 89-102.

26. Koehler, K.R., Malone, A.K., Hashino, E., *Recapitulating Inner Ear Development With Pluripotent Stem Cells: Biology and Translation*, in *Development of Auditory and Vestibular Systems*, R. Romand, Varela-Nieto, I., Editor. 2014, Academic Press: Oxford, UK. p. 214-249.

27. Schlosser, G., *Early embryonic specification of vertebrate cranial placodes.* Wiley Interdiscip Rev Dev Biol, 2014. **3**(5): p. 349-63.

28. Bruska, M., et al., *Differentiation of the facio-vestibulocochlear ganglionic complex in human embryos of developmental stages 13-15.* Folia Morphol (Warsz), 2009. **68**(3): p. 167-73.

29. Riccomagno, M.M., et al., *Specification of the mammalian cochlea is dependent on Sonic hedgehog.* Genes Dev, 2002. **16**(18): p. 2365-78.

30. Riccomagno, M.M., S. Takada, and D.J. Epstein, *Wnt-dependent regulation of inner ear morphogenesis is balanced by the opposing and supporting roles of Shh.* Genes Dev, 2005. **19**(13): p. 1612-23.

31. Brown, A.S. and D.J. Epstein, *Otic ablation of smoothened reveals direct and indirect requirements for Hedgehog signaling in inner ear development.* Development, 2011. **138**(18): p. 3967-76.

32. Streeter, G.L., *On the development of the membranous labyrinth and the acoustic and facialis nerves in the human embryo.* Am. J. Anat. , 1906. **6**: p. 139-165.

33. Pechriggl, E.J., et al., *Development of the innervation of the human inner ear.* Dev Neurobiol, 2015. **75**(7): p. 683-702.

34. Silva, J. and A. Smith, *Capturing pluripotency.* Cell, 2008. **132**(4): p. 532-6.

35. Thomson, M., et al., *Pluripotency factors in embryonic stem cells regulate differentiation into germ layers.* Cell, 2011. **145**(6): p. 875-89.

36. Takahashi, K., et al., *Induction of pluripotent stem cells from adult human fibroblasts by defined factors.* Cell, 2007. **131**(5): p. 861-72.

37. Takahashi, K. and S. Yamanaka, *Induction of pluripotent stem cells from mouse embryonic and adult fibroblast cultures by defined factors.* Cell, 2006. **126**(4): p. 663-76.

38. Brons, I.G., et al., *Derivation of pluripotent epiblast stem cells from mammalian embryos.* Nature, 2007. **448**(7150): p. 191-5.

39. Tesar, P.J., et al., *New cell lines from mouse epiblast share defining features with human embryonic stem cells.* Nature, 2007. **448**(7150): p. 196-9.

40. Watanabe, K., et al., *Directed differentiation of telencephalic precursors from embryonic stem cells.* Nat Neurosci, 2005. **8**(3): p. 288-96.

41. Watanabe, K., et al., *A ROCK inhibitor permits survival of dissociated human embryonic stem cells.* Nat Biotechnol, 2007. **25**(6): p. 681-6.

42. Mertens, J., et al., *Evaluating cell reprogramming, differentiation and conversion technologies in neuroscience.* Nat Rev Neurosci, 2016. **17**(7): p. 424-37.

43. Costa, A., et al., *Generation of sensory hair cells by genetic programming with a combination of transcription factors.* Development, 2015. **142**(11): p. 1948-59.

44. Li, H., et al., *Generation of hair cells by stepwise differentiation of embryonic stem cells.* Proc Natl Acad Sci U S A, 2003. **100**(23): p. 13495-500.

45. Oshima, K., et al., *Mechanosensitive hair cell-like cells from embryonic and induced pluripotent stem cells.* Cell, 2010. **141**(4): p. 704-16.

46. Keller, G.M., *In vitro differentiation of embryonic stem cells.* Curr Opin Cell Biol, 1995. **7**(6): p. 862-9.

47. Ouji, Y., et al., *In vitro differentiation of mouse embryonic stem cells into inner ear hair cell-like cells using stromal cell conditioned medium.* Cell Death Dis, 2012. **3**: p. e314.

48. Koehler, K.R. and E. Hashino, *3D mouse embryonic stem cell culture for generating inner ear organoids.* Nat Protoc, 2014. **9**(6): p. 1229-44.

49. Uhl, E.W. and N.J. Warner, *Mouse Models as Predictors of Human Responses: Evolutionary Medicine.* Curr Pathobiol Rep, 2015. **3**(3): p. 219-223.

50. Czajkowski, A., et al., *Pluripotent stem cell-derived cochlear cells: a challenge in constant progress.* Cell Mol Life Sci, 2019. **76**(4): p. 627-635.

51. Chen, W., et al., *Restoration of auditory evoked responses by human ES-cell-derived otic progenitors.* Nature, 2012. **490**(7419): p. 278-82.
52. Ding, J., et al., *Induction of differentiation of human embryonic stem cells into functional hair-cell-like cells in the absence of stromal cells.* Int J Biochem Cell Biol, 2016. **81**(Pt A): p. 208-222.

53. Ohnishi, H., et al., *Limited hair cell induction from human induced pluripotent stem cells using a simple stepwise method.* Neurosci Lett, 2015. **599**: p. 49-54.

54. Lahlou, H., et al., *Modeling human early otic sensory cell development with induced pluripotent stem cells.* PLoS One, 2018. **13**(6): p. e0198954.

55. Ronaghi, M., et al., *Inner ear hair cell-like cells from human embryonic stem cells.* Stem Cells Dev, 2014. **23**(11): p. 1275-84.

56. Lahlou, H., et al., *Enriched Differentiation of Human Otic Sensory Progenitor Cells Derived From Induced Pluripotent Stem Cells.* Front Mol Neurosci, 2018. **11**: p. 452.

57. Jeong, M., et al., *Generating inner ear organoids containing putative cochlear hair cells from human pluripotent stem cells.* Cell Death Dis, 2018. **9**(9): p. 922.

58. Simmons, D.D., et al., *Oncomodulin identifies different hair cell types in the mammalian inner ear.* J Comp Neurol, 2010. **518**(18): p. 3785-802.

59. Gale, J.E., et al., *FM1-43 dye behaves as a permeant blocker of the hair-cell mechanotransducer channel.* J Neurosci, 2001. **21**(18): p. 7013-25.

60. Lao, K.Q., et al., *mRNA-sequencing whole transcriptome analysis of a single cell on the SOLiD system.* J Biomol Tech, 2009. **20**(5): p. 266-71.

61. Hwang, B., J.H. Lee, and D. Bang, *Single-cell RNA sequencing technologies and bioinformatics pipelines.* Exp Mol Med, 2018. **50**(8): p. 96.

62. Haque, A., et al., *A practical guide to single-cell RNA-sequencing for biomedical research and clinical applications.* Genome Med, 2017. **9**(1): p. 75.

63. Islam, S., et al., *Quantitative single-cell RNA-seq with unique molecular identifiers.* Nat Methods, 2014. **11**(2): p. 163-6.

64. Burns, J.C., et al., *Single-cell RNA-Seq resolves cellular complexity in sensory organs from the neonatal inner ear.* Nat Commun, 2015. **6**: p. 8557.

65. Briscoe, J. and P.P. Therond, *The mechanisms of Hedgehog signalling and its roles in development and disease.* Nat Rev Mol Cell Biol, 2013. **14**(7): p. 416-29.

66. Nusslein-Volhard, C. and E. Wieschaus, *Mutations affecting segment number and polarity in Drosophila.* Nature, 1980. **287**(5785): p. 795-801.

67. Lai, L.P. and J. Mitchell, *Indian hedgehog: its roles and regulation in endochondral bone development.* J Cell Biochem, 2005. **96**(6): p. 1163-73.

68. Bitgood, M.J., L. Shen, and A.P. McMahon, *Sertoli cell signaling by Desert hedgehog regulates the male germline.* Curr Biol, 1996. **6**(3): p. 298-304.

69. Mirsky, R., et al., *Schwann cell-derived desert hedgehog signals nerve sheath formation.* Ann N Y Acad Sci, 1999. **883**: p. 196-202.

70. Parmantier, E., et al., *Schwann cell-derived Desert hedgehog controls the development of peripheral nerve sheaths.* Neuron, 1999. **23**(4): p. 713-24.

71. Varjosalo, M. and J. Taipale, *Hedgehog: functions and mechanisms.* Genes Dev, 2008. **22**(18): p. 2454-72.

72. Huangfu, D., et al., *Hedgehog signalling in the mouse requires intraflagellar transport proteins.* Nature, 2003. **426**(6962): p. 83-7.

73. Hui, C.C. and S. Angers, *Gli proteins in development and disease.* Annu Rev Cell Dev Biol, 2011. **27**: p. 513-37.

74. Bok, J., et al., *Opposing gradients of Gli repressor and activators mediate Shh signaling along the dorsoventral axis of the inner ear.* Development, 2007. **134**(9): p. 1713-22.

75. Durruthy-Durruthy, R., et al., *Reconstruction of the mouse otocyst and early neuroblast lineage at single-cell resolution.* Cell, 2014. **157**(4): p. 964-78.

76. Roccio, M., et al., *Molecular characterization and prospective isolation of human fetal cochlear hair cell progenitors.* Nat Commun, 2018. **9**(1): p. 4027.

77. Nie, J., K.R. Koehler, and E. Hashino, *Directed Differentiation of Mouse Embryonic Stem Cells Into Inner Ear Sensory Epithelia in 3D Culture.* Methods Mol Biol, 2017. **1597**: p. 67-83.

78. Meijer, L., M. Flajolet, and P. Greengard, *Pharmacological inhibitors of glycogen synthase kinase 3.* Trends Pharmacol Sci, 2004. **25**(9): p. 471-80.

79. Cohen, P. and M. Goedert, *GSK3 inhibitors: development and therapeutic potential.* Nat Rev Drug Discov, 2004. **3**(6): p. 479-87.

80. Ring, D.B., et al., *Selective glycogen synthase kinase 3 inhibitors potentiate insulin activation of glucose transport and utilization in vitro and in vivo.* Diabetes, 2003. **52**(3): p. 588-95.

81. Sinha, S. and J.K. Chen, *Purmorphamine activates the Hedgehog pathway by targeting Smoothened.* Nat Chem Biol, 2006. **2**(1): p. 29-30.

82. Torres, M., E. Gomez-Pardo, and P. Gruss, *Pax2 contributes to inner ear patterning and optic nerve trajectory.* Development, 1996. **122**(11): p. 3381-91.

83. Terzic, J., et al., *Expression of PAX2 gene during human development.* Int J Dev Biol, 1998. **42**(5): p. 701-7.

84. Burton, Q., et al., *The role of Pax2 in mouse inner ear development.* Dev Biol, 2004. **272**(1): p. 161-75.

85. Sanyanusin, P., et al., *Mutation of the PAX2 gene in a family with optic nerve colobomas, renal anomalies and vesicoureteral reflux.* Nat Genet, 1995. **9**(4): p. 358-64.

86. Schimmenti, L.A., et al., *Further delineation of renal-coloboma syndrome in patients with extreme variability of phenotype and identical PAX2 mutations.* Am J Hum Genet, 1997. **60**(4): p. 869-78.

87. Tellier, A.L., et al., *Expression of the PAX2 gene in human embryos and exclusion in the CHARGE syndrome.* Am J Med Genet, 2000. **93**(2): p. 85-8.

88. de Felipe, P., et al., *Use of the 2A sequence from foot-and-mouth disease virus in the generation of retroviral vectors for gene therapy.* Gene Ther, 1999. **6**(2): p. 198-208.

89. Wu, X., et al., *A small molecule with osteogenesis-inducing activity in multipotent mesenchymal progenitor cells.* J Am Chem Soc, 2002. **124**(49): p. 14520-1.

90. Wu, X., et al., *Purmorphamine induces osteogenesis by activation of the hedgehog signaling pathway.* Chem Biol, 2004. **11**(9): p. 1229-38.

91. Herget, M., et al., *A simple method for purification of vestibular hair cells and non-sensory cells, and application for proteomic analysis.* PLoS One, 2013. **8**(6): p. e66026.

92. Butler, A., et al., *Integrating single-cell transcriptomic data across different conditions, technologies, and species.* Nat Biotechnol, 2018. **36**(5): p. 411-420.

93. Satija, R., et al., *Spatial reconstruction of single-cell gene expression data.* Nat Biotechnol, 2015. **33**(5): p. 495-502.

94. AlJanahi, A.A., M. Danielsen, and C.E. Dunbar, *An Introduction to the Analysis of Single-Cell RNA-Sequencing Data.* Mol Ther Methods Clin Dev, 2018. **10**: p. 189-196.

95. Nornes, H.O., et al., *Spatially and temporally restricted expression of Pax2 during murine neurogenesis.* Development, 1990. **109**(4): p. 797-809.

96. Steevens, A.R., et al., *SOX2 is required for inner ear neurogenesis.* Sci Rep, 2017. **7**(1): p. 4086.

97. Nelson, R.F., et al., *Selective cochlear degeneration in mice lacking the F-box protein, Fbx2, a glycoprotein-specific ubiquitin ligase subunit.* J Neurosci, 2007. **27**(19): p. 5163-71.

98. Hartman, B.H., et al., *Identification and characterization of mouse otic sensory lineage genes.* Front Cell Neurosci, 2015. **9**: p. 79.

99. Goodrich, L.V., et al., *Conservation of the hedgehog/patched signaling pathway from flies to mice: induction of a mouse patched gene by Hedgehog.* Genes Dev, 1996. **10**(3): p. 301-12.

100. Hooper, J.E. and M.P. Scott, *Communicating with Hedgehogs.* Nat Rev Mol Cell Biol, 2005. **6**(4): p. 306-17.

101. Morsli, H., et al., *Otx1 and Otx2 activities are required for the normal development of the mouse inner ear.* Development, 1999. **126**(11): p. 2335-43.

102. Torres, M. and F. Giraldez, *The development of the vertebrate inner ear.* Mech Dev, 1998. **71**(1-2): p. 5-21.

103. Ma, Q., et al., *neurogenin1 is essential for the determination of neuronal precursors for proximal cranial sensory ganglia.* Neuron, 1998. **20**(3): p. 469-82.

104. Yang, T., et al., *The molecular basis of making spiral ganglion neurons and connecting them to hair cells of the organ of Corti.* Hear Res, 2011. **278**(1-2): p. 21-33.

105. Schaefer, S.A., et al., *From Otic Induction to Hair Cell Production: Pax2(EGFP) Cell Line Illuminates Key Stages of Development in Mouse Inner Ear Organoid Model.* Stem Cells Dev, 2018. **27**(4): p. 237-251.

106. Radde-Gallwitz, K., et al., *Expression of Islet1 marks the sensory and neuronal lineages in the mammalian inner ear.* J Comp Neurol, 2004. **477**(4): p. 412-21.

107. Lu, C.C., et al., *Developmental profiling of spiral ganglion neurons reveals insights into auditory circuit assembly.* J Neurosci, 2011. **31**(30): p. 10903-18.

108. Shepherd, R.K., et al., *Chronic depolarization enhances the trophic effects of brain-derived neurotrophic factor in rescuing auditory neurons following a sensorineural hearing loss.* J Comp Neurol, 2005. **486**(2): p. 145-58.

109. Beanan, M.J. and T.D. Sargent, *Regulation and function of Dlx3 in vertebrate development.* Dev Dyn, 2000. **218**(4): p. 545-53.

110. Bouchard, M., et al., *Nephric lineage specification by Pax2 and Pax8.* Genes Dev, 2002. **16**(22): p. 2958-70.

111. Liu, M., et al., *Essential role of BETA2/NeuroD1 in development of the vestibular and auditory systems.* Genes Dev, 2000. **14**(22): p. 2839-54.

112. Raft, S., et al., *Cross-regulation of Ngn1 and Math1 coordinates the production of neurons and sensory hair cells during inner ear development.* Development, 2007. **134**(24): p. 4405-15.

113. Gu, R., et al., *Lineage tracing of Sox2-expressing progenitor cells in the mouse inner ear reveals a broad contribution to non-sensory tissues and insights into the origin of the organ of Corti.* Dev Biol, 2016. **414**(1): p. 72-84.

114. Robledo, R.F., et al., *The Dlx5 and Dlx6 homeobox genes are essential for craniofacial, axial, and appendicular skeletal development.* Genes Dev, 2002. **16**(9): p. 1089-101.

115. Groves, A.K. and D.M. Fekete, *Shaping sound in space: the regulation of inner ear patterning.* Development, 2012. **139**(2): p. 245-57.

116. Wu, H., et al., *Comparative Analysis and Refinement of Human PSC-Derived Kidney Organoid Differentiation with Single-Cell Transcriptomics.* Cell Stem Cell, 2018. **23**(6): p. 869-881 e8.

117. Kwon, H.J., et al., *Identification of early requirements for preplacodal ectoderm and sensory organ development.* PLoS Genet, 2010. **6**(9): p. e1001133.

118. Pieper, M., et al., *Differential distribution of competence for panplacodal and neural crest induction to non-neural and neural ectoderm.* Development, 2012. **139**(6): p. 1175-87.

119. Bok, J., M. Bronner-Fraser, and D.K. Wu, *Role of the hindbrain in dorsoventral but not anteroposterior axial specification of the inner ear.* Development, 2005. **132**(9): p. 2115-24.

120. Bok, J., W. Chang, and D.K. Wu, *Patterning and morphogenesis of the vertebrate inner ear.* Int J Dev Biol, 2007. **51**(6-7): p. 521-33.

121. Chen, J.K., et al., *Small molecule modulation of Smoothened activity.* Proc Natl Acad Sci U S A, 2002. **99**(22): p. 14071-6.

122. Gorojankina, T., et al., *Discovery, molecular and pharmacological characterization of GSA-10, a novel small-molecule positive modulator of Smoothened.* Mol Pharmacol, 2013. **83**(5): p. 1020-9.

123. Ohta, S., et al., *BMP regulates regional gene expression in the dorsal otocyst through canonical and non-canonical intracellular pathways.* Development, 2016. **143**(12): p. 2228-37.

124. Shi, F., et al., *BMP4 induction of sensory neurons from human embryonic stem cells and reinnervation of sensory epithelium.* Eur J Neurosci, 2007. **26**(11): p. 3016-23.

125. Gonmanee, T., et al., *Differentiation of stem cells from human deciduous and permanent teeth into spiral ganglion neuron-like cells.* Arch Oral Biol, 2018. **88**: p. 34-41.

126. Reyes, J.H., et al., *Glutamatergic neuronal differentiation of mouse embryonic stem cells after transient expression of neurogenin 1 and*

treatment with BDNF and GDNF: in vitro and in vivo studies. J Neurosci, 2008. **28**(48): p. 12622-31.

127. Boddy, S.L., et al., *Inner ear progenitor cells can be generated in vitro from human bone marrow mesenchymal stem cells.* Regen Med, 2012. **7**(6): p. 757-67.

128. Coleman, B., et al., *Auditory hair cell explant co-cultures promote the differentiation of stem cells into bipolar neurons.* Exp Cell Res, 2007. **313**(2): p. 232-43.

CURRICULUM VITAE

Emma Longworth-Mills

Education

Ph.D. in Anatomy and Cell Biology 2013-2019
- Indiana University, Indianapolis, IN

B.S. in Biology, B.A. in Music 2007-2012
- Webster University, St. Louis, MO

Research Experience

Ph.D, Indiana University 2013-2019
- Doctoral research project investigating strategies for cochlear cell induction in a three-dimensional model for the differentiation of inner ear sensory epithelia
- Mentor: Dr. Eri Hashino

Research Assistant, Donald Danforth Plant Science Center 2012-2013
- Performed genotyping and maintenance of transgenic plant lines, assisted with data collection
- Mentor: Dr. Sona Pandey

Undergraduate researcher, Webster University 2011-2012
- Completed undergraduate thesis investigating the effects of antioxidants on ethyl methanesulfonate-induced chromosomal recombination in *Drosophila melanogaster*
- Mentor: Dr. Stephanie Schroeder

Research Fellowship

Ruth L. Kirschstein National Research Service Award (NRSA) for Individual Predoctoral Fellowship (F31). Awarded July 2016 and renewed yearly through Summer 2019.

Honors and Awards

IU School of Medicine Student Travel Award 2018
IUPUI Graduate & Professional Educational Grant 2018

Molecular Biology of Hearing Research Travel Award	2018
Indiana University School of Medicine University Travel Award	2013
Summa cum laude, Webster University	2012
Missouri Department of Higher Education Gear Up Award	2007-2012
Missouri Bright Flight Scholarship	2007-2012

Publications

1. **Longworth-Mills E**, Koehler KR, Hashino E. Generating inner ear organoids from mouse embryonic stem cells. *Methods Mol Biol*, 2016

2. Koehler KR, Nie J, **Longworth-Mills E**, Liu XP, Lee J, Holt J, Hashino E. Generation of inner ear organoids with functional hair cells from human pluripotent stem cells. *Nature Biotechnology*, 2017

3. **Longworth-Mills E**, Nie J, Harkin J, Srour EF, Hashino E, Sonic hedgehog signaling in dorso-ventral specification of human inner ear organoids. *In preparation*

Podium Presentations

Longworth-Mills E, Nie J, Harkin J, Srour EF, Hashino E, Dorso-Ventral Specification of Human Inner Ear Organoids in Response to Sonic Hedgehog Pathway Modulation. Association for Research in Otolaryngology Midwinter Meeting, Baltimore, MD, 2019

Poster Presentations

Conferences:

Longworth-Mills E, Nie J, Hashino E, Generation and characterization of human embryonic stem cell reporter lines for in vitro otic progenitor development. Association for Research in Otolaryngology Midwinter Meeting, Baltimore, MD, 2017

Longworth-Mills E, Nie J, Srour EF, Hashino E, Sonic Hedgehog signaling in dorso-ventral specification of human inner ear organoids. Molecular Biology of Hearing and Deafness Meeting, Göttingen, Germany, 2018

University associated:

Longworth-Mills E, Hashino E, Inner ear organogenesis in 3D culture. Indiana University School of Medicine Graduate Program Poster Showcase, Indianapolis, IN (2016)

Koehler KR, Liu XP, Mikosz AM, **Longworth-Mills E**, Holt JR, Hashino E, Functional interrogation of the sensorineural circuit in inner ear organoids. Indiana University School of Medicine Graduate Program Poster Showcase, Indianapolis, IN (2015)

Professional Membership

Association for Research in Otolaryngology student member 2016-present

Departmental Contributions

IU School of Medicine travel award review committee 2014-2017

- Anatomy and Cell Biology Department student representative
- Performed bi-annual grant reviews to award travel grants to IUSM graduate students